



**UNIVERSIDADE FEDERAL DO PARÁ  
INSTITUTO DE GEOCIÊNCIAS  
PROGRAMA DE PÓS-GRADUAÇÃO EM GEOLOGIA E GEOQUÍMICA**

---

**TESE DE DOUTORADO Nº 178**

**O CAMP NAS BACIAS DOS SOLIMÕES, AMAZONAS,  
PARNAÍBA E PARECIS, NORTE DO BRASIL:  
IMPLICAÇÕES GEOTECTÔNICAS E DEPOSICIONAIS  
PARA O JURÁSSICO DO GONDWANA OCIDENTAL**

**Tese apresentada por:**

**GABRIEL LEAL REZENDE**

**Orientador: Prof. Dr. Afonso César Rodrigues Nogueira (UFPA)**

---

**Belém – Pará  
2024**

**Dados Internacionais de Catalogação na Publicação (CIP) de acordo com ISBD  
Sistema de Bibliotecas da Universidade Federal do Pará  
Gerada automaticamente pelo módulo Ficat, mediante os dados fornecidos pelo(a) autor(a)**

---

R467c Rezende, Gabriel Leal.  
O Camp nas bacias dos Solimões, Amazonas, Parnaíba e  
Parecis, Norte do Brasil: implicações geotectônicas e deposicionais  
para o jurássico do Gondwana Ocidental / Gabriel Leal Rezende. —  
2024.  
xx,99 f. : il. color.

Orientador(a): Prof. Dr. Afonso César Rodrigues Nogueira  
Nogueira  
Tese (Doutorado) - Universidade Federal do Pará, Instituto de  
Geociências, Programa de Pós-Graduação em Ciências Ambientais,  
Belém, 2024.

1. Geologia-Amazônia. 2. Modelagem Crustal. 3.  
Anomalia Gravimétrica. 4. Espessura Crustal. 5. Pangea.. I.  
Título.

CDD 551.7009811



**Universidade Federal do Pará**  
**Instituto de Geociências**  
**Programa de pós-graduação em geologia e geoquímica**

**O CAMP NAS BACIAS DOS SOLIMÕES, AMAZONAS,  
PARNAÍBA E PARECIS, NORTE DO BRASIL:  
IMPLICAÇÕES GEOTECTÔNICAS E DEPOSICIONAIS  
PARA O JURÁSSICO DO GONDWANA OCIDENTAL**

**Tese apresentado por**

**GABRIEL LEAL REZENDE**

**Como requisito parcial à obtenção de Grau de Doutor em Ciências na Área  
de GEOLOGIA e Linha de Pesquisa Análise de Bacias Sedimentares**

**Data de Aprovação:** 23 / 08 / 2024

**Banca Examinadora:**

Prof. Dr. Afonso César Rodrigues Nogueira (Orientador-UFGA)

Prof.<sup>a</sup> Dr.<sup>a</sup> Juliana Charão Marques (Membro-UFRGS)

Documento assinado digitalmente  
**gov.br** JULIANA CHARAO MARQUES  
Data: 26/08/2024 11:26:30-0300  
Verifique em <https://validar.iti.gov.br>

Prof. Dr. Claudio Riccomini (Membro-USP)

Documento assinado digitalmente  
**gov.br** CLAUDIO RICCOMINI  
Data: 26/08/2024 15:58:35-0300  
Verifique em <https://validar.iti.gov.br>

Prof. Dr. Rodrigo Bijani Santos (Membro-UFF)

Documento assinado digitalmente  
**gov.br** RODRIGO BIJANI SANTOS  
Data: 29/08/2024 10:12:14-0300  
Verifique em <https://validar.iti.gov.br>

Prof. Dr. Joelson Lima Soares (Membro-UFGA)

*Dedico esse trabalho à minha família:  
Ana Rute Silva Leal, minha mãe.  
André Camara Rezende, meu pai.  
Danielle Lopes de Freitas, minha amada  
esposa e a Deus.*

## AGRADECIMENTOS

Primeiramente e acima de tudo, agradeço a **Deus** por ter abençoado e dado forças em todos os momentos dessa jornada e por sua presença constante na minha vida. À minha família que sempre me apoiou, financiando meus estudos e que esteve sempre ao meu lado em todos os momentos. Um agradecimento especial a minha mãe que sempre me apoiou e esteve comigo nos piores momentos da minha vida. À minha esposa, que sempre orou e acreditou no meu potencial, apoiando e lutando lado a lado para conseguir os nossos objetivos, garantindo a tranquilidade para finalizar a minha tese. As minhas duas avós, que sempre acreditaram em mim e estavam sempre cuidando quando eu mais precisava, principalmente, da minha saúde, dando muito amor e carinho para prosseguir na minha jornada. Ao Conselho Nacional de Desenvolvimento Científico e Tecnológico (CNPq) pela concessão de 19 meses de bolsa de doutorado. À Coordenação de Aperfeiçoamento de Pessoal de Nível Superior – Brasil (CAPES) – Código de Financiamento 001. Ao orientador Dr. Afonso César Rodrigues Nogueira, que em mais de oito anos de convivência nunca me abandonou, sendo um “paizão” e estando sempre disposto a ajudar com seus ensinamentos e amizade, além de todos os momentos de descontrações e críticas construtivas que tiveram ao longo desses anos. A Cleida por sua amizade e paciência em toda as fases dessa vida acadêmica, facilitando tudo que estava nas suas possibilidades e atribuições. Ao amigo e Dr. Nelson de Lima Ribeiro Filho que ajudou e sempre esteve disposto a agregar e melhorar a tese, além de ter contribuído na fase de revisão, formatação e processamento de dados deste trabalho. Aos amigos e companheiros do GSED em especial ao Drs. Renato Sol Paiva de Medeiros, Alexandre Ribeiro Cardoso e Cleber Eduardo Neri Rabelo que contribuíram nas imagens ou discussões .

“ O SENHOR é a minha luz e a minha salvação; a quem temerei? O SENHOR é a força da minha vida; de quem me recearei? Quando os malvados, meus adversários e meus inimigos, se chegaram contra mim, para comerem as minhas carnes, tropeçaram e caíram. Ainda que um exército me cercasse, o meu coração não temeria; ainda que a guerra se levantasse contra mim, nisso confiarei” (Salmos 27-1:3)”.

## RESUMO

Estudos geológicos em conjunto com aplicações de técnicas geofísicas estão sendo bastante utilizados para destacar e caracterizar anomalias gravimétricas do CAMP ao longo do Norte do Brasil, incluindo as bacias dos Solimões, Parecis, do Amazonas e Parnaíba. Interpretações de anomalias gravimétricas residuais destas bacias foram utilizadas para ampliar a compreensão da distribuição do CAMP ao longo da subsuperfície. Este estudo foi realizado por meio de interpretações qualitativas e quantitativas de dados gravimétricos, apoiadas em informações geológicas superficiais, principalmente dados estratigráficos baseados em afloramentos. A partir de uma modelagem gravimétrica direta, baseada em modelos de estrutura gravitacional da crosta disponíveis para separar um sinal de gravidade residual dos dados de gravidade observados, interpretou-se características geológicas e tectônicas realisticamente detalhadas, fornecendo informações úteis para uma interpretação geofísica de fontes geológicas. Com a anomalia residual, obteve-se o mapa da espessura elástica ( $T_e$ ) das bacias, a partir de um novo procedimento, permitindo presumidamente preencher algumas lacunas apresentadas na literatura atual sobre o CAMP. Para cada valor de  $T_e$  foi calculado o sinal gravimétrico residual, considerando as superfícies descritas pela topografia e profundidade da Moho para um modelo regional com densidade padrão e discretizado em prismas. A correlação cruzada entre o sinal gravimétrico observado e o sinal gravimétrico calculado permitiu obter o mapa da espessura elástica das áreas estudadas. O maior valor de correlação está diretamente relacionado ao melhor valor de espessura elástica e profundidade da Moho associados à deformação da crosta. Nosso estudo utilizou a combinação dessas técnicas para presumidamente definir a possível extensão do magmatismo do Jurássico, a reologia das bacias na intrusão de corpos ígneos e a história de subsidência térmica que controlou amplamente o controle deposicional durante e depois do CAMP. A presença de baixos valores de gravidade está intimamente relacionada as unidades litológicas menos densas da crosta superior, enquanto os altos valores de gravidade são relacionados as rochas de alta densidade, correlacionadas aos basaltos de inundação toleíticos continentais do CAMP. O uso da anomalia gravimétrica residual, baseada em modelagem crustal e combinada com dados geológicos prévios, foi eficaz na identificação no registro do CAMP nestas bacias sedimentares da Amazônia. Outrossim, algumas assinaturas gravimétricas correlacionam-se bem com as principais discontinuidades estruturais, particularmente com o Domo Monte Alegre e arcos de Xambioá, Serra Formosa e Vilhena, respectivamente, nas bacias do Amazonas, Parnaíba e Parecis. Esta interpretação fornece uma explicação razoável para a compreensão de lineamentos estruturais sem conotações exclusivamente tectônicas, presumindo uma nova interpretação para o campo gravitacional

relacionado ao contraste de densidade intracrustal ou campo gravimétrico residual para essas bacias. O Gondwana ocidental foi gradualmente soerguido pelos corpos subvulcânicos do magmatismo Penatecaua nas bacias do Amazonas e do Solimões. Em contrapartida, o vulcanismo extrusivo caracteriza o magmatismo Mosquito na bacia do Parnaíba intercalado com sedimentos intertrap. Informações obtidas a partir do mapa da espessura elástica, profundidade da moho e sinal gravimétrico residual indicam uma crosta mais fina na bacia do Parnaíba favorecendo a erupção magmática induzida por um hot spot instalado na borda oeste da bacia. Por outro lado, nas bacias com crosta mais densa e espessa, o magma acumula-se principalmente como soleiras, proporcionando maior resistência à ruptura pelo intumescimento do CAMP. A Bacia do Parnaíba experimentou três pulsos magmáticos em intervalos de aproximadamente 1 milhão de anos, alternando com o desenvolvimento de sistemas eólico-fluvial-lacustres (sedimentos intertrap) durante períodos não magmáticos, indicando curtos intervalos de retomada magmática e resfriamento no CAMP, contrastando com o magmatismo mais longo e contínuo nas bacias do Amazonas e do Solimões, que carecem de depósitos intertraps. Estes resultados são importantes para uma nova disposição da história tectonomagmática, estrutural e estratigráfica destas bacias, pois a partir de um novo contexto ou evolução geológica para a área permitirá uma melhor compreensão das bacias estudadas na interação lava-sedimento, preservadas do Jurássico e relacionado aos eventos CAMP, que precederam a principal ruptura continental no noroeste da Pangeia.

**Palavras-chave:** geologia-Amazônia; camp; modelagem crustal; anomalia gravimétrica; espessura crustal.



## ABSTRACT

Geological studies in conjunction with applications of geophysical techniques are being widely used to highlight and characterize CAMP gravimetric anomalies throughout Northern Brazil, including the Solimões, Parecis, Amazonas and Parnaíba basins. Interpretations of a residual gravimetric anomaly from these basins were used to expand the understanding of the distribution of CAMP throughout the subsurface. This study was carried out through qualitative and quantitative interpretations of gravimetric data, supported by surface geological information, mainly stratigraphic data based on outcrops. From direct gravimetric modeling, based on available crustal gravitational structure models to separate a residual gravity signal from observed gravity data, realistically detailed geological and tectonic features were interpreted, providing useful information for a geophysical interpretation of geological sources. With the residual gravity anomaly, a map of the elastic thickness ( $T_e$ ) of the basins was obtained, using a new procedure, presumably allowing some gaps presented in the current literature on the CAMP to be filled. For each  $T_e$  value, the residual gravimetric signal was calculated, considering the surfaces described by topography and Moho for a regional model with standard density and discretized into prisms. The cross-correlation between the observed gravity signal and calculated gravity signal made it possible to obtain a map of the elastic thickness of the studied areas. The highest correlation value is directly related to the best value of elastic thickness and Moho depth associated with crustal deformation. Our study used a combination of these techniques to presumably define the possible extent of Jurassic magmatism, the basin rheology of igneous body intrusion and history of thermal subsidence that largely controlled depositional control during and after the CAMP. The presence of low gravity values is closely related to the less dense lithological units of the upper crust, while the high gravity values are related to high-density rocks correlated to the continental tholeiitic flood basalts of the CAMP. The use of residual gravity anomaly based on crustal modeling combined with previous geological data was effective in identifying the CAMP record in these Amazonian sedimentary basins. Furthermore, some gravimetric signatures correlate well with the main structural discontinuities, particularly with the Monte Alegre Dome and Xambioá, Serra Formosa and Vilhena arches, respectively, in the Amazon, Parnaíba and Parecis basins. This interpretation provides a reasonable explanation for understanding structural lineaments without exclusively tectonic connotations, assuming a new interpretation for the gravitational field related to intracrustal density contrast or residual gravity field for these basins. Eastern Gondwana was gradually uplifted by subvolcanic bodies of the Penatecaua magmatism in the Amazon and Solimões basins. In contrast, extrusive volcanism characterizes Mosquito

magmatism in the Parnaíba basin interspersed with intertrap sediments. Information obtained from the elastic thickness map, Moho depth and residual gravity signal indicate a thinner crust in the Parnaíba basin favoring the magmatic eruption induced by a hot spot installed on the western edge of the basin. On the other hand, in basins with denser and thicker crust, magma accumulates mainly as sills, providing greater resistance to rupture due to the swelling of the CAMP. The Parnaíba Basin experienced three magmatic pulses at intervals of approximately 1 Myr, alternating with the development of aeolian-fluvial-lacustrine systems (intertrap sediments) during non-magmatic periods, indicating short intervals of magmatic resumption and cooling in the CAMP, contrasting with the longer and continuous magmatism in the Amazon and Solimões basins, which lack intertrap deposits. These results are important for a new disposition of the tectonomagmatic, structural and stratigraphic history for these basins, since from a new context or geological evolution for the area it will allow a better understanding of the studied basins in lava-sediment interaction, preserved from the Jurassic and related to the CAMP events, which preceded the main continental rupture in northwestern Pangea.

**Keywords:** geology-Amazon; camp; forward gravity modeling; gravity anomaly; crustal thickness.

## LISTA DE ILUSTRAÇÕES

### CAPÍTULO 1

- Figura 1- Ocorrências do CAMP no Oeste do Gondwana (adaptado de McHone 2000). A) Distribuição do CAMP nos continentes, principalmente nas áreas estudadas (bacias do Parnaíba, Parecis, Solimões e Amazonas) do Cratón Amazônico. B) Mapa estratigráfico das bacias amazônicas com rochas vulcânicas relacionadas ao CAMP (modificado de Milani & Zalán 1999b, Nogueira *et al.* 2021). Discordâncias generalizadas estão documentadas nas bacias do Solimões, Amazonas, Parecis e Parnaíba com rochas predominantemente subvulcânicas..... 6

### CAPÍTULO 3

- Figura 2- Representação de um modelo Simplificado da Crosta Terrestre composta por fontes da crosta. A) Modelo representativo da crosta. B) Crosta terrestre discretizada em N prismas retangulares 3D. B') Representação detalhada do N-ésimo prisma na discretização pelo algoritmo de Plouff (1976)..... 17
- Figura 3 - Topografia da área de estudo. A) Topografia da Bacia do Parnaíba. B) Topografia da Bacia dos Parecis. C) Topografia das bacias do Amazonas e Solimões..... 18
- Figura 4 - Profundidade da Moho obtida por Uieda & Barbosa. A) Profundidade da Moho da America do Sul, destacando as bacias da área de estudo. B) Profundidade da Moho da Bacia do Parnaíba. C) Profundidade da Moho da Bacia dos Parecis. D) Profundidade da Moho das bacias do Amazonas e Solimões..... 18
- Figura 5 - Calculo do valor de  $T_e$  a partir da correlação cruzada, considerando uma varredura contínua dos dados observados e calculados ao longo de um *grid*..... 22
- Figura 6 - Mapas da Espessura Elástica. A) Espessura elástica da Bacia do Parnaíba. B) Espessura elástica das bacias do Amazonas e Solimões. C) Espessura elástica da Bacia dos Parecis..... 22

Figura 7- Mapa de coeficiente de correlação. A) Coeficiente de correlação da Bacia do Parnaíba. B) Coeficiente de correlação das bacias do Amazonas e Solimões. C) Coeficiente de correlação da Bacia dos Parecis.....	23
--	----

## CAPÍTULO 4

Figure 1 - (A) The CAMP occurrences distributed as dykes, sills and lava flows in a scenario before the opening of the Central Atlantic Ocean and the Pangea break-up during the Permian-Triassic (modified from McHone 2000). (B) Geology of the southern Amazonian Craton and locations of the mapped basalts in the Parecis and Araras-Alto Paraguay Basins (geologic framework based on Santos <i>et al.</i> 2017, Nogueira <i>et al.</i> 2019).....	27
Figure 2 - Lithostratigraphy, paleoenvironments and major geologic events in the Parecis and Araras-Paraguay basins of the southern Amazonian Craton (modified from Nogueira <i>et al.</i> 2019)....	30
Figure 3 - Observed Bouguer gravity anomalies using the WGS84 reference ellipsoid and longitudinal selection grid (-W58.8° to -E54° and -N11.5° to -S15°).....	32
Figure 4 - Residual gravity anomalies showing the gravity highs and lows in southwestern Tocantins Province and southern Tapajós Province. The orange dotted lines represent anomalies with high gravity signatures associated with large basalt volumes in the subsurface and at the surface, contrasting with the low gravity anomalies in the basin. The continuous black lines represent faults and fractures that may provide structural controls on the percolation of magmatic fluids in the basin.....	33
Figure 5 - Geological map showing the location of the CAMP basalts in the southern Amazonian Craton. Note the occurrences of the exposed CAMP basalts and those interpreted from the residual gravity anomalies (dashed and dotted polygons, anomalies 1 and 2).....	35

Figure 6 - Tectonomagmatic evolution of the CAMP in the southern Amazonian Craton. (A) Initial phase before Pangea break-up (c. 250 Ma). (B) Increase in basalt volume due to CAMP intumescence, Pangea break-up and opening of the Central Atlantic Ocean (c. 201-190 Ma). (C) Extensional event related to the opening of the South Atlantic (c. 140-110 Ma) and Equatorial Atlantic (c. 113-95 Ma), as well as the first tectonic event related to the Andean orogeny (c. 88 Ma) that favoured the deposition of Cretaceous sediments in the Parecis Basin (c. 88-72 Ma); (D) Uplift of the southern Amazonian Craton, leading to the erosion of the Cretaceous cover and CAMP basalts and exposing most of the magmatic conduits located in the Araras-Alto Paraguay Basin and basement rocks (c. 72-65 Ma). (Geological framework based on Santos *et al.* 2017, Nogueira *et al.* 2019).....

## CAPÍTULO 5

- Figure 1 - CAMP occurrences in West Gondwana (adapted from McHone, 2000).  
 A) Distribution of the CAMP on the continents, mainly in the studied areas (Parnaíba, Solimões, and Amazonas basins) of the Amazon Cratón.  
 B) Stratigraphic map of Amazon basins with volcanic rocks related to the CAMP (modified from Milani and Zalán 1999, Nogueira *et al.* 2021).  
 Widespread unconformities are documented in the Solimões, Amazonas, Parecis, and Parnaíba basins with predominantly subvolcanic rocks..... 43
- Figure 2 - Layout of the methodology for obtaining the residual gravity signal.  
 (a) Observed gravity signal. (b) Predicted gravity regional signal from the discretization of the prismatic model. (c) Residual gravity Signal..... 49
- Figure 3 - The CAMP basalts in Amazônia. A) Dike cutting organic matter-rich shale. B) and C), stratified sandstone and siltstone intruded by sill in Monte Alegre Dome. D) Contact of sill and eolian deposits. E) Spheroidal weathering. F) Feldspar phenocrystals in gabbroic texture from the central portion of the volcanic body. A-C, Penatecaua Formation, D-F, Mosquito Formation..... 52
- Figure 4 - Stratigraphic sections of the Jurassic- lower Cretaceous succession. The locations of the sections are shown in Fig. 1 of the Stratigraphic chart of the study area and a composite section of the Mosquito Formation. Modified from Ballén *et al.* (2013) and Nogueira *et al.* (2021)..... 53
- Figure 5 Depositional model of the upper portion of the Jurassic Mosquito Formation. Wet desert settings were developed concomitantly with fluvial channels incised into the basaltic substrate. The volcanic plain was successively filled by fluvial-eolian-lacustrine deposits. The 1-IZ-2-MA profile of Rezende (2002) depicts sandstone intercalations in both the base and upper portion of the Mosquito Formation overlying the eolian deposits from the Sambaíba Formation..... 54

Figure 6 - Residual gravity anomaly showing the gravimetric highs and lows of the Parnaíba, Amazonas, and Solimões basins..... 56

Figure 7 - (A) Residual anomaly map of the Paraíba Basin, which show geologic structures coincident with the distribution of the CAMP magmatic bodies. (B) Graph that show the behavior of the residual signal in a specific area, represented by the solid black line with an eastern and western direction. This delimited area shows the behavior of the gravimetric signal between the gravimetric highs and lows, suggesting that the main structural lineament trends into of this basin, such as Transbrasiliano and Pedro II, have different orientation compared with the Xambioá Arch, predominantly E-W directed, coinciding with crustal fracturing trend related to the Mesozoic magmatism of CAMP and Paraná-Entedeka..... 57

Figure 8 - (A) Residual gravimetric anomaly of the Parecis Basin, which show geologic structures (The Vilhena and Serra Formosa arcs, profile 1 and 2 respectively) coincident with the distribution of the CAMP magmatic bodies. (B) Graph that show the behavior of the residual signal in a specific area, represented by the solid black line with a South/North direction. Graph that show the behavior of the residual signal in a specific area, represented by the solid pink line with a northwest/southeast direction..... 58

Figure 9 - The Monte Alegre Dome in Amazonas Basin. The dome's origin has been attributed to magmatic intrusions or tectonic deformation. The geologic map and section were based on Pastana (1999) and Figueira *et al.* (2012)..... 60

Figure 10 - Correlation between geophysical and geological data from the Parnaíba Basin based on previous works. (A) Tectonic sketch of the structural framework of the Parnaíba Basin (modified from Cordani et al. 1984, De Castro et al. 2014, 2016, Chamani 2015). (B) Map of magnetic anomalies of the deep magnetic field (adapted from Mocitaiba *et al.* 2017). The dashed rectangle points to an area interpreted as a magnetic signal resulting from a structural source. However, this signal coincides with Mesozoic magmatism, thus requiring new processing and interpretation of the data. (C) Map of the location of the study areas in the Parnaíba Basin, highlighting the main lineaments (modified from Schobbenhaus et al. 1984, Santos and Carvalho 2004). (D) Morphostructural context of the central-western portion of the Parnaíba Basin (area of the red square indicated in A based on the analysis of images from SRTM-90 sensors ( Modified from Abrantes Jr 2016). (E) Main relief lineaments with the mountains oriented approximately E-W coinciding with the Xambioá Arch (amphiclisis; Modified from Abrantes Jr 2016). Thicker lines represent confirmed and probable failures (Modified de Abrantes Jr 2016). The N-S cross-section is based on field data. The area indicated in blue represents the zone of occurrence of Paraná-Etendeká magmatism with occurrences further east of this area.....

62

Figure 11 - (A) Residual gravimetric anomaly of the Amazonas e Solimoes Basins, which show geologic structures (Monte alegre Domo, profile 2) coincident with the distribution of the CAMP magmatic bodies. (B) Graph that show the behavior of the residual signal in a specific area, represented by the solid black line with. Graph that show the behavior of the residual signal in a specific area, represented by the solid pink line. By analyzing the residual gravity anomaly of the Amazon Basin with the available geological data, the location of the Monte Alegre Dome is observed (at the peak of the profile 2 at around -55 degrees longitude and 40 mgal), which presents a positive gravity signature at the top, similar to the



positive signature of the CAMP diabase.....	63
Figure 12 - (A) Moho depth map of the Parnaíba Basin (Uieda and Barbosa 2016). (B) Elastic thickness map of the Parnaíba Basin. (C) Moho depth graph generated from a point area on the map in A (solid black line). (D) Elastic thickness graph generated from a point area on the map in B (solid black line). It is noted that the elastic thickness increases from westen to easten, while the depth of the Moho is occasionally greater in the areas where the CAMP occurs (westen edge). ....	65
Figure 13 - (A) Moho depth map of the Solimoes and Amazonas basins (Uieda and Barbosa 2016). (B) Elastic thickness map of the Solimoes and Amazonas basins. (C) Moho depth graph generated from two profiles on the map in A (pink and black lines). It is noted that the elastic thickness decreases from westen to easten. (D) Elastic thickness graph generated from two profiles on the map in B (pink and black lines).....	66
Figure 14 - Representation of crust thickness model 2D of the Amazonas, Solimões, and Parnaíba basins based on interpretations geophysical and geological data.....	67
Figure 15 - CAMP Evolution in the Amazon Basins. 1) Previously the main continental break up in Northwestern Pangea the magma accumulation in a deep-seated basaltic chamber may have caused an infra-crust inflate uplifting the region. 2) Due to the thinner crust (elasticity) occurred concentration of the fissure eruptions in the western Parnaíba Basin that allowed the formation of a mantellic plume or hot spot, afterward causing eruption dykes induced by the magma injection pressure. 3) Migration of the CAMP mantle plume of the Parnaíba basin, due to the closure of the CAMP, to the Solimoes and Amazonas basins, allowing increased swelling of the CAMP diabbases and continued uplift of these basins until the Middle Jurassic. 4A) previously, the fissure-controlled lava flow event, developed a volcanic substrate in a dry desert setting (Sambaiba	

Formation). 4B) After a long time of exposure, and weathering of volcanic plain, ephemeral fluvial channels transported basaltic intraclasts that accumulated in depressions and shallow lakes, whereas eolian dunes migrate on the volcanic substrate. 4C) new magmatic pulse with basalts sandwiching the intertrap sands, causing local compaction the eruption climax is associated with the thickest basalt body. 4D) again the implantation of ephemeral fluvial channels incised in volcanic substrate, producing several basaltic intraclasts, and concentrated on depressions that were filled by coarse grains, and fine grains transported toward shallow lakes. 4E) The last magmatic pulse with basalts sandwiched the underlaid intertrap sands. 4F) After the definitive end of the CAMP magmatic pulses, fluvial channels related to the wet desertic system of the Upper Jurassic-Early Cretaceous Corda Formation reworked both volcanic plains and intertrap deposits, producing an unconformity..... 72

Figure 16 - Paleoenvironmental Reconstruction of the Upper Jurassic and Lower Cretaceous Successions of the Parnaíba Basin and its relationship with West Africa and Solimões and Amazonas basins in the Post- CAMP. Lakes characterized the eastern portion of the basin with deltaic deposits and distal turbidites. The region of the Solimões and Amazon basins, mainly the Amazon Basin, functioned as the main source area for river channels coming from higher areas to the west due to the uplift caused by the CAMP..... 75

## SUMÁRIO

<b>DEDICATÓRIA</b> .....	iv
<b>AGRADECIMENTO</b> .....	v
<b>EPIGRAFE</b> .....	vi
<b>RESUMO</b> .....	vii
<b>ABSTRACT</b> .....	ix
<b>LISTA DE ILUSTRAÇÕES</b> .....	xi
<b>CAPÍTULO 1 INTRODUÇÃO</b> .....	1
1.1 ORGANIZAÇÃO DA TESE.....	1
1.2 APRESENTAÇÃO.....	1
1.3 JUSTIFICATIVA.....	4
1.4 OBJETIVOS DO TRABALHO.....	5
<b>CAPÍTULO 2 CONTEXTO GEOLÓGICO</b> .....	7
2.1 LOCALIZAÇÃO DA ÁREA DE ESTUDO.....	7
<b>2.1.1 Bacia do Parnaíba</b> .....	7
<b>2.1.2 Bacia dos Parecis</b> .....	8
<b>2.1.3 Bacia do Amazonas</b> .....	9
<b>2.1.4 Bacia dos Solimões</b> .....	10
2.2 MAGMATISMO DO CAMP NAS BACIAS ESTUDADAS.....	11
<b>CAPÍTULO 3 MATERIAIS E MÉTODOS</b> .....	16
3.1 PESQUISA BIBLIOGRÁFICA.....	16
3.2 OBTENÇÃO DE DADOS GRAVIMÉTRICOS.....	16
<b>3.2.1 Problema Direto: Modelagem Crustal</b> .....	16
3.2.1.1 Solução Analítica do cálculo da anomalia regional por discretização de prismas.....	19
<b>3.2.3 Cálculo da Espessura Elástica (Te) das Bacias</b> .....	20
3.2.3.1 Cálculo da profundidade Moho a partir da deflexão .....	20
3.2.3.2 Mapeamento da espessura elástica por meio da correlação cruzada.....	21
<b>CAPÍTULO 4 ARTIGO PUBLICADO NO JOURNAL OF SOUTH AMERICAN EARTH SCIENCES</b> .....	25
4.1 INTRODUCTION.....	24
4.2 GEOLOGICAL SETTING.....	28
<b>4.2.1 Mapped and unmapped CAMP records in the southern Amazonian Craton</b> .....	29
4.3 GEOPHYSICAL DATA.....	31
<b>4.3.1 Bouguer anomaly</b> .....	31
<b>4.3.2 Residual gravity anomaly</b> .....	32
4.4 RESULT AND DISCUSSION.....	34

<b>4.4.1 Association of the CAMP continental tholeiitic flood basalts (CTFB) from gravity and geological interpretations.....</b>	<b>34</b>
<b>4.4.2 Tectonomagmatic evolution from residual gravimetric anomalies and geological data interpretations.....</b>	<b>35</b>
4.5 FINAL REMARKS .....	37
Acknowledgement.....	37
<b>CAPÍTULO 5 THE CRUSTAL ELASTICITY AND GRAVIMETRIC DATA IN THE STRATIGRAPHIC EVALUATION OF THE JURASSIC CAMP SUCCESSION IN THE SOLIMÕES, AMAZONAS E PARNAÍBA BASINS, NORTHERN BRAZI.....</b>	<b>38</b>
5.1 INTRODUCTION.....	40
5.2 GEOLOGICAL SETTING.....	44
<b>5.2.1 The Solimões e Amazonas basins.....</b>	<b>44</b>
<b>5.2.2 The Parnaíba Basin.....</b>	<b>46</b>
5.3 METHODOLOGY.....	48
<b>5.3.1 Determination of the Residual anomaly .....</b>	<b>48</b>
5.3.1.1 Forward Gravity Problem from elementary prism.....	49
<b>5.3.2 Elastic thickness determination .....</b>	<b>50</b>
5.3.2.1 Moho depth calculation from deflection.....	50
5.3.2.2 Mapping elastic thickness to effects of correlation.....	49
5.4 RESULTS.....	51
<b>5.4.1 The jurassic succession in Amazon Basins.....</b>	<b>51</b>
<b>5.4.2 Residual anomalies X Camp signatures.....</b>	<b>54</b>
5.4.2.1 Geological structures.....	55
5.5 INTERPRATATION.....	64
<b>5.5.1 Correlation between elastic thickness and CAMP rheology.....</b>	<b>64</b>
<b>5.5.2 Plume establishment X crustal elasticity .....</b>	<b>67</b>
<b>5.5.3 Magmatic pulse time estimation.....</b>	<b>69</b>
<b>5.5.4 Post-Camp Scenario.....</b>	<b>73</b>
5.6 CONCLUSION.....	76
<b>CAPÍTULO 6 CONSIDERAÇÕES FINAIS.....</b>	<b>78</b>
<b>REFERÊNCIAS .....</b>	<b>80</b>

## CAPÍTULO 1 INTRODUÇÃO

### 1.1 ORGANIZAÇÃO DA TESE

A presente tese está organizada em 6 itens principais. O item um apresenta a proposta dessa pesquisa com suas respectivas justificativas e objetivos. No item dois é contextualizado a geologia das bacias dos Parecis, Parnaíba, Amazonas e Solimões com ênfase nos eventos magmáticos relacionados ao contexto do CAMP. No item três apresenta os materiais e as metodologias utilizadas. O item quatro apresenta os resultados sobre a Bacia dos Parecis, em um artigo publicado, que já alcança metade do objetivo da conclusão da tese de doutorado. O item cinco apresenta novos dados da área de estudo, a partir da utilização de métodos geofísicos e interpretações geológicas, ressaltando os principais temas abordados em um segundo artigo da tese já submetido. Por fim, o item seis será apresentado as considerações finais da tese, enfatizando lacunas para futuros trabalhos.

### 1.2 APRESENTAÇÃO

O período de transição do Triássico ao Jurássico-Eocretáceo (~248 a 100 Ma) representa um dos intervalos sedimentares mais intrigantes na história evolutiva das bacias sedimentares do Norte do Brasil. Este período foi marcado pela fragmentação do supercontinente Pangeia e abertura do Oceano Atlântico Norte, Equatorial e Sul, registrados principalmente na porção ocidental deste supercontinente, envolvendo intenso vulcanismo que ocorreu antes, durante ou após o rifteamento do Oceano Atlântico (Teisserene & Villmin 1989, Condie 2004, Cunha *et al.* 2007, Kearey *et al.* 2009, Vaz *et al.* 2007). Enquanto a zona de fragmentação dos Pangea na África ocidental, leste da América do Norte e Europa foi coincidente com a direção da paleosutura relacionada à orogênese Aleghaniana-Herciniana do Paleozóico Superior (Manspeizer 1988, Piqué & Laville 1996, Withjack *et al.* 1998), na América do Sul, a propagação deste *rifte* atingiu o Cráton Amazônico e as bacias sedimentares adjacentes, tais como as bacias do Solimões, Amazonas, Parnaíba e Parecis (Baski & Arckhibald 1997, Marzoli *et al.* 1999, Hameset *al.* 2000, Marzoli *et al.* 2004, Klöcking *et al.* 2018). Enquanto a história de abertura do Oceano Atlântico inclui a separação do Gondwana, a formação do atual *rift* intercontinental oceânico e da Cadeia Mesoatlântica, todas estas bem documentadas (Zalán 1991, Milani & Zalán 1999, Zalán 2004), os eventos pré-ruptura ainda são pouco registrados. O intenso vulcanismo pré-ruptura e sua interação com a sedimentação continental desenvolvida no Oeste do Gondwana é a chave para desvendar a história inicial de separação do Pangeia.

A primeira quebra do Pangeia está relacionada a abertura do Oceano Atlântico Central (ca. 190 Ma) que foi concomitante com a instalação de extensas províncias ígneas (Large Igneous Province-LIPs), como a Província Magmática do Atlântico Central ou CAMP (Marzoli *et al.* 1999). O CAMP compreende vários pulsos de atividade vulcânica ocorridos em torno de 200 e 202 Ma na forma de diques, soleiras e fluxo de lavas ou sequências piroclásticas que se infiltraram em depósitos sedimentares, estendendo-se por cerca de 11 milhões de km<sup>2</sup> com volume total estimado de magma de 3 milhões de km<sup>3</sup> (Marzoli *et al.* 2018) (Figuras 1A e B). O evento do CAMP abrange bacias de *riftes* da América do Norte Oriental e Marrocos, onde está bem exposto e tem sido intensamente estudado (Hames *et al.* 2000, McHone & Puffer 2003, Knight *et al.* 2004, McHone 2006, Verati *et al.* 2007, Jourdan *et al.* 2009, Bensalah *et al.* 2011, Schaller *et al.* 2012, Marzoli *et al.* 2018, Korte *et al.* 2019). Remanescentes do CAMP são encontrados em quatro continentes (leste da América do Norte, África Ocidental, Europa e algumas regiões da América do Sul) e consistem principalmente de basaltos toleíticos continentais colocados como fluxos subaéreos e corpos intrusivos. O registro da CAMP nas bacias estudadas é representado pelo Magmatismo Penatecaua do Jurássico Inferior, nas bacias do Solimões e Amazonas (190 ± 20Ma); pela Formação Mosquito do Jurássico Inferior (199,7 ± 2,45 Ma) na Bacia do Parnaíba e pelas formações Anarí e Tapirapuã do Jurássico Inferior (197-200 ± 6 Ma) na Bacia dos Parecis. Os basaltos da Formação Serra Geral da Bacia do Paraná, não fazem parte da CAMP, sendo relacionados à fase tardia do Oeste Gondwana e abertura do Atlântico Sul, por volta de 134 - 137 Ma (Renne *et al.* 1992, Melfi *et al.* 1988, Rocha-Campos *et al.* 1998, Vaz *et al.* 2007, Merle *et al.* 2011, Abrantes Jr 2016, Svensen *et al.* 2018).

O intumescimento crustal causado pela colocação de corpos subvulcânicos ligados a CAMP nas bacias da Amazônia Ocidental causou o soerguimento e o desenvolvimento de discordâncias regionais. Por outro lado, na Amazônia Oriental, particularmente na porção Oeste da Bacia do Parnaíba, a CAMP foi registrada por erupções vulcânicas da Formação Mosquito de caráter fissural intercaladas com depósitos siliciclásticos continentais ou sedimentos intertrap (Northfleet & Melo 1967, Rezende 2002, Beutel *et al.* 2005; Vaz *et al.* 2007, Ballén *et al.* 2013, Nogueira *et al.* 2021) (Fig. 1). O evento sedimentar pós-CAMP é representado pela instalação de um sistema eólico-fluvial e lacustre de clima úmido registrado nas formações Corda e Pastos Bons do Eo-Cretáceo (Rabelo & Nogueira 2015, Rabelo *et al.* 2019; Cardoso *et al.* 2019, Nogueira *et al.* 2021).

A combinação de dados geológicos prévios (Montes-Lauar *et al.* 1994, Barros *et al.* 2006, Oliveira *et al.* 2018, Marzoli *et al.* 2018, Heilbron *et al.* 2018, Nogueira *et al.* 2021), associados

com análise do campo gravimétrico das bacias estudadas, obtidas pela separação regional/residual por meio da modelagem crustal (Rbeiro-Filho 2018, Ghomsi 2021, 2022), revelaram anomalias que indicam a ocorrência de valores positivos de gravidade associados a rochas de grande densidade em subsuperfície. Esta correlação dos dados geofísicos com mapas geológicos disponíveis (Bahia *et al.* 2007, Mocitaiba *et al.* 2017, Soares *et al.* 2018, Moreira 2019), sugere que os corpos de basaltos jurássicos atribuídos a CAMP aflorantes nas bacias dos Parecis, Parnaíba, Amazonas e Solimões de idades fanerozóica, projetam-se para o interior destas em subsuperfície. A aplicação avançada de técnicas geofísicas (Wienecke 2007, Ribeiro filho *et al.* 2023) permitiu obter a avaliação da elasticidade da crosta, definindo a possível extensão deste magmatismo, a reologia da bacia em acomodar corpos ígneos, e a história de subsidência térmica que controlou em grande parte a assinatura deposicional durante e depois do CAMP. Secundariamente, é discutida a origem das principais estruturas geradas durante as diversas fases de desenvolvimento destas bacias do Pré-cambriano ao Fanerozóico, tais como arcos estruturais, sistemas de falhas e Domos estruturais influenciadas ou reativadas durante a colocação do CAMP no Mesozóico. Finalmente, desvendar a influência do CAMP nas bacias amazônicas fornecerá *insights* sobre o cenário inicial que levou à separação da Pangéia, que será apresentada neste trabalho, fornecendo uma nova abordagem de detecção de corpos ígneos não-aflorantes e permitindo identificar novos locais deste evento magmático, fornecendo um melhor entendimento da história geológica da região.

### 1.3 JUSTIFICATIVA

As bacias do Amazonas, Solimões, Parecis e do Parnaíba fazem parte de um conjunto de sinéclises intracratônicas paleozoicas da América do Sul. Suas histórias deposicionais abrangem o tempo Siluriano ao Cenozoico e são normalmente associadas aos eventos estensionais em domínio de intraplacas, ocorridos em diversas regiões cratônicas pelo mundo, tais como as bacias de Williston e Illinois no Norte América, as bacias do Congo e Taoudeni na África e a Bacia Siberiana na Rússia (cf. Condie 2004, Kearey *et al.* 2009, Allen & Allen 2013). Todas estas bacias representam extensões tectônicas no supercontinente Gondwana após a Orogenia Brasileira/Pan-Africana no final do Neoproterozóico e o início do Paleozóico (Soares *et al.* 2018).

Rifts continentais que não evoluem para crosta oceânica se tornam rifts abortados, configurando ambientes tectônicos oportunos para o desenvolvimento de bacias intracratônicas. Os processos de subsidência em áreas cratônicas são gerados por variações na direção da deformação na litosfera, geralmente, relacionados aos eventos orogênicos em cinturões

vizinhos (Zálan 1991, Almeida 2000). A subsidência ocorre quando a rigidez litosférica é atenuada, permitindo massa descompensada na crosta superior, relacionada aos remanescentes dos rifts abortados, para diminuir em uma grande região, devido à reativação de estruturas crustais antigas. No entanto, durante os períodos de atividades de não-orogenicidade, ocorre o enrijecimento da litosfera e uma interrupção concomitante no processo de equilíbrio isostático (Zálan 1991, Almeida 2000, Soares *et al.* 2018).

A estrutura mais profunda dessas bacias, até agora, tem sido principalmente inferida a partir de dados geológicos (por exemplo, Cordani *et al.* 1984, Montes Lauer *et al.* 1994, Bahia 2006, Bahia 2007, Barros *et al.* 2007, Davies *et al.* 2017, Korte *et al.* 2019, Nogueira *et al.* 2021), assim como dados geofísicos ainda pouco estudados (Feng *et al.* 2004, Bahia *et al.* 2007, Assumpção *et al.* 2013a, Assumpção *et al.* 2013b, Daly *et al.* 2014, Uieda & Barbosa 2016, Trosdorf *et al.* 2018, Heilbron *et al.* 2018, Soares *et al.* 2018 Rezende *et al.* 2021). Tanto a estrutura e a gênese, quanto a análise de dados geofísicos ainda são objetos de alguma controvérsia e debate nessas bacias atualmente. Desvendar a influência do CAMP nessas bacias fornecerá subsídios para o entendimento deste evento nas bacias aqui estudadas. Este estudo poderá abrir uma janela de oportunidade para o entendimento da evolução geológica desta parte da Plataforma Sul-Americana, contribuindo para o detalhamento dos eventos de soerguimento e subsidência térmica que controlaram em grande parte os eventos deposicionais durante e após o CAMP.

#### 1.4 OBJETIVOS DO TRABALHO

O objetivo geral deste trabalho é caracterizar a influência do CAMP na evolução paleoambiental, estratigráfica, deposicional e tectônica das bacias intracratônicas aqui estudadas. Tendo como objetivos específicos:

1. Inferir o volume de magma associado ao CAMP nas bacias sedimentares dos Parecis, Amazonas, Solimões e Parnaíba;
2. Presumir a relação da extensão do CAMP em superfície e subsuperfície;
3. Entender a influência do CAMP em termos de soerguimento e subsidência e sua implicação na evolução deposicional das unidades sedimentares (formações Mosquito, Tapirapuã, Corda e Pastos Bons) durante e após o evento magmático;



4. Verificar se existe relação entre os trends estruturais e os principais lineamentos das bacias com a orientação dos corpos magmáticos mesozoico, utilizando como elemento principal o Arco de Xambioá, na Bacia do Parnaíba, os Arcos de Serra Formosa e Vilhena, na Bacia dos Parecis e Domo de Monte Alegre, na Bacia do Amazonas. Esta relação avaliará se a estruturação serviu também para alojar os corpos magmáticos do evento Paraná-Etendeká;
5. Tecer considerações geotectônicas, Tectonomagmáticas, estruturais e estratigráficas, utilizando informações disponíveis sobre o modo de colocação dos corpos magmáticos (por exemplo: Formação Mosquito predominantemente extrusiva e Formação Penetecaua exclusivamente subvulcânica).

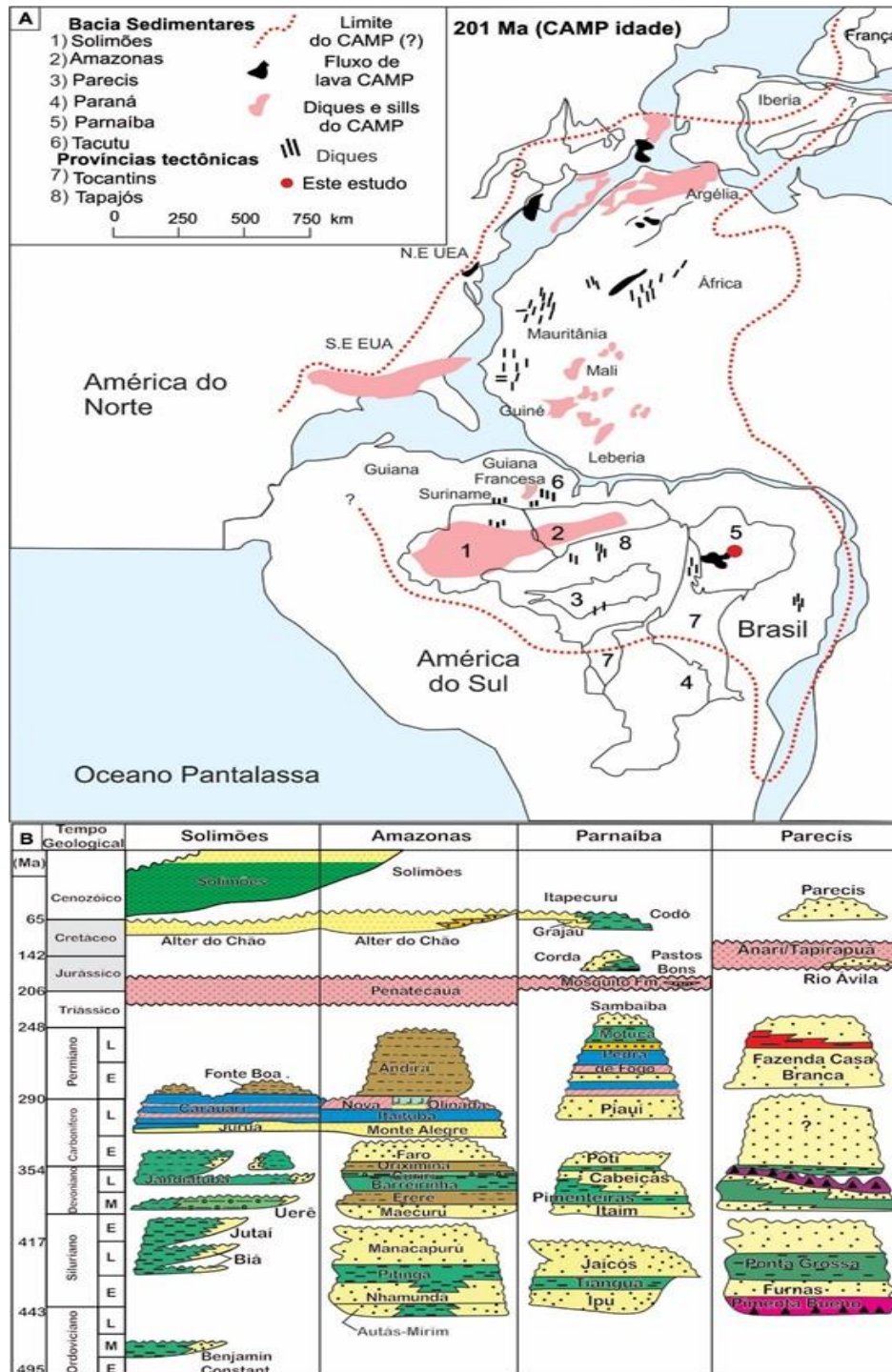


Figura 1 - Ocorrências do CAMP no Oeste do Gondwana (adaptado de McHone 2000). A) Distribuição do CAMP nos continentes, principalmente, nas áreas estudadas (bacias do Parnaíba, Parecis, Solimões e Amazonas) do Cratón Amazônico. B) Mapa estratigráfico das bacias amazônicas com rochas vulcânicas relacionadas ao CAMP (modificado de Milani & Zalán 1999, Nogueira *et al.* 2021). Discordâncias generalizadas estão documentadas nas bacias do Solimões, Amazonas, Parecis e Parnaíba com rochas predominantemente subvulcânicas.

## CAPÍTULO 2 CONTEXTO GEOLÓGICO

### 2.1 LOCALIZAÇÃO DA ÁREA DE ESTUDO

#### 2.1.1 Bacia do Parnaíba

A Bacia do Parnaíba está localizada na porção norte da Plataforma Sul-Americana e pode ser classificada como uma bacia intracratônica que se estende por uma área superior a 600.000 km<sup>2</sup> (Fig. 1A). O preenchimento sedimentar atinge uma espessura máxima de 3.500 m e é composto principalmente por sedimentos paleozoicos e, em menor quantidade, derrames vulcânicos (Milani & Thomaz Filho 2000, Cordani *et al.* 2003, Brito Neves *et al.* 2004) (Fig. 1B). A subsidência térmica ocorreu em uma extensa área intracratônica composta por rochas ígneas e metamórficas do Arqueano ao Neoproterozóico, limitada por arcos estruturais e cinturões móveis de alto grau retrabalhados durante a tectônica Pan-Afro-Brasileiro (Cordani *et al.* 2003, Almeida & Carneiro 2004). A fase cratônica da bacia foi marcada por extensa sedimentação em ciclos regionais transgressivos-regressivos organizados em supersequências (Vaz *et al.* 2007). Os estresses extensionais antecederam a abertura do Oceano Atlântico por meio da reativação de falhas do embasamento, que também representaram os principais condutos de colocação magmática derivados do manto nas bacias (Mizusaki *et al.* 1998, Milani & Thomaz Filho 2000).

O depocentro inicial da bacia do Paleozóico Inferior deslocou-se para a parte central do domínio da bacia durante o período Carbonífero-Jurássico Inferior e migrou, novamente, para noroeste no Cretáceo (Vaz *et al.* 2007), sugerindo uma relação temporal com o magmatismo Mosquito e Sardinha, respectivamente. O domínio da bacia era inicialmente mais amplo do que é hoje, com ligação com as bacias do Amazonas e Paraná e, possivelmente, até com a bacia do Congo na África (Melo 1988).

Atualmente, a Bacia do Parnaíba apresenta um contato de falha acentuada com a Província do Tocantins (Faixa Araguaia) a oeste (Daly *et al.* 2014), um contato tectônico/erosivo com a Província do Tocantins ao sul e um contato sedimentar suave ao norte com o Cráton São Luís e com o Cráton São Francisco a sudeste. Na borda leste, o limite da bacia com o bloco Borborema é erosivo com os sedimentos basais do Siluriano da bacia sendo expostos. O embasamento da Bacia do Parnaíba é constituído por uma colagem de pelo menos três domínios principais, classificados como blocos Amazônia, Parnaíba e Borborema, que são marcados por fortes contatos entre eles (Daly *et al.* 2014, Castro *et al.* 2014, Soares *et al.* 2018).

### 2.1.2 Bacia dos Parecis

A Bacia dos Parecis paleozoica, abrangendo os estados de Mato Grosso e a porções leste do estado de Rondônia, centro-oeste do Brasil, e uma Bacia Intracratônica pré-cambriana-paleozoica (Siqueira 1989, Nogueira & Riccomini 2006, Bahia *et al.* 2006, Bahia 2007, Bahia *et al.* 2007, Nogueira *et al.* 2019; Fig.1). A sucessão de capa carbonática do sudoeste do Cráton Amazônico ocorre em duas localidades na borda sul do Graben Pimenta Bueno, no município homônimo, e na borda sul do graben Colorado, próximo ao município de Chupinguaia. A sucessão de capa carbonática é associada à Formação Espigão d'Oeste e faz contato com os diamictitos da Formação Cacoal (Gaia *et al.* 2017, Afonso & Nogueira 2018, Nogueira *et al.* 2019).

O embasamento da Bacia dos Parecis é composto por rochas intrusivas e metamórficas de baixo grau do Cráton Amazônico (Bahia *et al.* 2006, Bahia 2007). Na porção oeste da bacia, ocorrem os granulitos do Complexo Jamarí. Nos estados de Mato Grosso e Goiás, regiões Norte e Sul da bacia, ocorrem os gnaisses, migmatitos e granitóides de idade arqueana/mesoproterozoica do Complexo Xingu, assim como, rochas metassedimentares. Relacionado ao Mesoproterozoico, intrusões básica e ultrabásica estão presentes nesta bacia (Bahia *et al.* 2007; Fig. 1A). A evolução da Bacia dos Parecis ocorreu em duas fases distintas (Pedreira & Bahia 2004), tais como: 1) fase de tafrogênese; e 2) fase de sinéclise. A primeira fase, corresponde a formação dos Grabens Pimenta Bueno e Colorado, cuja evolução é associável à implementação desta Bacia intracratônica do tipo *rift-sag* e um evento extensional seguindo o término do supercontinente Rodínia (~1.0 - 0.75 Ga). Nesta fase, ocorre a deposição de conglomerados em sistemas de leques aluviais, glaciais, fluviais e marinhos costeiros. A fase de sinéclise, corresponderia ao desenvolvimento da bacia em decorrência da subsidência térmica. Durante esta etapa, teria ocorrido o magmatismo básico continental e implementação de sistemas deposicionais eólicos e fluviais em um contexto de bacia intracratônica (Cordani *et al.* 2000, Pedreira & Bahia 2000, Siqueira & Teixeira 1993; Fig. 1B).

Incluindo sedimentos paleozoicos, mesozoicos e cenozoicos, além de rochas intrusivas básicas e ultrabásicas de idade Cretácea, a Bacia dos Parecis é caracterizado por um preenchimento sedimentar-magmático alcançando espessura superior a 6.000 m (Siqueira 1989, Siqueira & Teixeira 1993, Bahia *et al.* 2006, Bahia 2007; Fig. 1B). O arcabouço estratigráfico da Bacia dos Parecis é subdividido em seis supersequências, tais como: Ordoviciano, Devoniano, Carbonífero-Permiano, Jurássico, Juro-cretáceo e Cretáceo (Siqueira 1989, Siqueira & Teixeira 1993, Bahia & Pedreira 1996, Bahia 2007; Fig.1B).

### 2.1.3 Bacia do Amazonas

A Bacia do Amazonas localiza-se na região Norte do Brasil, englobando os estados do Amazonas e Pará. A bacia está limitada ao norte pelo Escudo das Guianas, ao sul pelo Cráton do Guaporé, a leste pelo arco de Gurupá e a oeste pelo Arco de Purus (Fig. 1A). Possui uma área de 500.000 km<sup>2</sup> e um preenchimento sedimentar máximo de até 6000 m de espessura em seu depocentro. Seu formato é alongado e estreito de direção WSW-ENE (Cunha *et al.* 1994, Costa 2001, Zálán 1991, 2004, Cunha *et al.* 2007). A gênese da bacia está ligada aos processos distensivos, oriundos do fechamento do Ciclo Brasileiro (Cunha *et al.* 1994). Estes esforços estariam associados a uma zona de alívio desenvolvida a partir da Faixa Móvel Araguaia-Tocantins e corresponderia ao *rift* precursor da Bacia do Amazonas, tendo se propagado de Leste para Oeste devido à reativação de zonas de fraquezas pré-cambrianas (Wanderley Filho 1991, Mizusaki & Wanderley Filho 1992). Após o evento distensivo ocorreu o resfriamento magmático, gerando subsidência termal e o posterior estabelecimento de uma sinéclise intracontinental (Cunha *et al.* 1994, Zálán 1991, 2004, Cunha *et al.* 2007).

A geração do *rift* inicial da bacia foi sucedida pela acumulação de unidades sedimentares e vulcano-sedimentares no final do Ciclo Brasileiro (700 a 470 Ma), com idades neoproterozoicas (Almeida & Hasui 1984). Estas unidades afloram contiguamente ao longo do Arco de Purus e são representadas pelos arenitos fluviais da Formação Prosperança e carbonatos de planície de maré da Formação Acari, ambas estão inseridas no Grupo Purus (Cunha *et al.* 2007). As unidades litoestratigráficas da Bacia do Amazonas foram reavaliadas seguindo os conceitos da estratigrafia de seqüências, e foram agrupadas em duas megasseqüências de primeira ordem, a Paleozoica e a Mesozoica-Cenozoica (Cunha *et al.* 2007, Matsuda *et al.* 2009). A megasseqüência paleozoica é dividida em quatro seqüências de segunda ordem: ordovício-devoniana, devono-tournasiana, neoviseana e pensilvaniana-permiana.

Os processos tectônicos que resultaram na abertura do Oceano Atlântico e a consolidação da zona de subducção andina promoveram também a reativação de estruturas tectônicas pretéritas, de direções ENE-WSW e WNW-ESE, chamado de Diastrofismo Juruá (Zálán 2004). Em seguida ao Diastrofismo Juruá um relaxamento tectônico estabeleceu-se, gerando uma zona de subsidência para a acumulação da megasseqüência Mesozoica-Cenozoica, constituída pelas seqüências cretácea e terciária que constituem o Grupo Javari, representado pelas formações Alter do Chão (composta de conglomerados, arenitos, argilitos, siltitos e folhelhos) e Solimões (composição arenosa e pelítica). Durante o Cretáceo houve o estabelecimento de um sistema fluvial que corria de leste para oeste, porém devido ao

soerguimento andino ocorrido no limite Cretáceo/Terciário os rios cretáceos transformaram-se em lagos rasos de água doce, contendo restos vegetais e conchas de moluscos (Nogueira 2008). Após o completo desenvolvimento dos Andes durante o Mioceno, a Bacia do Amazonas passou a ser suprida pelos sedimentos oriundos desta cadeia de montanhas e o fluxo passou a correr para leste em direção ao Oceano Atlântico (Nogueira *et al.* 2013).

#### **2.1.4 Bacia dos Solimões**

A Bacia do Solimões apresenta orientação leste-oeste, localizada a oeste da Amazônia Central, entre os escudos das Guianas e do Brasil (Wanderley-Filho *et al.* 2009). É separada das bacias do Acre e Pastaza/Marañon a leste, pelo Arco de Iquitos, e da bacia do Amazonas a leste, pelo Arco Purus (Fig. 1A). O registro sedimentar da Bacia do Solimões é marcado por múltiplas mudanças climáticas, regressão marinha e transgressão durante o Paleozóico e atividades tectônicas que promovem subsidência e soerguimento de arcos estruturais (Caputo & Silva 1991; Fig.1B).

A sequência paleozóica na bacia do Solimões é dividida em duas sub-bacias pelo Arco Caruari, controlando a distribuição e espessura das sucessões sedimentares, principalmente anteriores à época pensilvaniana. Contudo, o arco Caruari parece ter influenciado a deposição do Cretáceo e do Neógeno, representadas respectivamente pelas formações Alter do Chão e Solimões, ambas unidades separadas por uma discordância regional (Eiras *et al.* 1994). A Formação Alter do Chão do Cretáceo corresponde a um sistema fluvial de alta energia de migração para oeste desenvolvido sob um clima úmido que se estende desde a Bacia do Amazonas até as bacias subandinas (Caputo 1984; Fig. 1B). A história tectônica neogênica da Bacia do Solimões e de outras bacias do Norte da América do Sul foi marcada pelo soerguimento do nordeste dos Andes com o desenvolvimento do cinturão de dobras subandino, produto de reajustes das placas tectônicas (Hoorn *et al.* 1995).

A propagação oriental da orogênese produzida pela atividade andina causou um estágio de carregamento no sistema amazônico de foreland (Roddaz *et al.* 2005), resultando na reativação tectônica de arcos estruturais. A influência do Arco de Iquitos nessas regiões foi comprovada por análises sedimentológicas, de pólen e de proveniência (Hoorn *et al.* 2010, Roddaz *et al.* 2005, Espurt *et al.* 2007, Horbe *et al.* 2013, 2014 2019).

## 2.2 MAGMATISMO DO CAMP NAS BACIAS ESTUDADAS

Grandes volumes de basaltos toleíticos foram amplamente identificados no intervalo Triássico-Jurássico nas bacias sedimentares estudadas, atribuídos ao rompimento da Pangeia e abertura do Oceano Atlântico Central (ca. 190 Ma), representando uma Grande Província Ígnea (LIP) denominada como Província Magmática do Atlântica Central ou CAMP (Marzoli *et al.* 1999; Fig. 1A). A Província Magmática do Atlântico Central apresenta geometria alongada N-S, com eixo maior de 7500 km, cobrindo uma área de pelo menos 106 km<sup>2</sup>, abrangendo a América do Sul, América do Norte, África Ocidental e Europa, tornando-a uma das principais províncias ígneas (LIP-*Large Igneous Province*) do mundo (McHone 2000, Marzoli *et al.* 2018, Klöcking *et al.* 2018). LIPs consistem em volumosos pulsos magmáticos de composição tipicamente básica-ultrabásica cobrindo áreas maiores que 1,0 x 10<sup>5</sup> km<sup>2</sup>. As grandes províncias ígneas são formadas em um tempo relativamente curto (<50 Ma) e são caracterizadas por pulsos magmáticos de curta duração (menor que 1 Ma até 10 Ma) (Coffin & Eldholm 1993, Sheth 2007, Bryan & Ernst 2008).

A CAMP foi um evento magmático com duração de 10 Ma (200-190 Ma; Marzoli *et al.* 2018), com sua origem ainda debatida por muitos autores, com dois principais mecanismos discutidos e aceitos até o momento: (1) impacto da pluma do manto sob a litosfera continental (McHone 2000, De Min *et al.* 2003) ou (2) concentração de calor sob a litosfera continental espessa e/ou convecção resultante das diferenças de diversos domínios litosféricos (McHone 2000).

Na Bacia dos Parecis os basaltos mapeados pelo CAMP são encontrados pelas formações Anarí e Tapirapuã, expostas na região sudeste do Graben do Colorado e Chupinguaia, respectivamente (Fig. 1A). Os basaltos sobrepostos a essas supersequências foram datados pelo método K/Ar que indicou idade Jurássica Inferior para a Formação Anarí (Pinto Filho *et al.* 1977, Santos *et al.* 1980, Barros *et al.* 2006). Montes Lauer *et al.* (1994) utilizando o método de datação Ar/Ar, sugeriram idades em torno de 197 Ma para as formações Anarí e Tapirapuã, próximas às idades encontradas por Marzoli *et al.* (1999) e Barros *et al.* (2006). Essas idades e a geoquímica, relacionada às formações Anari e Tapirapuã, são compatíveis com uma mesma origem mantélica (Montes Lauer *et al.* 1994, Baksi & Archibald 1997).

Os derrames básicos considerados de caráter fissural, denominados de Formação Tapirapuã, afloram numa área de aproximadamente 115 km de extensão por 10 a 20 km de largura, na Serra de Tapirapuã, município de Tangará da Serra, Mato Grosso. A cidade de Tangará da Serra está localizada a aproximadamente 250 km de Cuiabá no Mato Grosso (Barros

*et al* 2007). Os basaltos da Formação Tapirapuã, na porção oeste da área, mostram composições de ambiente intra-placa continental. Sua composição é básica, não tendo sido encontrado até o momento rochas mais fracionadas, como os riolitos associados à Formação Serra Geral. Os teores de SiO<sub>2</sub> variam de 49,5 a 50,7% e os valores de TiO<sub>2</sub> são em torno de 1,3% (Barros *et al.* 2007). A natureza toleítica é sugerida pela alta razão FeO<sub>t</sub>/MgO, aliada a conteúdos elevados de CaO, baixos teores de Sr e Ba e pelo alinhamento das amostras no diagrama de Miyashiro (1974). Os padrões dos elementos de Terras Raras mostram enriquecimento leves sobre pesados durante a evolução do líquido. A ausência de anomalia negativa de Eu no plagioclásio associada com o empobrecimento de ETR pesados e a observação de textura subofítica demonstram que o plagioclásio não participou do fracionamento sozinho, mas acompanhado de clinopiroxênio. Os dados geoquímicos associados aos resultados dos isótopos de <sup>87</sup>Sr/<sup>86</sup>Sr (0,70758 a 0,706446) e <sup>144</sup>Nd/<sup>143</sup>Nd (0,512609 a 0,512662) e ε<sub>Nd</sub> variando de - 0,01 a + 2,32 demonstram que estas rochas se originaram de fontes mistas (manto enriquecido + manto astenosférico; Barros *et al.* 2007). É sugerido que a idade mais precisa para a cristalização, embora ainda levemente afetada pelos processos de alteração, é 206 ± 6 Ma. Esta idade pode ser considerada concordante com determinações anteriores pelo método K-Ar que indicavam valores de 197-198 Ma (Pinto Filho *et al.* 1977, Santos *et al.* 1980), posicionando este evento no limite Triássico Superior - Jurássico Inferior. Eventos intrusivos desta faixa de idade são observados nas bacias do Solimões e do Amazonas, além de diques básicos na costa do Pará e Amapá, entre outras áreas. Eles têm sido associados à abertura do Atlântico Norte (Mizusaki *et al.* 2002) e antecedem o início do magmatismo da Formação Serra Geral na Bacia do Paraná e Formação Sardinha na Bacia do Parnaíba com idade aproximadamente 133 Myr (Oliveira *et al.* 2023).

O CAMP nas bacias do Amazonas e Solimões é exposto pelo magmatismo Penetecaua. Datações de <sup>40</sup>Ar/<sup>39</sup>Ar e U/Pb para as soleiras de diabásio da Amazônia, associadas a idades de outras regiões (Santos 2000, Davies *et al.* 2017, 2019) atribuem uma idade de 201.52 ± 0.07 Ma para o pico desse magmatismo e que se coloca muito próximo do limite Triássico-Jurássico (201.36 ± 0.17 Ma). Estes novos resultados no Penetecaua indicam uma idade compatível com a interpretação que o CAMP possa ser um mecanismo gatilho para mudanças climáticas relacionadas à extinção em massa no final do Triássico, embora essa associação já tenha sido contestada (Whiteside *et al.* 2010). O principal mecanismo proposto é a liberação de voláteis pelas camadas sedimentares ricas em carbono em que se encaixam as intrusões, adicionando à atmosfera uma enorme quantidade de gases SO<sub>2</sub> e CO<sub>2</sub>.



Os afloramentos foram primeiramente descritos pelo projeto RADAM e também pela CPRM (Vasquez 2008), principalmente, nas margens das bacias e com direções aproximadamente paralelas ao curso atual do rio Amazonas. As soleiras apresentam grandes extensões laterais de até 50 km, como é o caso da soleira de Medicilândia (PA). A maioria das ocorrências é identificada como soleiras, porém no Noroeste da bacia também são descritos diques. Na Bacia do Amazonas as soleiras apresentam basculamento desprezível diferentemente do que ocorre na Bacia do Solimões, provavelmente afetada pela orogenia andina. Em sub-superfície foram reconhecidos na bacia Amazônica até oito níveis de diabásio encaixados nos sedimentos paleozoicos e com até algumas centenas de metros de espessura (Svesen *et al.* 2018)

O magmatismo Penatecaua, em geral, ainda é pouco estudado, mas recentemente, alguns estudos concentrados em regiões ou soleiras foram divulgados (Svesen *et al.* 2018, Davies *et al.* 2019). A soleira de Medicilândia, localizada em cidade homônima no estado do Pará é a maior em extensão aflorante na borda sul da Bacia Amazônica. Abrange cerca de 300 km<sup>2</sup> e é composta por diabásios. Alguns trabalhos da literatura têm caráter mais estrutural. Por exemplo, Montalvão & Oliveira (1975) procuraram explicar a ocorrência do domo de Monte Alegre, aproximadamente, 10 km a noroeste da cidade homônima na borda norte da bacia, associando-o às intrusões toleíticas. Figueira *et al.* (2012) estudaram o registro das deformações nas soleiras e diques do magmatismo Penatecaua que afloram nessa região buscando determinar as paleoextensões que atuaram após o evento Penatecaua.

Na bacia do Parnaíba o CAMP é marcado pelo magmatismo máfico regional da Formação Mosquito Triássico-Jurássico Inferior (199±2,4 Ma, Merle *et al.* 2011; Fig. 1A), relacionado à abertura do Oceano Atlântico central. A espessura total das rochas magmáticas derivadas desses dois eventos é c. 600-800 m intrudidos em uma pilha sedimentar de espessura máxima de 3500 m (Daly *et al.* 2014; Fig. 1B). Os fluxos de basalto da Formação Mosquito estão concentrados no centro-oeste da bacia do Parnaíba (Fodor *et al.* 1990) e estão intervalados com arenitos eólicos chamados de intertraps (Nogueira *et al.* 2021). Um fino depósito jurássico lacustre (Formação Pastos Bons) é o registro sedimentar local de um período de soerguimento e erosão (Cardoso *et al.* 2019).

O intervalo mesozoico na Bacia do Parnaíba foi caracterizado por expressivos eventos magmáticos que resultaram na colocação de derrames, diques e soleiras de basaltos toleíticos (Bellieni *et al.* 1990, Ernesto 2003). Na Bacia do Parnaíba são reconhecidas até três fases de atividade magmática. A primeira precede a formação da bacia e ocorreu durante o Cambro-Ordoviciano (Oliveira & Mohriak 2003; Daly *et al.* 2018, Heilbron *et al.* 2018). As demais fases ocorrem durante o Mesozoico e são representadas pelas formações Mosquito (Jurássico) e Sardinha (Cretáceo). A Formação Mosquito é composta por derrames e soleiras que predominam na porção centro-oeste da bacia, sendo estas rochas relacionadas à Província Magmática do Atlântico Central (CAMP). A Formação Mosquito possui, na base e no topo, intercalações de arenito que são conhecidos como “arenitos *intertrap*” (Moore 1961, Aguiar 1969, Bellieni *et al.* 1990, Baksi & Archibald 1997, Ernesto 2003, Vaz *et al.* 2007, Nogueira *et al.* 2018). Dados recentes obtido por datações U-Pb, Ar-Ar e K-Ar tem confirmado idades distintas para as Formações Mosquito ( $201 \text{ Ma} \pm 2$ ) com um intervalo de 215 a 150 Ma e média de 178 Ma (Eojurássico) (Cordani *et al.* 1970, Mizusaki *et al.* 2002, Vaz *et al.* 2007, Rodrigues 2014, Oliveira *et al.* 2018).

Segundo Merle *et al.* (2011) utilizando método de datação Ar-Ar, indicou idades três assinaturas composicionais para as rochas básicas da Bacia do Parnaíba: com baixo TiO<sub>2</sub>, Alto TiO<sub>2</sub> e Alto TiO<sub>2</sub> evoluído. As idades atribuídas às rochas básicas da Formação Mosquito indicam que elas são correlacionadas com as rochas básicas da Formação Penatecaua registradas nas bacias do Solimões e Amazonas e com idades próximas a atividade da CAMP a qual foi resultado da fragmentação do Supercontinente Pangeia com posterior abertura do Oceano Atlântico Central (Marzoli *et al.* 1999, Milani & Thomaz Filho 2000, Merle *et al.* 2011, Oliveira *et al.* 2018, Davies *et al.* 2019, Oliveira *et al.* 2023 ).

Petrograficamente a Formação Mosquito é bem similar a Formação Tapirapuã, sendo ambas caracterizadas como rochas com textura levemente porfirítica (5- 10% de fenocristais e microfenocristais), predominantemente amigdaloidais/vesiculares e menos frequentemente maciças. A assembleia mineralógica é constituída por dois piroxênios (augita e pigeonita), plagioclásio, óxidos de Fe-Ti (magnetita com exsolução de ilmenita) e vidro vulcânico. Ocasionalmente minerais de calcita e zeólita ocorrem preenchendo amígdalas na Formação Mosquito (Rabelo *et al.* 2019).

A Formação Mosquito é caracterizada quimicamente por basaltos toleíticos de baixo Ti (B-Ti) e alto Ti (A-Ti), sendo os basaltos de B-Ti mais abundantes (Bellieni *et al.* 1990, Fodor *et al.* 1990, Ernesto 2003). Merle *et al.* (2011) subdividiram o grupo de A-Ti em dois subgrupos, sendo (a) A-Ti com aproximadamente 2% de TiO<sub>2</sub> e (b) alto Ti evoluído (AE-Ti) com TiO<sub>2</sub> acima de 3%. Os basaltos de B-Ti são considerados em concentrações menores que 1,3% de TiO<sub>2</sub>. A derivação dos basaltos da Formação Mosquito de B-Ti foi caracterizada pela fusão parcial das porções mais férteis do manto litosférico subcontinental metassomatizado durante um processo pretérito de subducção; os toleítos de A-Ti referem-se à fusão parcial da astenosfera com contaminação durante a ascensão pela interação com o manto litosférico subcontinental (MLSC) e, alguns toleítos de AE-Ti, apesar de terem sido originados dessa mesma fonte, mostraram evidências de assimilação por cristalização fracionada (AFC). Estas constatações foram obtidas a partir de dados isotópicos (Sr-Nd-Pb-Os) e litogeoquímicos (Merle *et al.* 2011).

## CAPÍTULO 3 MATERIAIS E MÉTODOS

### 3.1 PESQUISA BIBLIOGRÁFICA

Houve a consulta das principais referências sobre a geologia da região que engloba as bacias estudadas, inseridas no contexto antes, durante e Pós-CAMP, visando integrar o maior número de informações para embasar e analisar criticamente as ideias sobre o arcabouço tectônico, estratigráfico, paleogeográfico e magmático do Mesozoico (Basei 1974, Almeida & Mantovani 1975, Almeida *et al.* 1981, Caputo 1984, Caputo & Silva 1990, Wanderley Filho 1991, Mizusaki *et al.* 1992, Montes Lauer *et al.* 1994, Baski & Archibald 1997, Zalán 2004, Barros *et al.* 2007, Almeida & Pinheiro 2007, Ballen *et al.* 2013, Rabelo & Nogueira 2015, Abrajante Junior 2016, Svensen *et al.* 2018, Abelha *et al.* 2018, Daly *et al.* 2018, Cardoso *et al.* 2019, Nogueira *et al.* 2021). Além disso, houve também a compilação de dados geofísicos de artigos publicados, enfatizando a reologia e resultados advindos de diversos métodos geofísicos referente ao evento do CAMP, próximo ou nas bacias estudadas (Teixeira 2001, Siqueira & teixeira 2003, Bahia *et al.* 2007, Assumpção *et al.* 2013a, De Castro *et al.* 2016, Mocitaiba *et al.* 2017, Soares *et al.* 2018, Manenti *et al.* 2018, Heilbron *et al.* 2018, Trosdorf *et al.* 2018, Ghomsi 2020, Rezende *et al.* 2021, Ghomsi 2022, Castro *et al.* 2022, Ribeiro Filho *et al.* 2023).

### 3.2 OBTENÇÃO DE DADOS GRAVIMÉTRICOS

#### 3.2.1 Problema Direto: Modelagem Crustal

Este método é amplamente utilizado para identificação e interpretação de feições crustais com base no contraste de densidade das rochas na crosta (Telford *et al.* 1990). Para obter informações sobre o registro geológico a partir dos dados gravimétricos é necessário separar o sinal gravimétrico residual do sinal gravimétrico regional (Lowries 2007, Telford *et al.* 1990). Portanto, realizamos essa separação para os dados das bacias do Amazonas, Parnaíba, dos Parecis e Solimões. O campo gravimétrico regional é um sinal previsto pela crosta terrestre modelada com comprimentos de onda mais longos, produzido por grandes estruturas geológicas e mais profundas que o campo residual, que é fortemente afetado por variações de densidade mais próximas à superfície. Assim, a interpretação gravimétrica de sinais de comprimentos de onda mais curtos é necessária para caracterizar fontes próximas ao topo da crosta (Blakely 1996, Lowries 2007). Existem várias maneiras de determinar o campo regional-residual para um conjunto de dados de gravidade (Spector & Grant 1970, Beltrão 1989, Tenzer *et al.* 2012, Martínez-Moreno *et al.* 2015, Ribeiro-Filho *et al.* 2018, Ghomsi 2020, Ghomsi 2021, Ghomsi

2022). Obtivemos o sinal gravimétrico residual crustal a partir da anomalia gravimétrica calculada de uma crosta modelada e discretizada em prismas retangulares 3D (sinal gravimétrico regional). O sinal gravimétrico de  $N$  prismas em cada ponto de observação é obtido pelo algoritmo de Plouff (1976). As formas do modelo crustal são presumivelmente conhecidas e definidas por duas superfícies, topo e base (Fig. 2B). A forma da superfície superior é definida pelo ETOPO-1/Terrain digital Model (DTM) (Barthelmes & Köhler 2012, Fig. 3), obtido do serviço de navegação do *International Center for Global Earth Models* (ICGEM) (Amante & Eakins 2009). Além disso, a forma da superfície de base (profundidade da Moho das bacias estudadas) é fornecida por Uieda & Barbosa (2016) (Fig. 4). A anomalia gravimétrica residual foi obtida subtraindo a anomalia bouguer observada da anomalia regional da crosta modelada.

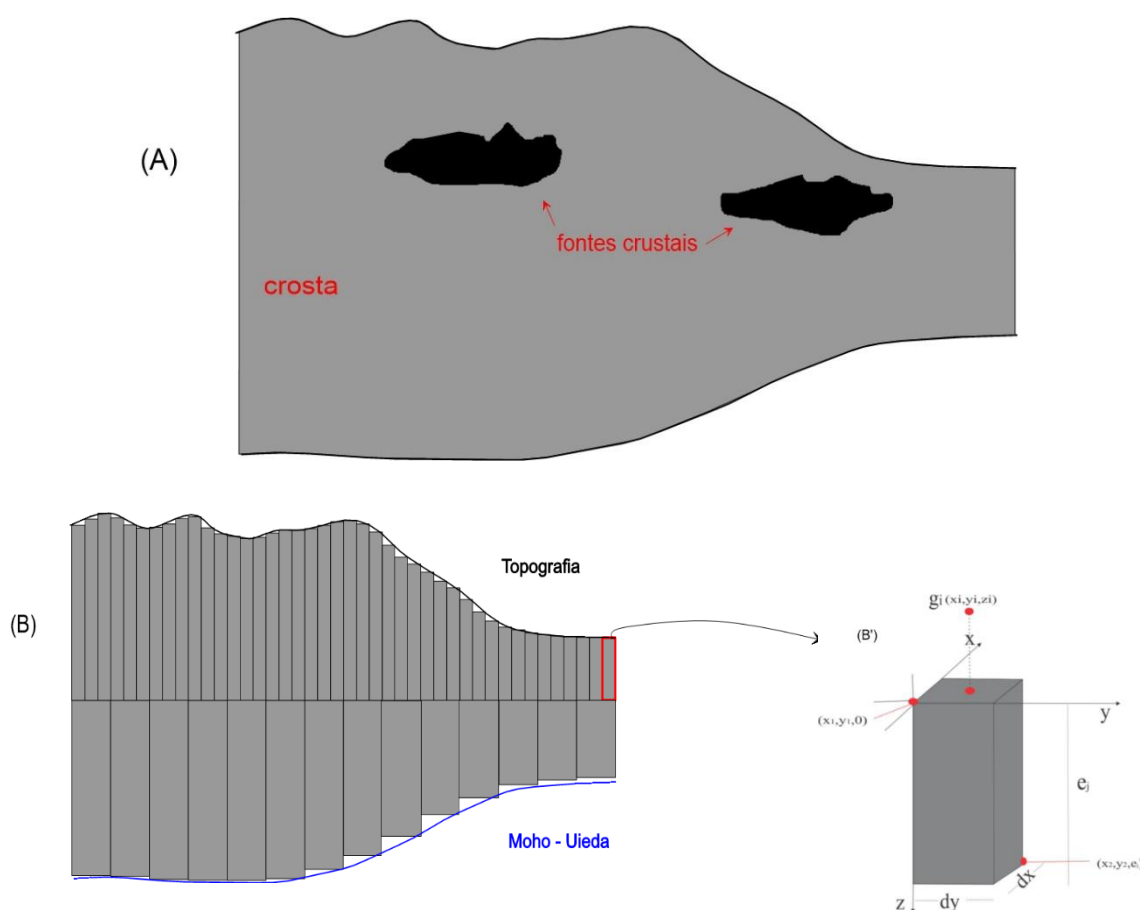


Figura 2 - Representação de uma modelo simplificado da Crosta terrestre, compostas por fontes da crosta. A) Modelo representativo da crosta. B) Crosta terrestre discretizada em  $N$  prismas retangulares 3D. B') Representação detalhada do  $N$ -ésimo prisma na discretização pelo a algoritmo de Plouff (1976).

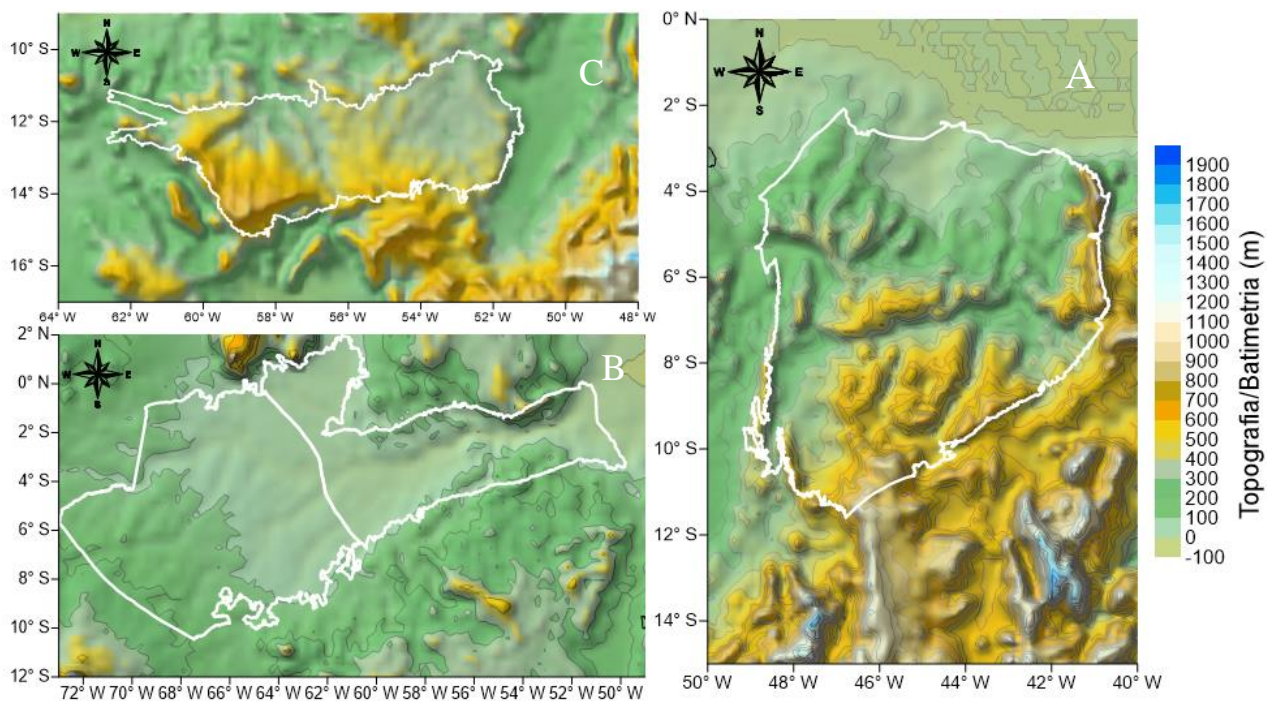


Figura 3 - Topografia da área de estudo. A) Topografia da Bacia do Parnaíba. B) Topografia das bacias do Amazonas e Solimões. C) Topografia da Bacia dos Parecis

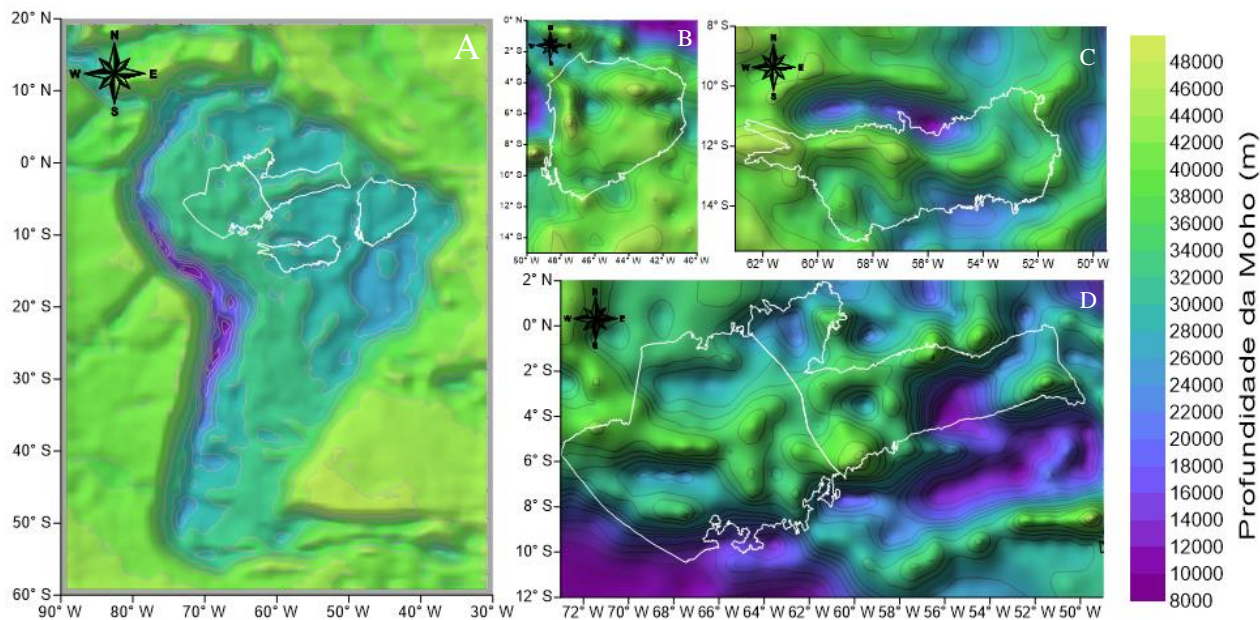


Figura 4 - Profundidade da Moho obtida por Uieda & Barbosa (2016). A) Profundidade da Moho da America do Sul, destacando as bacias da área de estudo. B) Profundidade da Moho da Bacia do Parnaíba. C) Profundidade da Moho da Bacia dos Parecis. D) Profundidade da Moho das bacias do Amazonas e Solimões.

### 3.2.1.1 Solução Analítica do cálculo da anomalia regional por discretização de prismas

A anomalia regional ou anomalia gravimétrica calculada é a anomalia de uma crosta modelada e discretizada em prismas retangulares 3D (Fig. 2B). O sinal gravimétrico dessa anomalia é dividida em N prismas em cada ponto de observação (Fig.2B') e foi obtido pelo algoritmo de plouff (1976), em que a função  $g_z$  que calcula a componente vertical do sinal gravimétrico avaliado no  $i$ -ésimo ponto de observação  $(x_i, y_i, z_i)$  produzida por um único prisma retangular 3D com densidade constante  $\rho$  e dimensões conhecidas  $dx$ ,  $dy$  e  $dz$ , com o centro localizado no ponto  $(x_j, y_j, z_j)$ , como:

$$g_z = \gamma \rho \int_{z_1}^{z_2} \int_{y_1}^{y_2} \int_{x_1}^{x_2} \frac{z - z_p}{\left[ (x - x_p)^2 + (y - y_p)^2 + (z - z_p)^2 \right]^{\frac{3}{2}}} dx dy dz \quad (1)$$

Em que o símbolo P representa cada prisma, ou seja, os termos  $x_p$ ,  $y_p$  e  $z_p$  representam o tamanho do prisma nas direções x, y e z, e os termos  $x_1$ ,  $x_2$ ,  $y_1$ ,  $y_2$ ,  $z_1$  e  $z_2$  representam os limites inferior e superior de cada dimensão,  $\rho$  é a densidade e  $\gamma$  representa a constante universal de Newton, dentro do volume do prisma (Fig. 2B'). Se considerarmos N prismas, essa integral deve ser resolvida N vezes, ou seja, para a quantidade de prismas existentes na malha regular discretizada. Logo, para um conjunto de N prismas, o dado gravimétrico predito pode ser escrito como a soma da contribuição calculada para cada célula prismática, ou seja:

$$g_p = \sum_{i=1}^N g_z(x_p, y_p, z_p) \quad (2)$$

A solução para a integral mostrada na Equação (1) é resolvida por Nagy (1966) e Plouf (1976) de modo numérico. Uma vez calculada a Equação (2), temos posse do dado gravimétrico calculado devido à discretização da superfície crustal em prismas retangulares justapostos, onde o topo de cada prisma coincide com um plano de observação próximo à superfície e a base é representada pela profundidade crustal da moho associada e calculada através da flexura devido à carga topográfica.

### 3.2.2 Cálculo da Espessura Elástica ( $T_e$ ) das Bacias

Utilizou-se de três etapas para determinar a espessura elástica. Primeiramente, calculou-se a profundidade da descontinuidade de Mohorovicic para um conjunto de valores de espessura elástica padrão, conforme descrito por Wienecke (2007). Posteriormente, para cada valor de  $T_e$ , calculamos o sinal gravimétrico residual, considerando dois cenários: 1) A superfície descrita pela topografia e a Moho de referência, e a superfície descrita pela topografia e Moho calculado a partir de  $T_e$ . Em seguida, calculamos a correlação cruzada entre o sinal gravimétrico observado e o sinal gravimétrico calculado (anomalia regional obtida pelo algoritmo de discretização de primas). O maior valor de correlação está diretamente relacionado a melhor espessura elástica e a melhor profundidade do Moho associada à deformação. O detalhamento desse método pode ser visualizado a partir de Ribeiro-Filho *et al.* (2023).

#### 3.2.2.1 Cálculo da profundidade Moho a partir da deflexão

Considere um conjunto de dados de alta resolução de dados topográficos e dados de gravidade observados. De acordo com os princípios da flexão elástica, qualquer carga topográfica causa deformação local e regional na crosta terrestre, onde tal deformação vertical pode ser calculada a partir da solução de uma equação diferencial parcial de quarta ordem.

$$\frac{\partial^4 w}{\partial r^2} - \frac{1}{\beta^4} w(r) = 0 \quad (3)$$

Onde  $r$  representa a distância radial escrita por

$$r = \sqrt{x^2 + y^2} \quad (4)$$

$\beta$  é a constante relacionada à espessura elástica

$$\beta^4 = \frac{12(1 - \nu^2)(\rho_m - \rho_c)g}{E \cdot T_e^3} \quad (5)$$

Na equação acima,  $\nu$  representa o coeficiente de Poisson,  $\rho$  representa a densidade do manto e da crosta,  $g$  representa o valor do campo gravitacional,  $E$  é o módulo de Young e  $T_e$  é o valor da espessura elástica. Portanto, a solução analítica calcula a deformação crustal para uma *grid* regular de pontos ao longo da área de estudo, permitindo uma representação detalhada da resposta elástica da crosta (Wienecke, 2006 e 2007), conforme equação abaixo:



$$w = w_0 + w_{sin} + w_{log}$$

onde  $w_0$ ,  $w_{sin}$  e  $w_{log}$  são as deformações pontuais, próximas e distantes.

Uma vez calculada a flexão da Moho, é possível determinar a profundidade da Moho, pois esta profundidade é obtida pela soma da deformação e a profundidade de referência ( $\sim 35$  km), conforme mostrado na seguinte equação:

$$z_M = w + z_R \quad (7)$$

Finalmente, estes procedimentos sistemáticos e analíticos fornecem uma abordagem rigorosa para estimar a rigidez flexural e compreender os processos geodinâmicos.

### 3.2.2.2 Mapeamento da espessura elástica por meio da correlação cruzada

Após calcular o valor para a profundidade de Moho e espessura elástica, criamos uma *grid* de valores de  $T_e$  em um conjunto de pontos discretos, permitindo uma avaliação sistemática da influência da espessura elástica em relação aos dados gravimétricos observados. Posteriormente, foi realizada uma correlação cruzada entre os dados gravimétricos observados e os dados gravimétricos calculados a partir da modelagem crustal pela discretização em prismas, seguindo a equação abaixo:

$$C(T_e) = \frac{\sum (g_o - \underline{g_o}) \cdot (g_c - \underline{g_c})}{\sum (g_o - \underline{g_o})^2 \cdot \sum (g_c - \underline{g_c})^2} \quad (8)$$

onde  $g_o$  e  $\underline{g_o}$  são os dados observados e os dados médios observados, e  $g_c$  e  $\underline{g_c}$  representam os dados calculados e a média calculada da modelagem.

Neste caso, para um valor  $T_e$ , calculamos uma correlação. Este procedimento foi caracterizado de forma dinâmica (Fig.5), considerando não apenas uma única comparação, mas uma varredura contínua dos dados observados e calculados ao longo de um *grid*. A melhor espessura elástica (Fig.6) para um ponto específico correspondeu ao maior coeficiente de correlação (Fig.7), associado também ao melhor valor para a profundidade de moho (Fig.4).

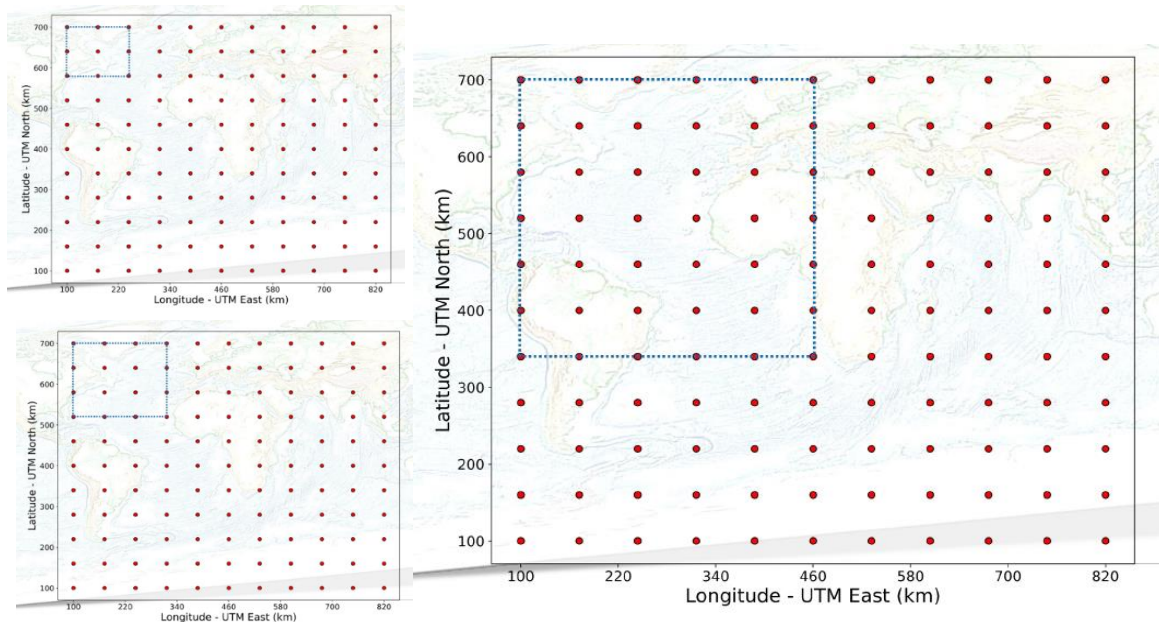


Figura 5- Cálculo do valor de  $T_e$  a partir da correlação cruzada, considerando uma varredura contínua dos dados observados e calculados ao longo de um *grid*.

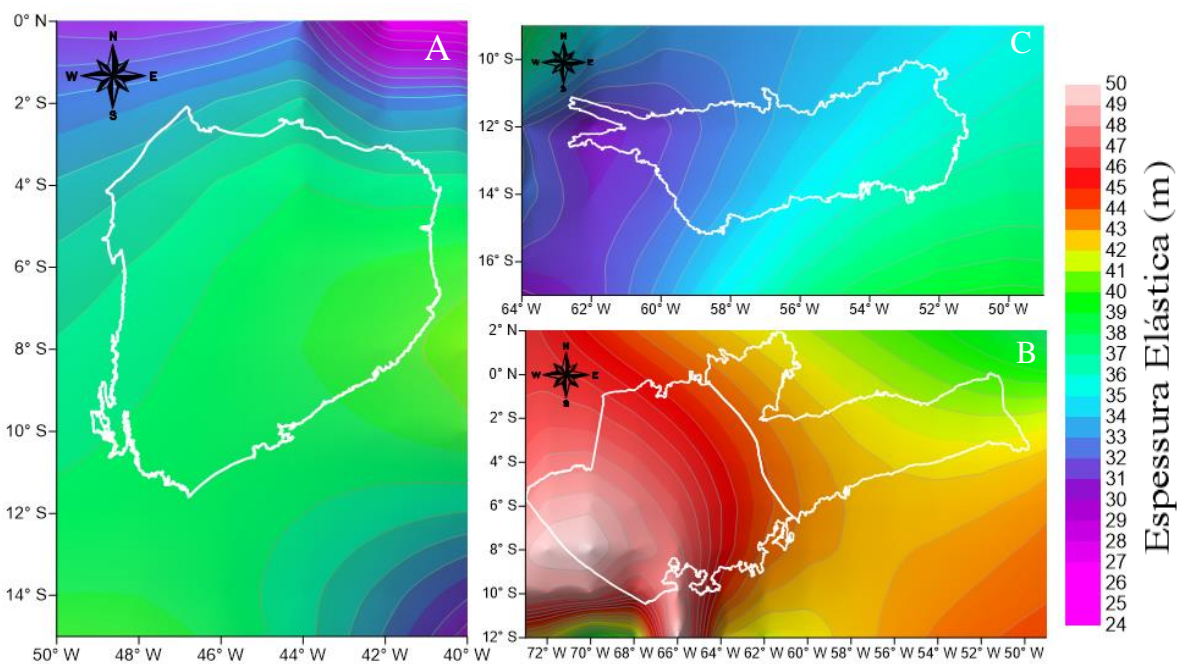


Figura 6 - Mapas da Espessura Elástica. A) Espessura elástica da Bacia do Parnaíba. B) Espessura elástica das bacias do Amazonas e Solimões. C) Espessura elástica da Bacia dos Parecis.

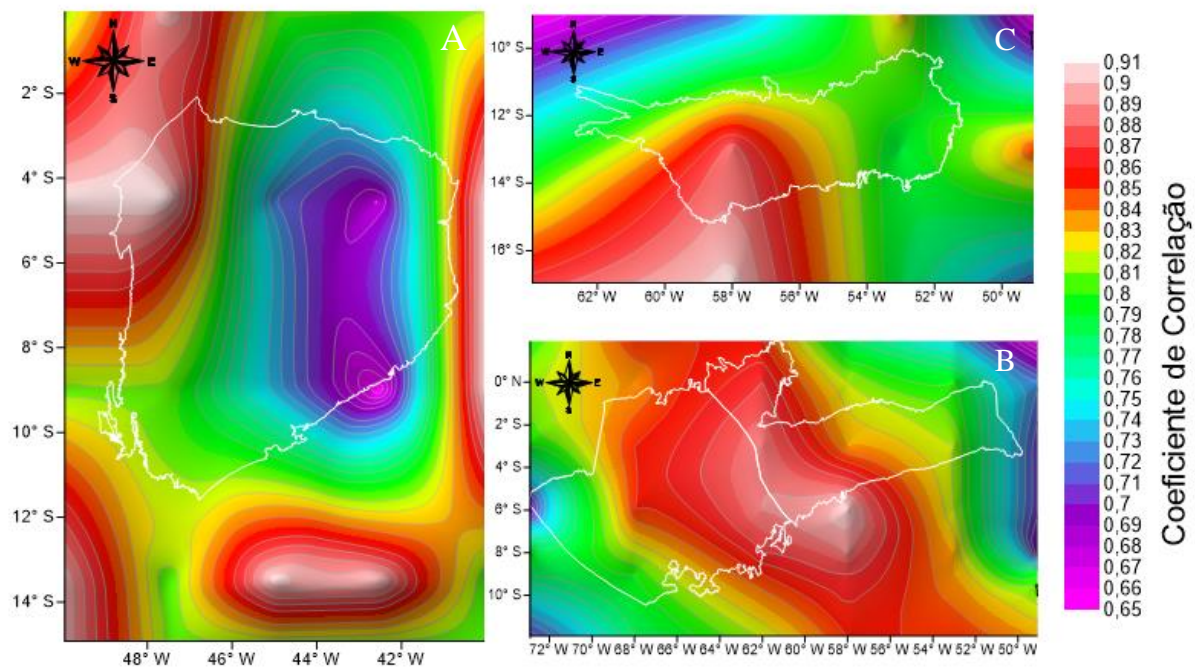


Figura 7 - Mapa do coeficiente de correlação. A) Coeficiente de correlação da Bacia do Parnaíba. B) Coeficiente de correlação das bacias do Amazonas e Solimões. C) Coeficiente de correlação da Bacia dos Parecis.

## **CAPÍTULO 4 EVIDENCE FOR THE CENTRAL ATLANTIC MAGMATIC PROVINCE (CAMP) IN PRECAMBRIAN AND PHANEROZOIC SEDIMENTARY BASINS OF THE SOUTHERN AMAZONIAN CRATON, BRAZIL**

**Gabriel L. Rezende<sup>1\*</sup>; Cristiano Mendel Martins<sup>2</sup>; Afonso C. R. Nogueira<sup>1,3,4</sup>; Fabio Garcia Domingos<sup>4</sup>; Nelson Ribeiro-Filho<sup>2</sup>**

<sup>1</sup>*Programa de Pós-Graduação em Geologia e Geoquímica (PPGG), Instituto de Geociências, Universidade Federal do Pará, 66075-110, Guamá, Belém, Pará, Brazil;*

<sup>2</sup>*Curso de Pós-Graduação em Geofísica (CPGF), Geociências, Universidade Federal do Pará, 66075-110, Guamá, Belém, Pará, Brazil;*

<sup>3</sup>*Faculdade de Geologia (FAGEO), Instituto de Geociências, Universidade Federal do Pará, 66075-110, Guamá, Belém, Pará, Brazil;*

<sup>4</sup>*Research Productivity of CAPES and CNPQ, Brazil.*

**\*Artigo published to Journal of South American Earth Sciences**

### **Abstract**

The Triassic-Jurassic emplacement of large volumes of basaltic rocks, termed the Central Atlantic magmatic province (CAMP), preceded the Pangea break-up and the opening of the Central Atlantic Ocean. Central Brazil is an important site where the CAMP record can be assessed in detail. Previously mapped basalts in this region, which includes southwestern Tocantins and southern Tapajós provinces, represent a volume of 0.19 million km<sup>3</sup>. Interpretations of existing geophysical and geological data combined with forward gravity modelling were carried out in the Paleozoic Parecis and late Cryogenian-Cambrian Araras-Alto Paraguay basins. This study allows a new interpretation of geologic structures from residual gravity anomalies in the southern Amazonian Craton. Additionally, the basalts exposed in these basins occur as lava flows, sills and dykes hosted in Neoproterozoic and Paleozoic rocks, presenting an estimated subsurface magma volume of 3 million km<sup>3</sup>. Moreover, these geological elements are interpreted as high-density rocks correlated to the continental tholeiitic flood basalts of the CAMP. Therefore, the combination of residual gravity anomalies and previous geological data verify the CAMP occurrence in these sedimentary basins of Amazonia.

**Keywords:** large igneous provinces; residual gravity field, gravity modelling, Parecis Basin, Araras-Alto Paraguay Basin, Jurassic-Triassic, Amazonian Craton.

## 4.1 INTRODUCTION

Large volumes of tholeiitic basalt have been broadly identified in the Triassic-Jurassic interval in several widespread sedimentary basins; they are attributed to the Pangea break-up and the opening of the Central Atlantic Ocean (c. 190 Ma) and represent a large igneous province (LIP) termed the Central Atlantic magmatic province or CAMP (Marzoli *et al.* 1999). Pangea rifting occurred shortly before (approximately 199-192 Ma) the opening of the Central Atlantic Ocean and involved the production of new oceanic crust in the mid-ocean ridge from the Early Jurassic to the present. The CAMP comprises several pulses of magmatic activity that occurred at approximately 201 Ma (Marzoli *et al.* 2018, Blackburn *et al.* 2013, Davies *et al.* 2017; Fig 5A). The CAMP magmatism in Brazilian Amazonia and northern and central South America is represented by the record of several units, such as the Penatecaua magmatism ( $190 \pm 20$  Ma) in the Solimões and Amazonas basins, the Mosquito Formation ( $199.7 \pm 2.45$  Ma) in the Parnaíba Basin, the Anarí and Tapirapuã formations ( $197-200 \pm 6$  Ma) in the Parecis Basin, the basaltic remnants in southern Bolivia (Tarabuco, entre Ríos and Camiri areas) with ages of  $198.1 \pm 1.5$ ~ $199.2 \pm 2.2$  Ma, and the Cururu diabase dyke swarm, which crops out to the west of the Tucumã swarm in the region of São Felix do Xingu and has been dated by the K-Ar method at  $180 \pm 9$  Ma (Melfi *et al.* 1988, Rocha-Campos *et al.* 1998, Renne *et al.* 1992, Góes & Feijó 1994, Montes-Lauar *et al.* 1994, Tassinari *et al.* 1996, Wilson 1997, Barros *et al.* 2006, Vaz *et al.* 2007, Merle *et al.* 2011, Bertrand *et al.* 2014, Texeira *et al.* 2018; Fig. 5A). The younger basalts of the Serra Geral Formation exposed in the Paraná Basin, southeastern South America, succeeded the CAMP and have been related to the late stage of the West Gondwanaland break-up and the opening of the South Atlantic at approximately 134 Ma, termed the Paraná-Etendenka magmatism (Mizusaki *et al.* 2002, Baksi and Archibald 1997).

The basalts of the CAMP flowed into large rift basins, also forming dykes and sills that intruded into the sedimentary deposits, extending over approximately 11 million km<sup>2</sup> with an estimated total magma volume of 3 million km<sup>3</sup> (Marzoli *et al.* 2018, Korte *et al.* 2019). This event triggered a whole range of paleoenvironmental, paleogeographic and paleoclimatic changes, such as climate warming, photic zone euxinia and ocean acidification (Kiessling *et al.* 2009, Schoene *et al.* 2010, Whiteside *et al.* 2010, Ruhl *et al.* 2011, Ruiz-Martínez *et al.* 2012, Greene *et al.* 2012, Kasprak *et al.* 2015, Davies *et al.* 2017, Korte *et al.* 2019). The large amounts of CAMP magma during this volcanic event were responsible for sharp global warming (Svensen *et al.* 2007, Blackburn *et al.* 2013, Korte *et al.* 2019, Capriolo *et al.* 2020). A direct consequence was the decrease in marine and continental biodiversity at the end of the Triassic, culminating in one of the five most expressive mass extinctions on the planet (Olsen 1999, Marzoli *et al.* 2004, Davies *et al.* 2017, Marzoli *et al.* 2018, Korte *et al.* 2019). The reduction in organic productivity modified the carbon cycle, causing significant paleoceanographic changes indicated by the  $\delta^{13}\text{C}$  values in marine and continental deposits (Ruhl *et al.* 2011, Korte *et al.* 2019; Fig. 5A).

The CAMP event spans rift basins in eastern North America and Morocco, where it is well exposed and has been intensely studied (Hames *et al.* 2000, McHone & Puffer 2003, Knight *et al.* 2004, McHone 2006, Verati *et al.* 2007, Jourdan *et al.* 2009, Marzoli *et al.* 2011, Bensalah *et al.* 2011, Schaller *et al.* 2012, Marzoli *et al.* 2018 and 2019, Korte *et al.* 2019). In contrast, the constituents of the CAMP have not been as well studied and understood in Western Africa, Europe and some regions of South America, where they are represented by subvolcanic bodies and extrusive deposits (Coffin & Eldholm 1993, Montes-Lauar *et al.* 1994, Deckart *et al.* 1997, Oyarzun *et al.* 1997, Wilson 1997, Cebriá *et al.* 2003, Deckart *et al.* 2005, Reis *et al.* 2006, Nomade *et al.* 2007, Verati *et al.* 2007, Barros *et al.* 2006, Martins *et al.* 2008, Callegaro *et al.* 2014a, Marzoli *et al.* 2018, Korte *et al.* 2019). In this work, we evaluated the presence of the CAMP in the southern Amazonian Craton based on the occurrences mapped in the Phanerozoic Parecis and the late Cryogenian-Ordovician Araras-Alto Paraguay Basins (Santos *et al.* 2017, Nogueira *et al.* 2019) (Fig. 1B). The exposed basalts in both intracratonic basins represent a small volume (Fig. 5).

To confirm the CAMP in the southern Amazonian Craton, we discuss here a new interpretation based on geophysical and geological data. Bouguer gravity anomaly data are separated, i.e., we apply a regional-residual separation by using a robust polynomial fitting technique (Beltrão 1991). In addition, this technique considers that the regional gravity field can be iteratively approximated by a low-order polynomial, and the residual anomaly is calculated from simple subtraction. Furthermore, the analysis of geophysical data in combination with geological information provides a consistent interpretation. It also allows the mapping of high-density rocks below the surface associated with the CAMP basalts. Therefore, we report that the methodology of robust polynomial fitting applied to the Bouguer anomaly data leads us to understand the distribution of the CAMP in the southern Amazonian Craton and its expansion. This new interpretation can provide a new approach for the detection of high-density igneous rocks that do not crop out in sedimentary basins of the Amazon.

First, we describe some concepts regarding the CAMP and its occurrence in the southern Amazonian Craton. Then, we comment about the geological setting in the Parecis Basin and map the CAMP. Next, a geophysical data section is presented, followed by a brief discussion of the new interpretation based on geophysical and geological data. We finish this manuscript by validating and interpreting our results.

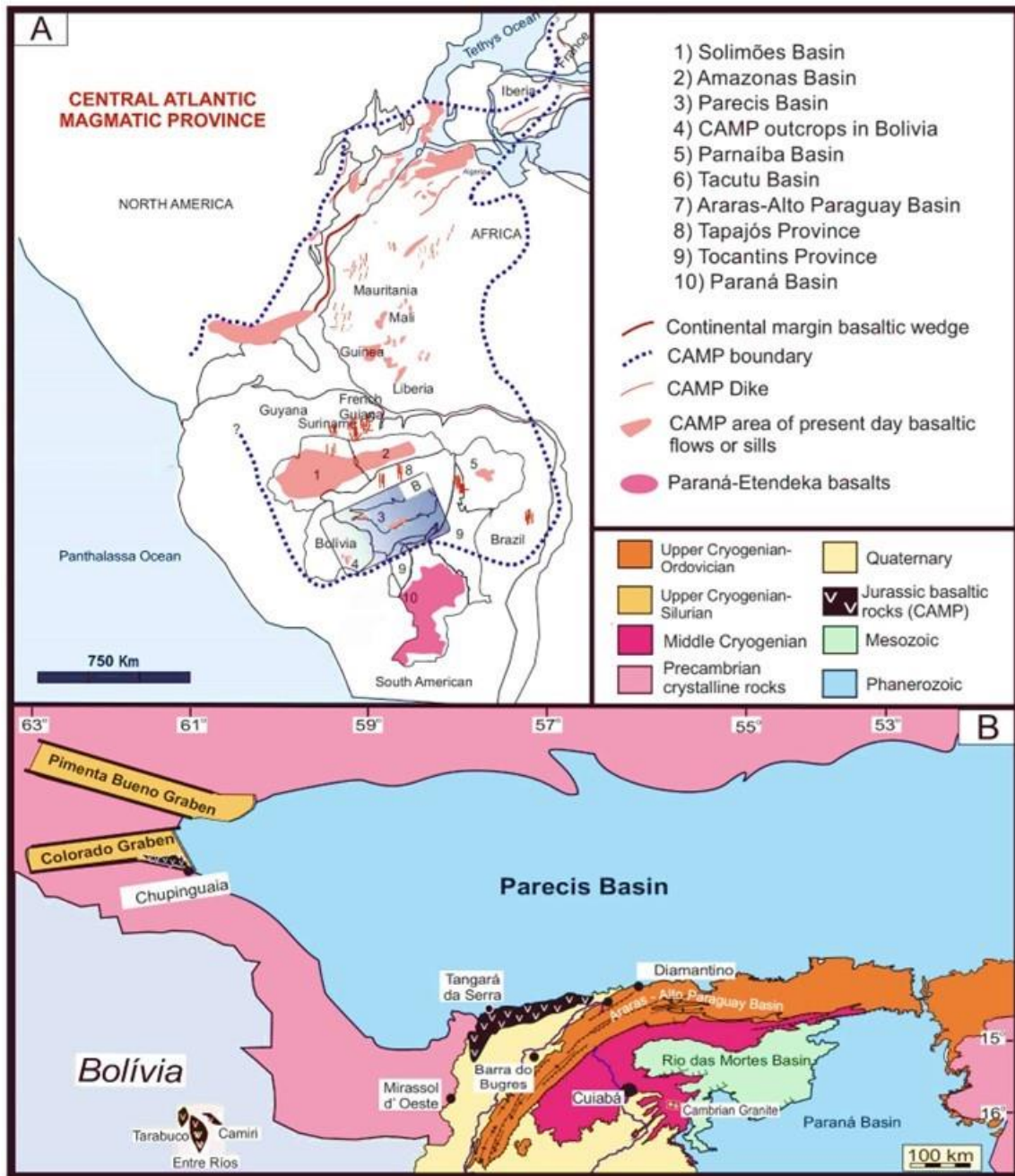


Figure 1 - The spatial relationship of the widespread CAMP. (A) The CAMP occurrences distributed as dykes, sills and lava flows in a scenario before the opening of the Central Atlantic Ocean and the Pangea break-up during the Permian-Triassic (modified from McHone 2000). (B) Geology of the southern Amazonian Craton and locations of the mapped basalts in the Parecis and Araras-Alto Paraguay Basins (geologic framework based on Santos *et al.* 2017, Nogueira *et al.* 2019).

## 4.2 GEOLOGICAL SETTING

The southern Amazonian Craton area is located in the southwestern Tocantins Province and southern Tapajós Province (Montes-Lauar *et al.* 1994, Barros *et al.* 2007, Cordani *et al.* 2000, Nogueira *et al.* 2019; Fig. 5B). Two basins, the subjects of this study, formed within the Tonian metamorphic rocks of the northern Paraguay Belt and the Paleo- to Mesoproterozoic rocks of the Amazonian Craton: 1) the Paleozoic Parecis Basin and 2) the late Cryogenian-Ordovician intracratonic basin or Araras-Paraguay Basin.

The Paraguay Belt originated during the Tonian-Cryogenian period (c. 900-640 Ma) mainly through a tectonic collision among the Amazonia, São Francisco and Paraná continental blocks in an event named the Brazilian-Pan-African orogeny (Cordani *et al.* 2000, Cordani *et al.* 2013, Nogueira *et al.* 2019). Furthermore, the Paraguay Belt is a complex of rocks deformed by ductile tectonic structures from transpressional structural domains and recorded mainly in the metamorphosed rocks of the Cuiabá Group (Almeida and Mantovani 1975, Siqueira and Teixeira 1993, Pedreira and Bahia 2000, Cordani *et al.* 2000, Alkmin *et al.* 2001, McGee *et al.* 2012, Nogueira *et al.* 2019; Fig. 6).

The Araras-Alto Paraguay Basin formed during the Cryogenian-Ordovician in the southeastern Amazonian Craton. This basin was inverted during the Ordovician, associated with the opening of the Paleozoic basins in the Amazon, and deformed during the Cretaceous by brittle to brittle-ductile transtensional tectonics (Cordani *et al.* 2000, Cordani *et al.* 2013, Santos *et al.* 2017, Nogueira *et al.* 2019; Fig. 6). This basin is filled by the following units: 1) the late Cryogenian Puga Formation, composed of glaciogenic diamictites, siltstones and sandstones; 2) the Ediacaran Araras Group, composed of limestones, dolostones and subordinate siliciclastic rocks; and 3) the Cambrian-Ordovician Alto Paraguay Group, which consists of sandstones and pelites (Fig. 6). The dolostones at the base of the Araras Group that overlie glaciogenic diamictites are interpreted as cap carbonates linked to Marinoan post-glacial events and related to the Snowball Earth hypothesis (c. 635 Ma). The deposits of the Araras-Alto Paraguay Basin unconformably overlie the crystalline rocks of the Amazonian Craton and metamorphic rocks of the Cuiabá Group exposed in the northern Paraguay Belt (Fig. 6).

The Parecis Basin is a rift-sag type basin that formed during an extensional event in the Amazonian Craton following the Rodinia break-up between 1.0 and 0.75 Ga (Pedreira and Bahia 2000, Teixeira 2001). This basin has a surface of approximately 500000 km<sup>2</sup> directly within the Amazonian Craton, central-western Brazil (Siqueira and Teixeira 1993, Bahia *et al.* 2006, Bahia 2007). The stratigraphic records present sedimentary-magmatic filling, which reaches 6000 m in thickness and consists of Paleozoic and Mesozoic deposits intruded by Cretaceous basic and ultrabasic rocks and overlain by Cenozoic rocks (Siqueira 1989, Siqueira and Teixeira 1993, Bahia *et al.* 2006, Bahia 2007). The basin was structured during the Late Ordovician, when the Amazonian Craton was affected by an extensional event yielding intracontinental rift systems generated by fault zone reactivation in the basement (Cordani *et al.* 2000). Six supersequences have been recognized in the Parecis Basin: Ordovician, Devonian, Carboniferous-Permian, Jurassic, Jurassic-Cretaceous and Cretaceous (Siqueira



1989, Siqueira and Teixeira 1993, Bahia and Pedreira 1996, Bahia 2007; Fig. 6).

The Paleozoic sediments of the Parecis Basin overlie late Cryogenian and Ediacaran sedimentary rocks exposed in the Colorado and Pimenta Bueno grabens and correlate with the successions exposed at the base of the Araras-Alto Paraguay Basin (Figs. 5B and 6). The late Cryogenian glaciogenic diamictites of the Cacoal Formation are overlain by dolostones and siltstones belonging to the Ediacaran Espigão d'Oeste Formation (Gaia *et al.* 2017, Afonso and Nogueira 2018, Nogueira *et al.* 2019; Fig. 6). Based on facies analysis, carbon isotopes and stratigraphic correlation, the Cacoal Formation (Bahia *et al.* 2007) was reinterpreted as a Neoproterozoic formation linked to the Marinoan and post-glacial events (~635 Ma), interpreted as only sedimentary fill in the basement, completely disconnected from the Paris Basin evolution (Gaia *et al.* 2017, Afonso and Nogueira 2018, Nogueira *et al.* 2019). Moreover, the Parecis Basin sedimentary rocks started with the Pimenta Bueno Formation, previously considered Carboniferous (Pedreira and Bahia 2004, Bahia *et al.* 2006) but repositioned in the Ordovician-Silurian interval (Afonso and Nogueira 2018; Fig. 6).

#### **4.2.1 Mapped and unmapped CAMP records in the southern Amazonian Craton**

Mapped CAMP basalts are found in the Phanerozoic Parecis Basin represented by the Anarí and Tapirapuã formations exposed in the southeastern Colorado graben and Tangará da Serra regions, respectively. Basalts overlying these supersequences were dated by the K/Ar method, which indicated a Lower Jurassic age for the Anarí Formation (Pinto Filho *et al.* 1977, Santos *et al.* 1980) (Tab. 1). Montes Lauer *et al.* (1994), using the Ar/Ar dating method, suggested ages of approximately 197 Ma for the Anarí and Tapirapuã formations, close to the ages found by Marzoli *et al.* (1999) and Barros *et al.* (2006) (Tab. 1). These ages and the geochemistry related to the Anari and Tapirapuã formations are compatible with the same mantle origin (Montes Lauer *et al.* 1994; Baksi and Archibald 1997, De Min *et al.* 2003). We emphasize that although Table 1 shows approximate values from previously published articles on the CAMP, these K/Ar ages are purely indicative, and the Ar/Ar ages obtained before 2010 need to be recalculated. These problems were improved with studies starting in 2011 (Marzoli *et al.* 2011). In addition, there are basalts mapped by the CPRM (Geological Survey of Brazil), located in the Emal Unit of the Itaipu mine in Barra do Bugres (Fig. 5B), which are possible occurrences of the CAMP located in the late Cryogenian-Ordovician Araras-Alto Paraguay Basin. These basalts are very close to those mapped and dated in Tangará da Serra (distance of approximately 5 km) and are presumed to be associated with this event (Fig. 5B).

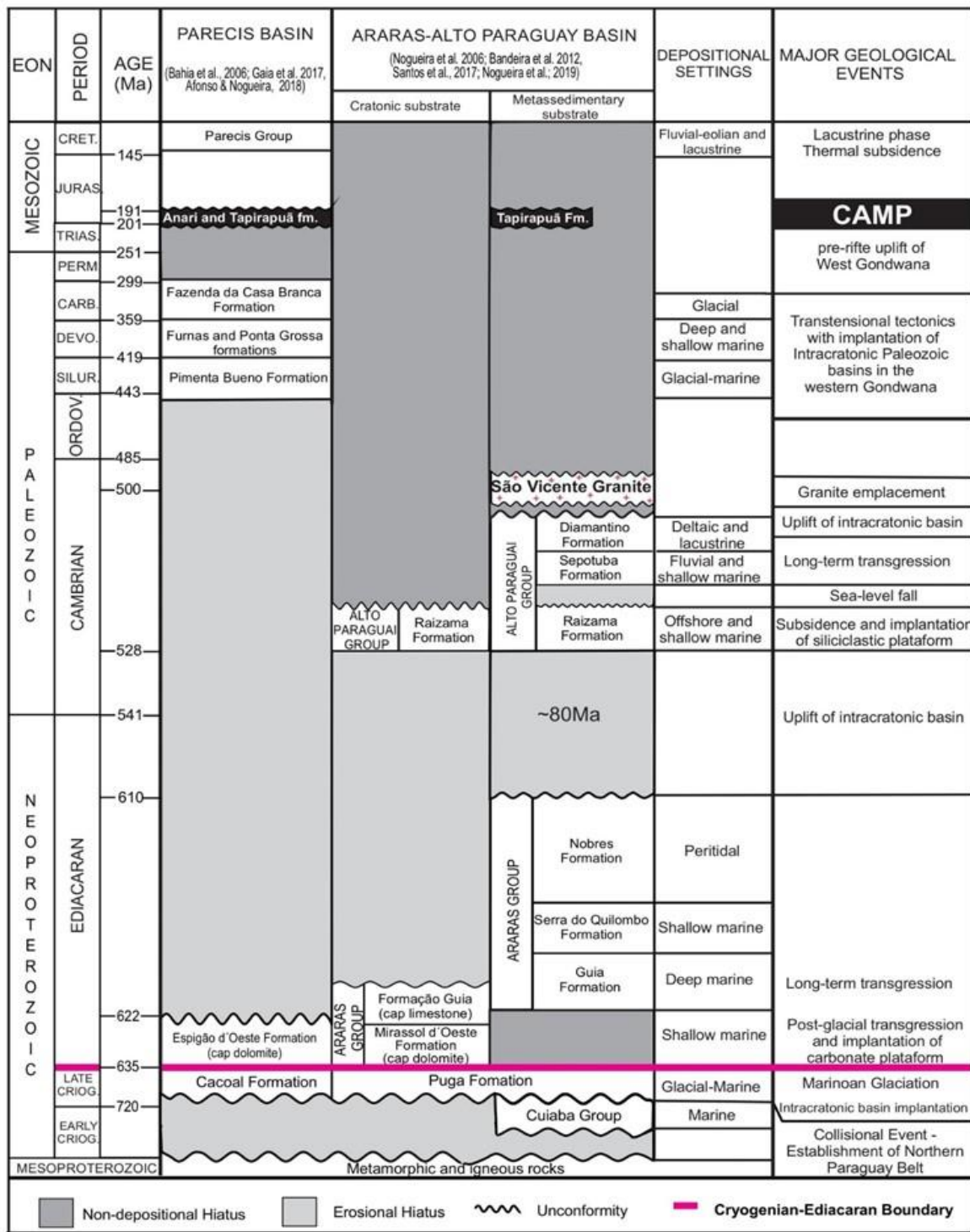


Figure 2- Lithostratigraphy, paleoenvironments and major geologic events in the Parecis and Araras-Paraguay basins of the southern Amazonian Craton (modified from Nogueira *et al.* 2019).

Due to the great CAMP extent (a widespread magmatic event whose products are located on 4 different continents) and the proximity of the Araras-Alto Paraguay Basin and Parecis Basin basalts, we infer that both basins contain basaltic bodies of the CAMP (Fig. 5B).

Table 1- The K/Ar and Ar/Ar ages of the Anari and Tapirapuã formations

Period (method)	Age (Ma)	Authors
Lower Jurassic (K/Ar)	197-198	Pinto Filho et al. (1977)
Lower Jurassic(K/Ar)	197-198	Santos et al. (1980)
Lower Jurassic (K/Ar) and (Ar/Ar)	197	Montes-Lauar et al. (1994)
Lower Jurassic (Ar/Ar)	198	Marzoli et al. (1999)
Lower Jurassic (Ar/Ar)	200±6	Barros et al. (2007)

#### 4.3 GEOPHYSICAL DATA

In this section, we describe how the gravity data were obtained and provide specific information about grid size and steps to reach the residual gravity anomalies.

##### 4.3.1 Bouguer anomaly

Bouguer anomaly data were collected from the online platform of the International Centre of Global Earth Models (ICGEM). This website provides topographic and bathymetric data, as well as gravity data from a variety of satellite models. For this work, we select the EIGEN-6C4 model, which presents the highest degree of spherical harmonic expansion of the gravity field. This model is also a combination of land, marine and satellite data. First, we select a window size in longitude and latitude, and then we convert these data to metric coordinates (i.e., UTM).

For this work, we choose an area where the coordinates range from longitude  $-64^{\circ}$  to  $-49^{\circ}$  (east) and from latitude  $-16^{\circ}$  to  $-9^{\circ}$  (north). Additionally, we note the grid step with a resolution of  $0.05^{\circ}$ , which means that there is a measurement of the Bouguer anomaly every 5 km inside the grid area, totalling 170841 points. Then, we convert the geographic coordinates to metric coordinates, which is necessary to apply any geophysical procedure (i.e., modelling and inversion).

The Bouguer anomaly map is illustrated in Figure 7. We can observe a northward-striking, elongated and positive anomaly at approximately  $57.5^{\circ}$ . This signature is associated with high-density values in the Parecis Basin. We also note negative areas near the positive anomalies in the central part of the map, probably associated with igneous intrusions, which extend northward. In addition, the data amplitude is not very large, and the minimum and maximum values are close, which means that the positive and negative density contrasts are small. Moreover, the last view shows that the Bouguer anomaly exhibits good behaviour; i.e., there are no abrupt changes. This setting is very important since we use robust polynomial fitting. In other words, fitting a polynomial to a very irregular anomaly is difficult; thus, the better the behaviour of the data is, the better the results.

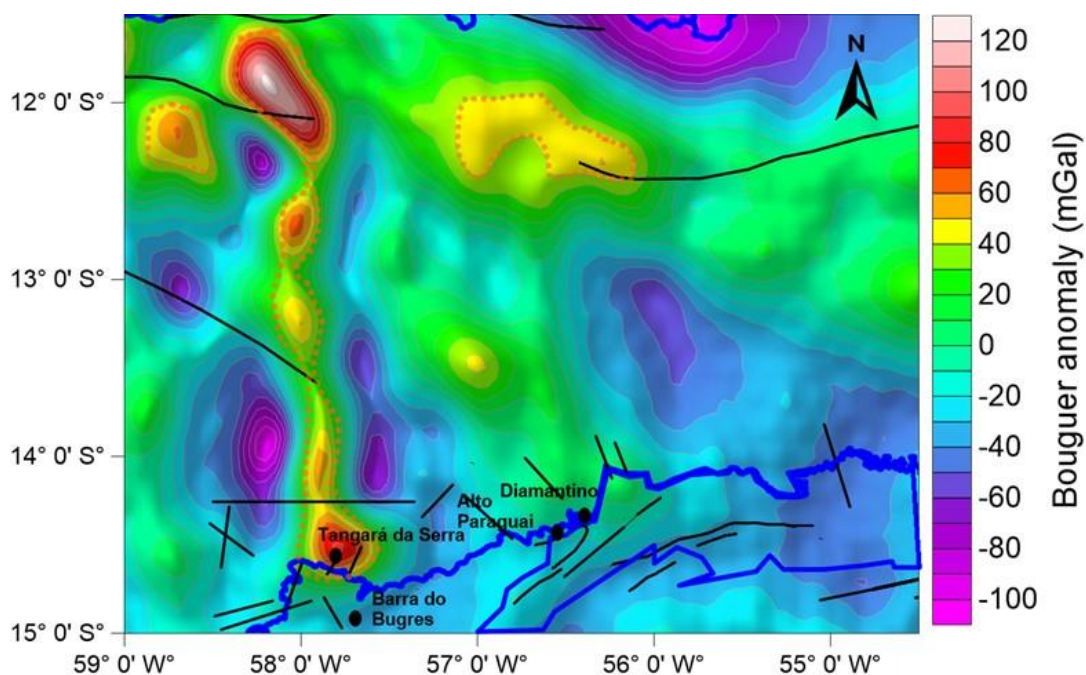


Figure 3 - Observed Bouguer gravity anomalies using the WGS84 reference ellipsoid and longitudinal selection grid (-W58.8° to -E54° and -N11.5° to -S15°).

#### 4.3.2 Residual gravity anomaly

Among several techniques to determine the regional-residual gravity field, we select the robust polynomial fitting approach proposed by Beltrão *et al.* (1991). In this method, the regional field exhibits good behaviour and can be approximated by a low-order polynomial surface, which is defined in the horizontal coordinates and represents the set of polynomial coefficients. Mathematically, this polynomial is calculated by minimizing the Euclidean norm between the observed data and the predicted data (i.e., the misfit) in the least squares sense. However, these authors use a robust procedure based on diagonal matrix elements to reduce the amplitude distortion. Once the observed signal is fitted, the residual anomaly can be obtained by subtracting the regional anomaly from the observed signal. More in-depth discussions about this method and some applications can be found in Ribeiro Filho (2018) and Ghoms (2020).

The residual anomaly (Fig. 8) is calculated by the Beltrão *et al.* (1991) method, as previously explained. We select polynomials of fifteen degrees for the regional anomaly data to verify the lowest misfit. First, we remove a linear trend from the Bouguer data; next, we proceed with Beltrão's method for polynomials from the 4th to the 15th degree and then apply the separation. The regional anomaly of the 11th degree is chosen because this anomaly best recovers the geologic features and geophysical signatures. Figure 8 shows the residual obtained by subtracting the selected regional anomaly from the Bouguer anomaly data. In the residual map, on the other hand, we can see positive and negative anomalies, probably associated with rock density contrasts beneath the surface. Negative values of residual anomalies are associated with negative contrasts between sediments and basement basins. Besides that, positive anomaly values confined inside the sedimentary basin contours cannot be explained only by structural highs in the basement of the basin. These types of anomalies must be associated with the presence of massive bodies in these highs. In fact, from the residual anomaly, we interpret large volumes of basalt on the surface and below, highlighting the residual map with red dotted lines.

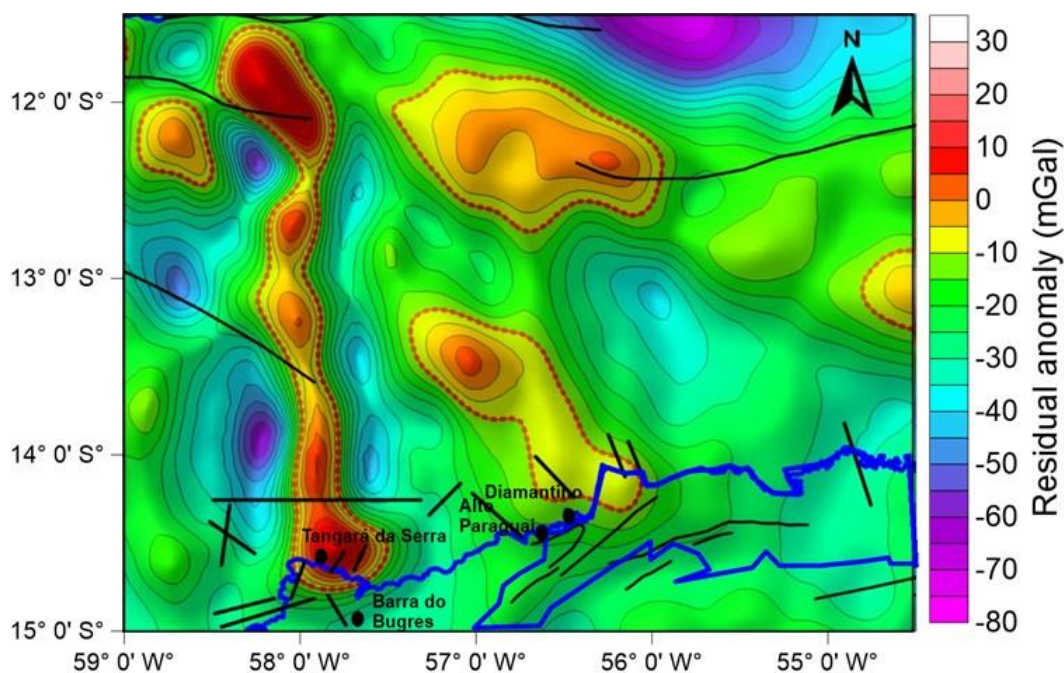


Figure 4 - Residual gravity anomalies showing the gravity highs and lows in southwestern Tocantins Province and southern Tapajós Province. The orange dotted lines represent anomalies with high gravity signatures associated with large basalt volumes in the subsurface and at the surface, contrasting with the low gravity anomalies in the basin. The continuous black lines represent faults and fractures that may provide structural controls on the percolation of magmatic fluids in the basin.

#### 4.4 RESULTS AND DISCUSSION

##### **4.4.1 Association of the CAMP continental tholeiitic flood basalts (CTFB) from gravity and geological interpretations.**

Residual gravity anomalies are associated with intracrustal density variations (see Fig. 8), which allows the identification of high-density rock signatures inside sedimentary basins. The highest positive values of the residual gravity anomalies occur in the Araras-Alto Paraguay and Parecis basins. Indeed, we can note that positive values of the residual gravity anomalies confined within a sedimentary basin cannot be explained only by horst basement structures. Alternatively, we should interpret these values as the result of high-density rocks associated with the CAMP basalts (Figs. 8 and 9). The use of residual gravity anomalies added to the analysis of previous geological data in the southern Amazonian Craton allows us to propose the following points: I) gravity signatures with high gravity values and elongation inside the Parecis Basin (N-S trend), associated with areas of both exposed and mapped basalts and mapped basalts that do not crop out (Montes-Lauar *et al.* 1994, Barros *et al.* 2007; Fig. 9, anomaly 1); and II) high gravity signatures, with NW-SE trends within the Araras-Alto Paraguay and Parecis basins (Fig. 9, anomaly 2), which are probably the results of basalts that do not crop out and related to possible occurrences of CAMP basalts.

There are mapped basalts, located in the Emal Unit of the Itaipu mine at Barra do Bugres that present low gravity signatures compared with other anomalies related to the basalt signature of the CAMP (anomalies 1 and 2). The relatively low gravity signatures at these sites may be related to the reduced thickness of the basalts due to relatively intense erosion of these rocks (dykes from 2 to 10 metres). Furthermore, identified occurrences of previously mapped basalts next to Tangará da Serra do not present a visible signature on the residual gravity anomaly. This extremely low gravity signature is incompatible with the gravity highs from high-density CAMP basalts, as well as with other sites having low gravity signatures. Deeper detailed geological and geophysical studies are needed for an accurate interpretation.

The Araras-Alto Paraguay Basin displays elongated N-S- and NW-SE-trending gravimetric signatures similar to the elongated N-S-trending gravity signatures of CAMP basalts of the Tapirapuã Formation. This correlation allows the discovery of other CAMP occurrences from the residual gravity anomaly interpretation in the southern Amazonian Craton and an interpretation of the tectono-magmatic evolution of this region (Fig. 10).

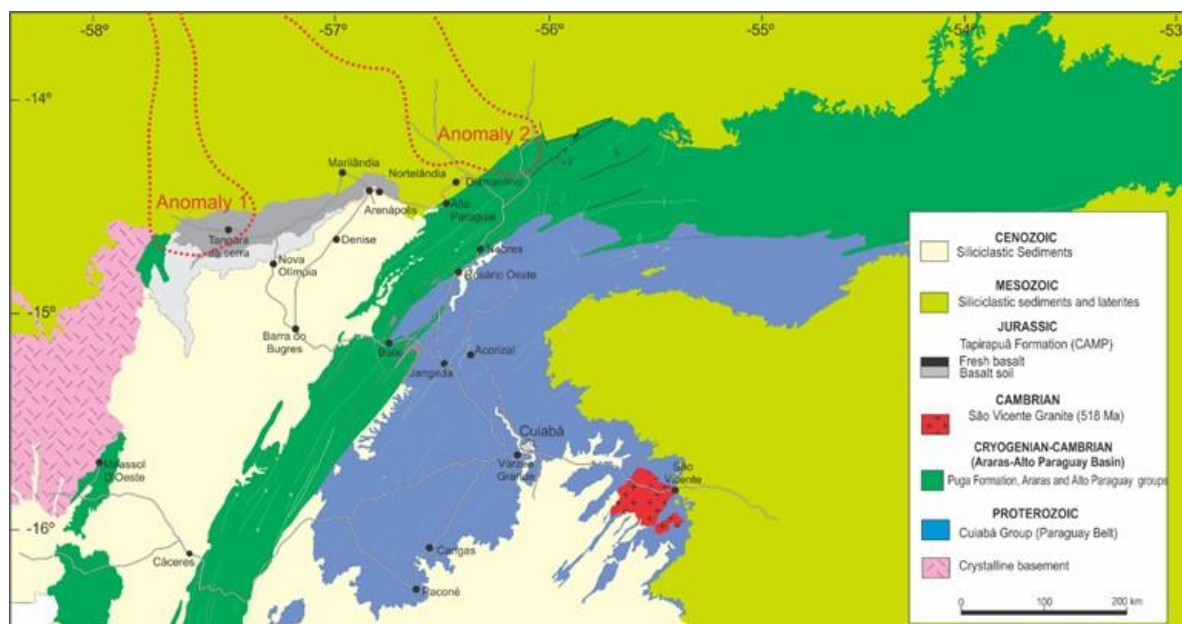


Figure 5 - Geological map showing the location of the CAMP basalts in the southern Amazonian Craton. Note the occurrences of the exposed CAMP basalts and those interpreted from the residual gravity anomalies (dashed and dotted polygons, anomalies 1 and 2).

#### 4.4.2 Tectonomagmatic evolution from residual gravimetric anomalies and geological data interpretations

Sub-lithospheric activity beneath the South American Platform originating from mantellic processes has promoted the formation of CAMP basalts in the southern Amazonian Craton (Almeida *et al.* 2000; Fig. 10A). Pangea rifting at approximately 225-220 Ma led to the production of large volumes of basaltic rocks during the first reactivation sub-phase of the South American Platform from the Late Triassic-Jurassic onwards (Marzoli *et al.* 1999, Almeida *et al.* 2000, Zalán 2004, McHone 2006; Fig. 10B). The large volumes of basaltic rocks are related to the CAMP event (c. 200-202 Ma) with peak activity at approximately 201 Ma, represented by the intrusive (sills and dykes) and/or extrusive (lava flows) rocks formed in the Paleozoic Parecis and late Cryogenian-Ordovician Araras-Alto Paraguay basins in the southern Amazonian Craton. Extensional fractures and faults formed during the opening of the Atlantic Ocean acted as pathways for CAMP basaltic magmas (Santos *et al.* 2017, Nogueira *et al.* 2019; Fig. 10B). Thermal subsidence in the southern Amazonian Craton took place after the Sinemurian (c. 190-160 Ma) caused by lowering of the isotherms and progressive decreases in the heat flow in the region. The opening of the Central Atlantic and the Waldenian reactivation (e.g., Zalán 2004) possibly favoured the deposition of Upper Jurassic eolian sediments in the Parecis Basin (Bahia *et al.* 2006, Batezelli *et al.* 2014, 2016). The extensional events related to the opening of the South Atlantic (c. 140-110 Ma) and Equatorial Atlantic (c. 113-95 Ma), as well as the first tectonic event related to the Andean orogeny (c. 88 Ma), which took place at the Turonian-Coniacian boundary (Peruvian orogenic phase), favoured an increase in the accommodation space expressed by the deposition of the Late Cretaceous Salto das Nuvens and Utariti formations in the Parecis Basin, overlying the CAMP basalts (Jaillard *et*

al. 2000, Zalán 2004, Bahia 2007, Granot and Dymant 2015, Menegazzo *et al.* 2016, Rubert 2019) (Fig. 10C). In the Late Cretaceous and early Cenozoic (c. 72-65 Ma), the southern Amazonian Craton experienced uplift and extreme erosion related to a new contractional pulse of the Peruvian orogeny that occurred in the late Campanian (Jaillard *et al.* 2000, Menegazzo *et al.* 2016). This orogenic event caused partial remobilization of deposits in the confluence zone between the basins. The exposure of the most superficial portion of the CAMP led to partial removal, contrasting with the low topography modelled for rocks of the late Cryogenian-Ordovician Araras-Alto Paraguay Basin. In this region, the root of this geotectonic structure is exposed, and the magmatic conduits of the CAMP may be observed (Fig. 10D).

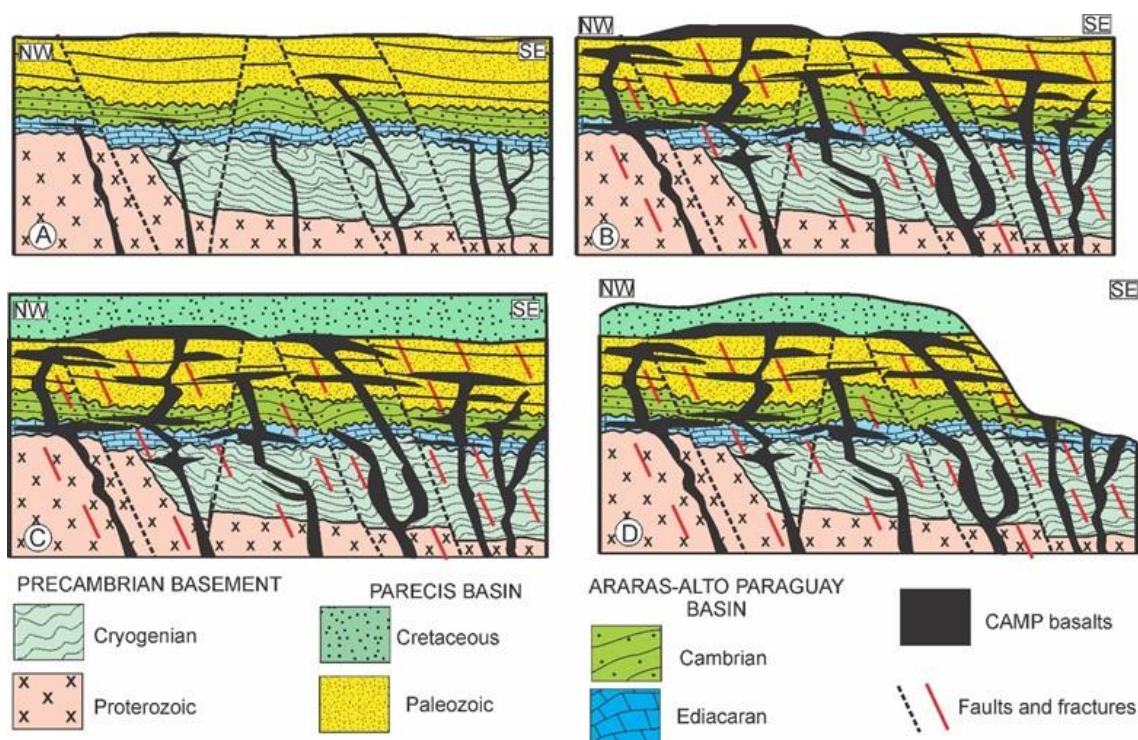


Figure 6 - Tectonomagmatic evolution of the CAMP in the southern Amazonian Craton. (A) Initial phase before Pangea break-up (c. 250 Ma). (B) Increase in basalt volume due to CAMP intumescence, Pangea break-up and opening of the Central Atlantic Ocean (c. 201-190 Ma). (C) Extensional event related to the opening of the South Atlantic (c. 140-110 Ma) and Equatorial Atlantic (c. 113-95 Ma), as well as the first tectonic event related to the Andean orogeny (c. 88 Ma) that favoured the deposition of Cretaceous sediments in the Parecis Basin (c. 88-72 Ma); (D) Uplift of the southern Amazonian Craton, leading to the erosion of the Cretaceous cover and CAMP basalts and exposing most of the magmatic conduits located in the Araras-Alto Paraguay Basin and basement rocks (c. 72-65 Ma). (Geological framework based on Santos *et al.* 2017, Nogueira *et al.* 2019).



#### 4.5 FINAL REMARKS

In this work, the analysis of existing geophysical and geological data allowed us to obtain surface and subsurface evidence for the CAMP event in the southern Amazonian Craton. The Paleozoic Parecis and late Cryogenian-Ordovician Araras-Alto Paraguay basins were the main candidates to test this methodology with reasonable responses. The CAMP basalts in this area probably correspond to intrusive (dykes or sills) and extrusive (lava flows) rocks coinciding with the N-S- and NW-SE-trending gravity signatures. Based on these data, we propose a tectono-magmatic evolution for this part of the Amazonian Craton, which includes 1) an initial phase before the rupture of Pangea (c. 250 Ma); 2) a progressive increase in the volume of basalts due to the rupture of Pangea, causing expansion from the CAMP basalts in the crust concomitant with the opening of the Central Atlantic Ocean; 3) an extensional event related to the opening of the South Atlantic and Equatorial Atlantic, as well as the first tectonic event related to the Andean orogeny, leading to the deposition of Cretaceous sediments in the Parecis Basin; and 4) the exposure of the southern Amazonian Craton, causing erosion of Cretaceous rocks, CAMP basalts and older rocks, exposing only the magmatic channels. We emphasize that studying the gravimetric signal in isolation would make the description and correlation of the high gravimetric signatures with the occurrences of the CAMP impracticable. However, with the data obtained for the formations (through a survey of previous bibliographies related to the study area), in combination with the gravimetric method (bodies with this signature within a basin indicate extremely dense magmatic bodies) and the proximity of the Araras-Alto Paraguay Basin to the Parecis Basin basalts, we can infer that the signatures inside the Parecis Basin are related to the magmatism of the CAMP. Thus, the correlation among geochronology, bibliographic surveys and gravity modelling is satisfactory, although future studies including magnetometry data, which can show CAMP intrusions in the region in more detail, may better clarify this relationship.

#### **Acknowledgement**

The authors thank Andrea Marzoli and the anonymous reviewer for the corrections that improve the final text. The acknowledges are extensive to the Coordenação de Aperfeiçoamento de Pessoal de Nível Superior (CAPES, grant 001) and the Conselho Nacional de Desenvolvimento Científico e Tecnológico (CNPQ) by the scholarship funding that supported for the master's degree and the current Ph.D. program of the first author.

**CAPÍTULO 5 THE CRUSTAL ELASTICITY AND GRAVIMETRIC DATA IN THE STRATIGRAPHIC EVALUATION OF THE JURASSIC CAMP SUCCESSION IN THE SOLIMÕES, AMAZONAS E PARNAÍBA BASINS, NORTHERN BRAZIL.**

**Gabriel Leal Rezende <sup>a</sup>, Afonso Cesar Nogueira <sup>a</sup>, Nelson de Lima Ribeiro-Filho <sup>b</sup>,  
Cristiano Mendel Martins <sup>b</sup>, Renato Sol Paiva de Medeiros <sup>a</sup>, Alexandre Ribeiro  
Cardoso, Davis Carvalho de Oliveira <sup>a</sup>**

*<sup>a</sup>Programa de Pós-Graduação em Geologia e Geoquímica (PPGG), Instituto de Geociências, Universidade Federal do Pará, 66075-110, Guamá, Belém, Pará, Brazil;*

*<sup>b</sup>Curso de Pós-Graduação em Geofísica (CPGF), Geociências, Universidade Federal do Pará, 66075-110, Guamá, Belém, Pará, Brazil;*

*<sup>c</sup> Universidade Estadual de Campinas (UNICAMP), Avenida Albert Einstein, n° 901 - Cidade Universitária "Zeferino Vaz" Barão Geraldo - Campinas, SP - CEP: 13083-852.*

**\*Article submitted to *gondwana research***

**Abstract**

Geological studies combined with geophysical techniques are widely utilized to highlight and characterize Central Atlantic Magmatic Province (CAMP) gravimetric anomalies across Northern Brazil, including the Amazon, Solimões and Parnaíba basins. Forward gravity modeling interpretations from the residual gravity anomalies in these basins enhance the understanding of CAMP's subsurface distribution, offering valuable data for geophysical interpretations of geological sources. This study's results supported by surface geological information, primarily outcrop-based stratigraphic data. Furthermore, the research calculated and determined the elastic thickness ( $T_e$ ) map of these basins, which Cross-correlation between observed and calculated gravity signals produced the elastic thickness map of the studied areas. The high gravity values are related to high-density rocks correlated to the continental tholeiitic flood basalts of CAMP. Penatecaua magmatism's subvolcanic bodies in the Amazon and Solimões basins gradually uplifted Eastern Gondwana. In contrast, the Parnaíba basin's Mosquito magmatism is characterized by extrusive volcanism interspersed with intertrap sediments. Data from the elastic thickness map, Moho depth, and residual gravimetric signal indicate a thinner crust in the Parnaíba basin, favoring magmatic eruptions induced by a hot spot on the basin's western edge. Conversely, in Amazon and Solimões basins present denser and thicker crust, accumulating magma primarily as sills, leading to crustal densification and

increased resistance to breakup due to CAMP swelling. The Parnaíba Basin experienced three magmatic pulses at intervals of approximately 1 Myr, alternating with the development of aeolian-fluvial-lacustrine systems (intertrap sediments) during non-magmatic periods, indicating short intervals of magmatic resumption and cooling in the CAMP, contrasting with the longer and continuous magmatism in the Amazon and Solimões basins, which lack intertrap deposits. The possible extent of Jurassic magmatism, the basin rheology of igneous body intrusion, and the history of thermal subsidence were extremely relevant for the control depositional systems before, during, and after the CAMP event.

**Keywords:** camp; forward gravity modeling; gravity anomaly; crustal thickness; Pangea.

## 5.1 INTRODUCTION

The fragmentation of Pangea and the subsequent opening of the Central Atlantic Ocean were accompanied by the formation of Large Igneous Provinces (LIPs), including the Central Atlantic Magmatic Province (CAMP) (Marzoli *et al.* 1999). This process evolved into the construction of the Mid-Atlantic Ridge, which began in the Early Jurassic and continues to the present day (Coffin and Eldholm 1993, Montes-Lauar *et al.* 1994, Olsen 1999, Oyarzun *et al.* 1997, Wilson 1997, Baksi and Archibald 1997, Mizusaki *et al.* 2002, Saunders 2005, Mchone 2006, Barros *et al.* 2007, Martins *et al.* 2008, Bensalah *et al.* 2011, Schaller *et al.* 2012, Davies *et al.* 2017, Svensen *et al.* 2018, Korte *et al.* 2019). CAMP is present across all Atlantic-bordering continents: North America, South America, Africa, and, to a lesser extent, Europe. It prominently features radiating dyke swarms, extensive sill provinces, and associated volcanic sequences (cf. Jourdan *et al.* 2009 and references therein).

In large rift basins, CAMP consists of multiple pulses of volcanic activity characterized by continental tholeiitic basalts and the formation of sills and dikes intruding into sedimentary deposits (Marzoli *et al.*, 2018). This extensive volcanism, occurring from the Late Triassic to Early Jurassic, was accompanied by significant oceanic and atmospheric geochemical changes, triggering notable paleoenvironmental, paleoclimatic, and paleogeographic shifts such as climate warming, anoxic events, and ocean acidification (Marzoli *et al.* 1999, Kiessling *et al.* 2009, Schoene *et al.* 2010, Whiteside *et al.* 2010, Ruhl *et al.* 2011, Greene *et al.* 2012, Ruiz-Martínez *et al.* 2012, Schaller *et al.* 2012, Kasprak *et al.* 2015, Davies *et al.* 2017, Korte *et al.* 2019, capriolo *et al.* 2020).

Large volumes of continental tholeiitic basalts have been widely identified in several sedimentary basins in Amazonia, Northern, and Central South America (Basei 1974, Santos *et al.* 1975, Bizinella *et al.* 1980, Silva 1980, Melfi *et al.* 1988, Rocha-Campos *et al.* 1998, Renne *et al.* 1992, Góes and Feijó 1994, Montes-Lauar *et al.* 1994, Barros *et al.* 2007, Vaz *et al.* 2007, Merle *et al.* 2011, Abrantes Jr 2016; Fig. 1A). These include the Solimões and Amazonas Basins, represented by the Penatecaua magmatism of the Lower Jurassic ( $190 \pm 20$  Ma); the Parnaíba Basin, represented by the Mosquito Formation of the Upper Triassic-Lower Jurassic ( $199 \pm 2.45$  Ma); and the Parecis Basin, represented by the Tapirapuã and Anarí formations of the Lower Jurassic ( $197\text{-}200 \pm 6$  Ma).

Geophysical studies in the Amazon region (Amazonas, Solimões, Parnaíba, and Parecis basins) have indicated large Bouguer gravity anomalies, particularly in the Amazonas Basin, which suggest the presence of dense ultrabasic rock masses within the acidic basement (Nunn and Aires 1988, Bahia *et al.* 2007, Sanchez-Rojas 2012, Rosa *et al.* 2016, Rezende *et al.* 2021). These are related to continental crust thinning, mantle upwelling, and basin genesis (Linsser 1958, 1974, Rezende *et al.* 2021). Gravitational studies have facilitated the delineation of platforms and the deep depositional axis of the basin. The deepest structures of these basins have been primarily inferred from geological data (Cordani *et al.* 1984, Montes Lauer *et al.* 1994, Bahia 2007, Barros *et al.* 2007, Davies *et al.* 2017, Korte *et al.* 2019, Tczeck *et al.* 2019, Nogueira *et al.* 2021) and from geophysical data, which are still underexplored (Feng *et al.* 2004, Bahia *et al.* 2007, Assumpção *et al.* 2013a, b, Daly *et al.* 2014, Uieda and Barbosa 2016, Trosdorf *et al.* 2018, Heilbron *et al.* 2018, Soares *et al.* 2018, Tczeck *et al.* 2019, Rezende *et al.* 2021).

The evaluation of deep structures to understand the Central Atlantic Magmatic Province (CAMP) processes in sedimentary basins has been more effective using the mapping of the effective elastic thickness (ET). Elastic thickness is a fundamental concept that describes the depth within the Earth's crust where elastic deformations occur in response to applied forces (Turcotte, 2002; Watts, 2001). In simple terms, it is the depth to which rocks behave as an elastic material, capable of reversible deformation under pressure without undergoing permanent rupture (Artemieva 2009, Watts 2010). Understanding the behavior of elastic thickness in sedimentary basins is crucial for assessing the potential for natural resource exploration.

In sedimentary basins, sediment accumulation occurs over geological time. Consequently, elastic thickness influences the subsidence and deformation of underlying layers under the weight of deposited sediments, directly affecting the formation and evolution of significant geological structures (Castro 2022, Ribeiro-Filho 2023). In regions where magma eruptions occur, elastic thickness affects the Earth's crust response to magma intrusion, influencing the formation of structures such as dykes, sills, and plutonic intrusions (Artemieva 2009, Turcotte 2002). Analyzing elastic thickness in sedimentary basins where magmatic intrusions occur allows for an understanding of the extent and geometry of these intrusions and the interaction between magmatic bodies and surrounding sedimentary layers (Kearey 2009).

The geophysical evaluation, supported by geological data, of the Solimões, Amazonas, and Parnaíba basins, will enable a comprehensive understanding of how the structuring of these geotectonic segments facilitated the accommodation of CAMP magmatic bodies. Some geotectonic features of the Parecis Basin will also be reinterpreted using previous studies and their relationship with CAMP. Gravity anomalies will be used in combination with the assessment of crustal elasticity to define the possible extent of this magmatism, the rheology of the basin in accommodating igneous bodies, and the thermal subsidence history that largely controlled the depositional signature before, during, and after CAMP.

Additionally, the study will discuss the origin of the main structures generated during the various phases of development of these basins from the Precambrian to the Phanerozoic, such as structural arches, fault systems, and structural domes influenced or reactivated during the emplacement of CAMP in the Mesozoic. The timing of magmatic pulses was tentatively estimated in succession, recording lava outpouring events that alternated with recurrent installation of depositional systems during periods without magmatic activity. Finally, this work aims to unravel the influence of CAMP on the Amazonian basins, providing new insights into the initial geological scenarios in South America that led to the separation of Pangea.

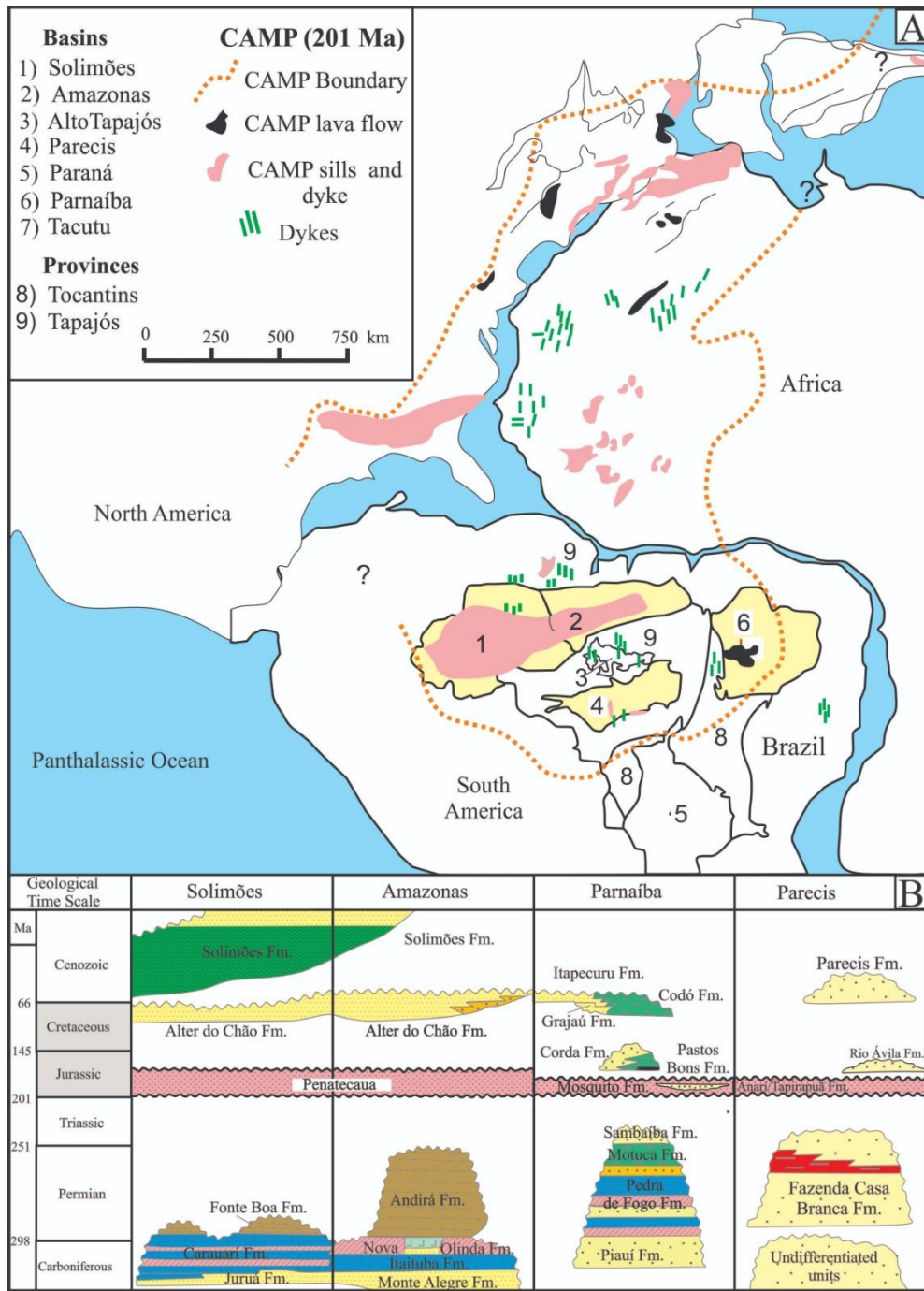


Figure 1- CAMP occurrences in West Gondwana (adapted from McHone, 2000). A) Distribution of the CAMP on the continents, mainly in the studied areas (Parnaíba, Solimões, and Amazonas basins) of the Amazon Cratón. B) Stratigraphic map of Amazon basins with volcanic rocks related to the CAMP (modified from Milani and Zalán 1999, Nogueira *et al.* 2021). Widespread unconformities are documented in the Solimões, Amazonas, Parecis, and Parnaíba basins with predominantly subvolcanic rocks.

## 5.2 GEOLOGICAL SETTING

### 5.2.1 The Solimões e Amazonas basins

The Meso-Cenozoic Amazonian retroarc foreland basin extends across western South America, encompassing the Amazonas-Putumayo, Oriente, Pastaza-Marañón, Huallaga, Madre de Dios, Beni-Mamore, Solimões, and Acre basins, located in Colombia, Ecuador, Peru, Bolivia, and Brazil respectively (Caputo *et al.* 1990, Roddaz *et al.* 2006, Hoorn *et al.* 2010, Louterbach *et al.* 2018, Hurtado *et al.* 2018). During the Miocene, the depositional environment of this basin was characterized by the Pebas-Solimões mega-wetland system, composed of lakes and swamps influenced by fluvial and marginal marine processes (Wesselingh and Salo 2006, Cozzuol 2006, Latrubesse *et al.* 2010, Hoorn *et al.* 2010, Silva-Caminha *et al.* 2010, Nogueira *et al.* 2013, Leite *et al.* 2017). Significant interfluvial reliefs, such as the Fitzcarrald, Iquitos, and Purus arches, influenced Neogene Amazonian drainage and sediment distribution within the basin (Roddaz *et al.* 2005, Espurt *et al.* 2007, Nogueira 2008, Hoorn *et al.* 2010, Nogueira *et al.* 2013, 2021). Before the Miocene (c. 23 Ma), westward cratonic drainage in lowland Amazonia was captured by Andean rivers that flowed into lakes and coastal regions connected to the Maracaibo Lake, forming a seaway to the Caribbean Sea (Hoorn *et al.* 1995, Lundberg *et al.* 1998, Wesselingh and Salo 2006, Roddaz *et al.* 2010, Nogueira *et al.* 2013, Hurtado *et al.* 2018).

The Solimões Basin, oriented east-west, is situated in western to central Amazonia, between the Guianas and Brazilian shields (Wanderley-Filho *et al.* 2010). It is bounded by the Acre and Pastaza/Marañón basins to the west, separated by the Iquitos Arc, and the Amazonas basin to the east, separated by the Purus Arc (Fig. 1A). The sedimentary record of the Solimões Basin is characterized by multiple climatic changes, marine regressions and transgressions during the Paleozoic, and tectonic activities that promoted the subsidence and uplift of structural arcs (Caputo and Silva 1991; Fig. 1B).

The Paleozoic sequence in the Solimões Basin is divided into two sub-basins by the Carauari Arch, which controls the distribution and thickness of sedimentary successions, especially before the Pennsylvanian period (Wanderley-Filho *et al.* 2010). The Carauari Arch also influenced Cretaceous and Neogene deposition, represented by the Alter do Chão and Solimões formations, respectively, which are separated by a regional unconformity (Eiras *et al.* 1994). The Cretaceous Alter do Chão Formation corresponds to a high-energy fluvial system migrating westward, developed under a humid climate and extending from the Amazonas Basin to the sub-Andean basins (Caputo 1984, Mendes *et al.* 2012; Fig. 1B).



The Neogene tectonic history of the Solimões Basin and other basins in northern South America is marked by the uplift of the northeastern Andes, leading to the development of the sub-Andean fold belt due to plate tectonic readjustments (Hoorn *et al.* 1995). The eastern propagation of orogenesis from Andean activity induced a loading stage in the foreland Amazon system, resulting in the tectonic reactivation of structural arcs (Roddaz *et al.* 2005). The influence of the Iquitos Arch in these regions has been corroborated by sedimentological, pollen, and provenance analyses (Hoorn *et al.* 2010, Roddaz *et al.* 2005, Espurt *et al.* 2007, Horbe *et al.* 2013, 2019).

The Amazonas Basin, located in northern Brazil between the Amazonas and Pará states, is bordered by the Guiana Shield to the north, the Brazilian Shield to the south, the Gurupá Arch to the east, and the Purus Arch to the west (Cunha *et al.* 1994, Cunha *et al.* 2007, Matsuda *et al.* 2010; Fig. 1A). It exhibits an elongated and narrow WSW-ENE orientation, covering approximately 500,000 km<sup>2</sup>, with the current course of the Amazonas River representing the depositional axis (Cunha *et al.* 2007; Fig. 1A). The basin is intracratonic, developed on the Amazonas Craton, with sedimentary deposits reaching a thickness of up to 6 km (Wanderley Filho 1991, Cunha *et al.* 1994).

The sedimentary fill of the Amazonas Basin comprises two first-order sequences separated by a regional unconformity (Cunha *et al.*, 1994). The first sequence, dating to the Paleozoic, includes sedimentary deposits, while the second sequence, spanning the Mesozoic to Cenozoic eras, includes both sedimentary and volcanic deposits (Cunha *et al.* 1994, Cunha *et al.* 2007; Fig. 1B). The Paleozoic sequence consists of four second-order sequences: Ordovician-Devonian, Devonian-Tournasian, Neovisean, and Pennsylvanian-Permian. This sequence resulted from a subsidence event, with a marine transgression from the west causing the inundation of wind dunes in the Solimões Basin, surpassing the Purus Arch, and interconnecting the Solimões and Amazonas basins (Caputo 1984, Caputo and Silva 1990, Cunha *et al.* 1994, Matsuda *et al.* 2006, Matsuda *et al.* 2010, Silva 2019).

The Tapajós Group includes the Monte Alegre, Itaituba, Nova Olinda, and Andirá formations (Matsuda 2002). The Monte Alegre and Itaituba formations, basal units of this group with a Bashkirian age, comprise sandstones, siltstones, and dolostones from aeolian-fluvial environments, and limestones, dolostones, sandstones, siltstones, and evaporites from tidal flats and carbonate shelves (Matsuda 2002, Cunha *et al.* 2007, Matsuda *et al.* 2004). The upper units, Nova Olinda and Andirá formations, represent a regressive event in the Amazonas Basin (Cunha *et al.* 1994, Cunha *et al.* 2007). The Nova Olinda Formation, a coastal sabkha paleoenvironment, dates to the Moscovian age, while the Andirá Formation, consisting of

continental lake deposits, dates to the Asselian-Sakmarian age (Caputo *et al.* 1971, Cunha *et al.* 2007, Scomazzon *et al.* 2016).

### 5.2.2 The Parnaíba Basin

The Parnaíba Basin, located in the northern portion of the South American platform, is an extensive intracratonic basin covering over 600,000 km<sup>2</sup> (Fig. 1A). Its sedimentary fill reaches a maximum thickness of 3,500 meters, predominantly composed of Paleozoic sediments, with lesser volcanic contributions (Milani and Thomaz Filho 2000, Cordani *et al.* 2003, Brito Neves *et al.* 2004) (Fig. 1B). The basin's thermal subsidence occurred within a broad intracratonic region consisting of igneous and metamorphic rocks from the Archean to the Neoproterozoic, bounded by structural arches and mobile belts reworked during the Pan-Afro-Brazilian tectonic event (Cordani *et al.*, 2003; Almeida and Carneiro, 2004).

The basin's cratonic phase was characterized by extensive sedimentation during regional transgressive-regressive cycles, organized into supersequences (Vaz *et al.* 2007). Prior to the opening of the Atlantic Ocean, extensional stresses reactivated basement faults, which served as primary conduits for the emplacement of mantle-derived magmas in the basin (Mizusaki *et al.* 1998, Milani and Thomaz Filho 2000).

The initial depocenter of the Lower Paleozoic Basin migrated to the central part of the basin domain during the Carboniferous-Lower Jurassic period and shifted northwestward again in the Cretaceous (Vaz *et al.* 2007). This migration suggests a temporal relationship with the Mosquito and Sardinha magmatic events, respectively. Historically, the basin domain was more extensive than it is today, with possible connections to the Amazonas and Paraná basins, and potentially to the Congo Basin in Africa (Melo 1988).

Currently, the Parnaíba Basin exhibits a pronounced fault contact with the Tocantins Province (Araguaia Belt) to the west (Daly *et al.* 2014), a tectonic/erosive contact with the Tocantins Province to the south, and a gentle sedimentary contact to the north with the São Luís Craton and the São Francisco Craton to the southeast. On the eastern edge, the basin boundary with the Borborema block is erosive, exposing basal Silurian sediments. The basement of the Parnaíba Basin is a collage of at least three main domains—Amazon, Parnaíba, and Borborema blocks—marked by strong contacts between them (Daly *et al.* 2014, Castro *et al.* 2014, Soares *et al.* 2018).

The evaluation of deep structures to understand the CAMP processes in sedimentary basins has been more effective using the mapping of effective elastic thickness. Elastic thickness is a critical concept describing the depth within the Earth's crust where elastic deformations occur in response to applied forces (Turcotte 2002; Watts 2001). It indicates the depth to which rocks behave elastically, capable of reversible deformation under pressure without permanent rupture (Artemieva 2009, Watts 2010). Understanding elastic thickness in sedimentary basins is crucial for assessing natural resource exploration potential.

In sedimentary basins, sediment accumulation over geological time affects the elastic thickness, influencing subsidence and deformation of underlying layers under the weight of sediments (Chang and Liu 2019). This, in turn, affects the formation and evolution of significant geological structures (Castro 2022, Ribeiro-Filho 2023). In areas of magma eruptions, elastic thickness influences the crust's response to magma intrusion, impacting the formation of structures such as dykes, sills, and plutonic intrusions (Artemieva 2009, Turcotte 2002).

Geophysical evaluations supported by geological data of the Solimões, Amazonas, and Parnaíba basins help understand how these geotectonic segments accommodated CAMP magmatic bodies. We use the interpretation of the residual gravity anomalies and assessing crustal elasticity to define the extent of magmatism, the rheology of basins in accommodating igneous bodies, and the thermal subsidence history controlling depositional signatures before, during, and after CAMP. Additionally, the origin of main structures generated during various developmental phases of these basins, from Precambrian to Phanerozoic, is discussed, including the influence of CAMP on structural arches, fault systems, and domes during the Mesozoic. This analysis proposes to unravel the influence of CAMP on Amazonian basins, providing new insights into the initial scenario in South America that led to the separation of Pangea.

### 5.3 METHODOLOGY

An extensive analysis was undertaken, utilizing a comprehensive compilation of geological data that encompassed tectonic processes, magmatic events, stratigraphic sequences, depositional systems, and weathering histories across several basins. This study aimed to enhance understanding of magmatic episodes and their impact on basin subsidence. Advanced techniques were employed for data processing, modeling, and interpreting gravitational data, enabling the identification and mapping of subsurface magma bodies.

The survey unveiled the spatial distribution of these magma bodies and their profound influence on local geological evolution over extended periods. Horizontal characteristics of these bodies were delineated and estimated through the analysis of high-resolution satellite data. This method facilitated the identification of residual gravitational anomalies, which were subsequently interpreted using forward gravitational modeling techniques.

Moreover, a meticulous assessment of crustal elasticity was conducted, providing crucial insights into the extent and rheological properties of magmatism within the studied basins. This approach not only enhanced our understanding of the deep-seated geological processes but also contributed significantly to the broader understanding of regional geological dynamics and their implications for basin evolution and resource exploration.

#### 5.3.1 Determination of the Residual anomaly

The residual gravity data were obtained subtracting the observed Bouguer Anomaly and the calculated gravity anomaly from crustal attributes, similar to the one proposed by Ghoms (2020); Ghoms (2021); Rezende et al (2021); Ghoms (2022), Fig. 2. For this work, we choose an area where the coordinates range from 83°W to 31°W of longitude and from -22°S to 16°N of latitude. Additionally, we selected the grid step with 0.05° of data resolution, which means that the observed Bouguer anomaly and the calculated anomaly were evaluated at 5 km approximately.

### 5.3.1.1 Gravity forward problem from elementary prisms

Initially, we establish a topography preliminary model, considering the geometry of the study area together the depth of the Moho obtained of the Uieda and Barbosa. Subsequently, the area of interest is discretized into a grid of vertical prisms, where the top of each prism coincides with the topographic surface and the base corresponds to the Moho depth. Then, we assign to each prism a standard density value ( $2,673 \text{ g/m}^3$ ) based on the lithology and expected composition, varying according to local geological characteristics. We compute the gravitational effect of the prism ensemble for each desired observation point using the equations proposed by Nagy (1966) and Plouff (1976). After this step, the effects that are summed by the equation above (2) obtain the predicted gravity signal for the study area (Fig.2B) Finally, the predicted gravity signal is compared with the observed gravity data (Fig.2A) to calculate the residual gravity signal by subtracting the observed data from the predicted data. This residual signal (Figs.2C and 5) represents the effect of all existing small and medium features

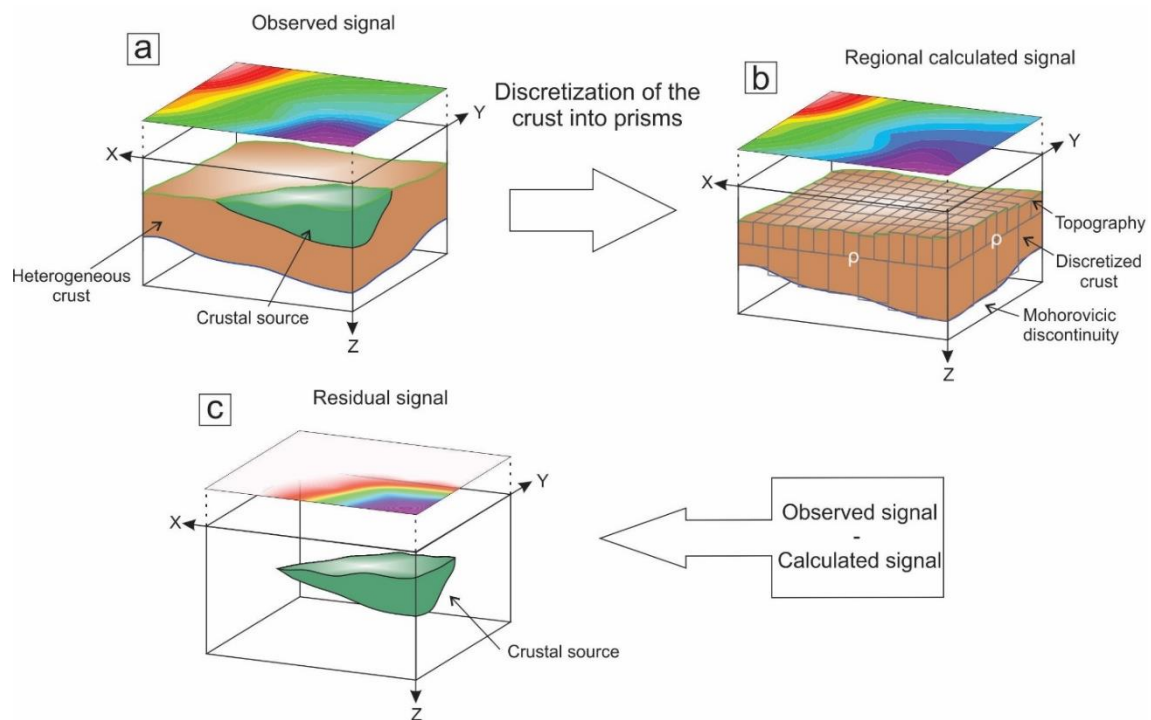


Figure 2 - Layout of the methodology for obtaining the residual gravity signal. (a) Observed gravity signal. (b) Predicted gravity regional signal from the discretization of the prismatic model. (c) Residual gravity Signal.

### 5.3.2 Elastic thickness determination

We will briefly describe the three steps for determining the elastic thickness. Firstly, we calculate the depth of the Mohorovicic discontinuity for a set of elastic thickness values, as described by Wienecke (2007). Subsequently, for each value of  $T_e$ , we compute the residual gravity signal considering two scenarios: the surface described by topography and the standard Moho, and the surface described by topography and Moho calculated from  $T_e$ . Then, we calculate the cross-correlation between the observed gravity signal and the calculated gravity signal. The highest correlation value is directly related to the elastic thickness and the depth of the Moho associated with deformation. It is worth noting that a more detailed description can be found in Ribeiro-Filho (2023).

#### 5.3.2.1 Moho depth calculation from deflection

Consider a high-resolution dataset of topographic data and observed gravity data. According to the principles of elastic flexure, any topographic load causes local and regional deformation in the Earth's crust, where such vertical deformation can be calculated from the solution of a fourth-order partial differential equation. Therefore, the analytical solution calculates the crustal deformation for a regular grid of points along the study area, allowing for a detailed representation of the elastic response of the crust (Wienecke, 2007).

Once the flexure of the Moho is calculated, it is possible to determine the final depth of the Moho, as this depth is obtained as the sum of the deformation and the reference depth. Finally, these systematic and analytical procedures provide a rigorous approach to estimating flexural rigidity and understanding geodynamic processes.

#### 5.3.2.2 Mapping elastic thickness to effects of correlation

After calculating a value for the Moho depth and elastic thickness, we created a grid of  $T_e$  values at a set of discrete points, enabling a systematic evaluation of the influence of elastic thickness relative to the observed gravity data. Subsequently, a moving correlation was performed between the observed gravity data and the data calculated from the direct prism modeling. In this case, for a  $T_e$  value, we computed a correlation. This procedure was characterized dynamically, considering not only a single comparison but rather a continuous scan of the observed and calculated data along the grid. The optimal elastic thickness for the specific point corresponded to the highest correlation coefficient, also associated with the best value for the Moho depth.

## 5.4. RESULTS

### 5.4.1. The Jurassic succession in Amazon Basins

The eastern part of Gondwanaland experienced gradual uplift during the Jurassic due to notable magmatic intrusions causing swelling in the central Amazon basins, evidenced by subsurface Penatecaua magmatism in the Amazonas and Solimões basins. These CAMP volcanic deposits were evaluated from a stratigraphic point of view using the formal nomenclature of the units, previous sedimentological description, and paleoenvironmental inferences mainly for the intertrap deposits from the Paranaíba Basin (cf. Nogueira *et al.* 2021). The Paleozoic and Mesozoic intervals in these basins were disturbed by the accumulation of magma in the subsurface that caused uplift and erosion forming basin-scale unconformities. Subvolcanic intrusive bodies are exposed in the form of sills and dikes in the Paleozoic and Mesozoic stratigraphic succession following the tabular strata mainly in the western Amazonia (Fig. 3). In the Parnaíba Basin, the Jurassic Mosquito Formation is well exposed (Fig. 3 and 4) and has been interpreted as a series of lava fissural outpouring interbedded with intertrap deposits (cf. Nogueira *et al.* 2021).

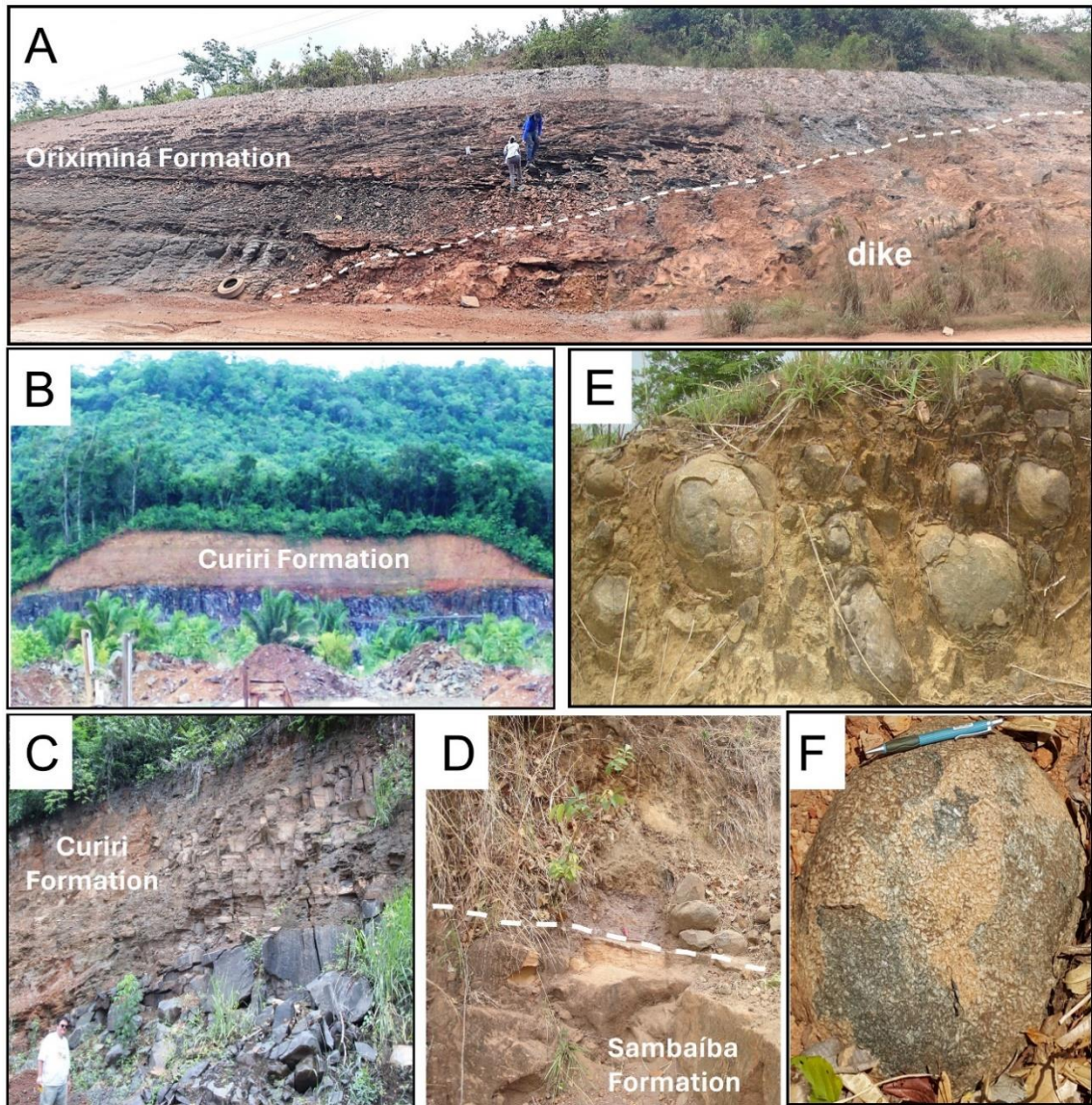


Figure 3 - The CAMP basalts in Amazônia. A) Dike cutting organic matter-rich shale. B) and C), stratified sandstone and siltstone intruded by sill in Monte Alegre Dome. D) Contact of sill and eolian deposits. E) Spheroidal weathering. F) Feldspar phenocrystals in gabbroic texture from the central portion of the volcanic body. A-C, Penatecaua Formation, D-F, Mosquito Formation.



The intertrap deposits are sandwiched by basalts and consist of pebbly sandstone, fine- to coarse sandstone with even parallel and trough cross stratifications, laminated siltstone, massive sandstone, and pelite/sandstone rhythmite (Fig. 4). The poorly sorted angular to sub-rounded grains are constituted predominantly of basaltic fragments and quartz. These deposits are representative of an ephemeral braided river, and pond/shallow Lake Paleoenvironments (Nogueira *et al.* 2021). In the Western Parnaíba Basin, the quiescent intervals between lava flow episodes formed extensive volcanic plains, whereas wet desert settings were developed concomitant with fluvial channels with subaqueous dunes and sand sheets were incised into the basaltic substrate (Fig. 5). The heat flow and hydrothermal activity of volcanic rocks increased the devitrification of glassy clasts, releasing silica and precipitating low-temperature authigenic mineral assemblages typical of early diagenetic-hydrothermal stage (Nogueira *et al.* 2021).

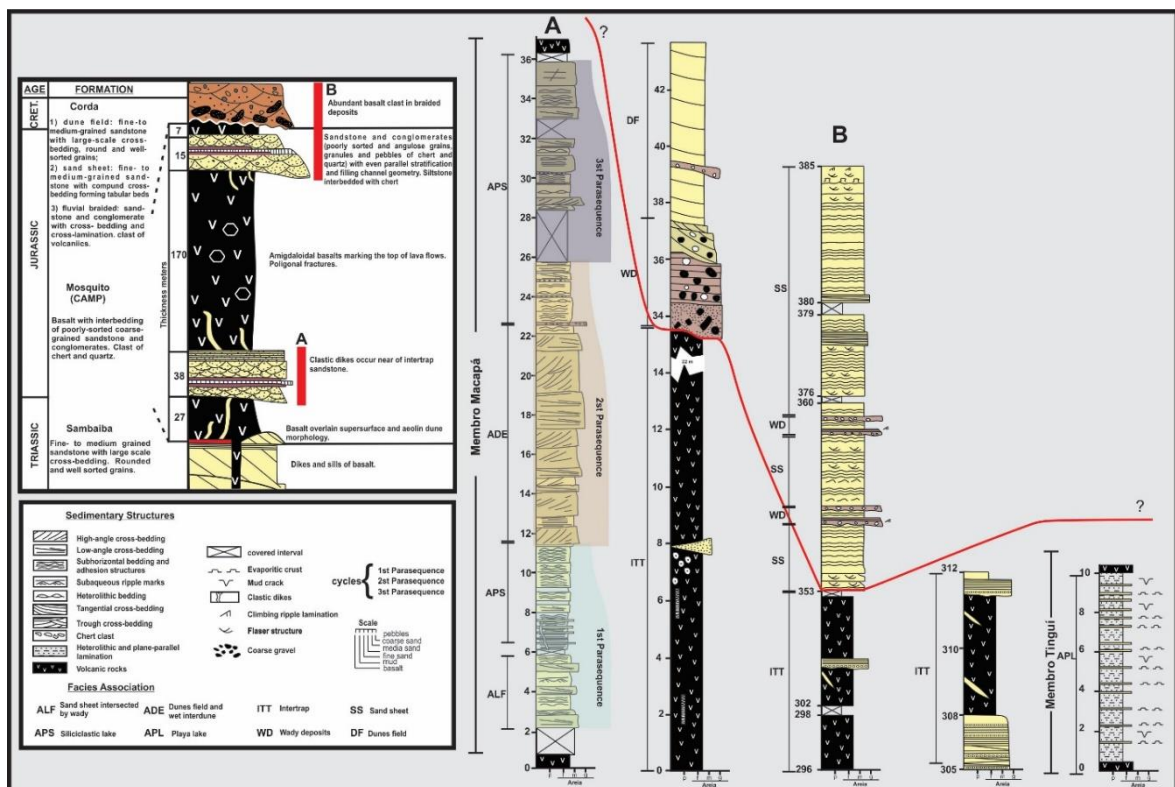


Figure 4 - Stratigraphic sections of the Jurassic- lower Cretaceous succession. The locations of the sections are shown in Figure. 1 of the Stratigraphic chart of the study area and a composite section of the Mosquito Formation. Modified from Ballén *et al.* (2013) and Nogueira *et al.* (2021).

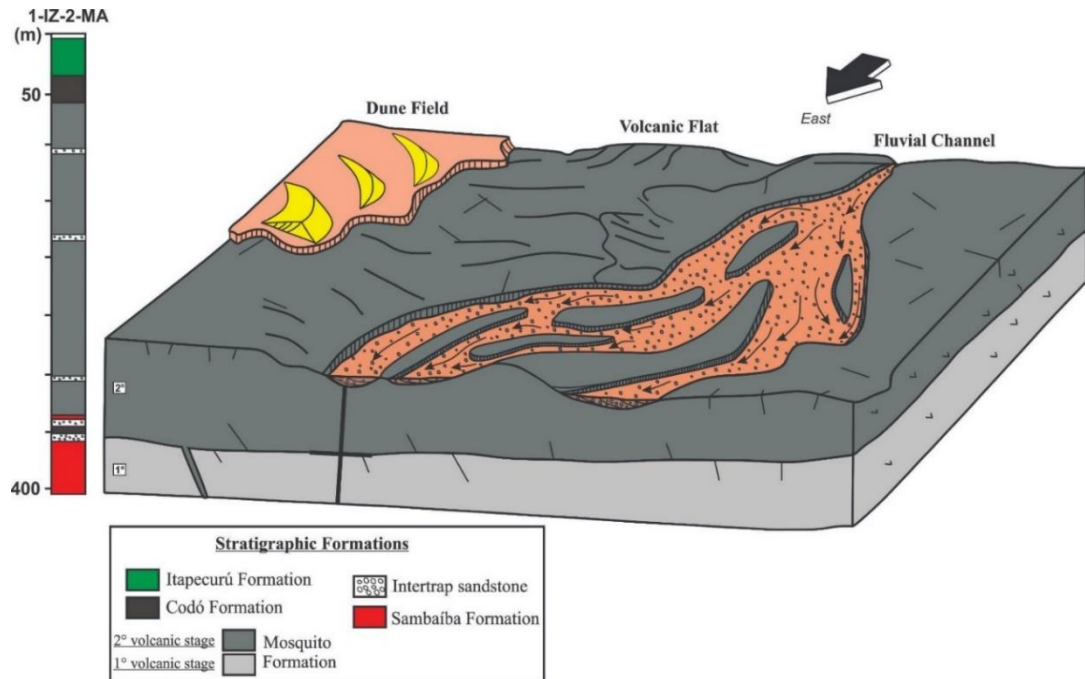


Figure 5 - Depositional model of the upper portion of the Jurassic Mosquito Formation. Wet desert settings were developed concomitantly with fluvial channels incised into the basaltic substrate. The volcanic plain was successively filled by fluvial-eolian-lacustrine deposits. The 1-IZ-2-MA profile of Rezende (2002) depicts sandstone intercalations in both the base and upper portion of the Mosquito Formation overlying the eolian deposits from the Sambaíba Formation.

#### 5.4.2 Residual anomalies x camp signatures

The utilization of methods to compute the crustal gravity signal, analyze elastic thickness, and determine Moho depth, coupled with an in-depth examination of geological data, yielded CAMP signatures that delineate the geometry and extent of magmatic intrusions. Additionally, it facilitated an estimation of their rheological properties, as well as phases of uplift and subsidence.

By analyzing the gravity signal associated with residual anomalies, we compared signatures of high-density rocks with previously mapped basalts in Amazonia. These anomalies were further juxtaposed with linear and domic (domical) geological structures to investigate their existence and potential coexistence with high-density rock anomalies. This comparative analysis contributes to refining our understanding of the geological framework and processes associated with CAMP magmatism in the studied regions.

#### 5.4.2.1 Geological structures

The maps of residual anomalies, in conjunction with geological data, indicate potential intracrustal density variations, suggesting the presence of high-density rock signatures within sedimentary basins, similar to findings by Rezende *et al.* (2021) (see Fig. 6). In this study, the highest positive values observed in the residual gravitational anomalies are linked to the CAMP, prominently in the Western Parnaíba Basin associated with the Mosquito Formation (Fig. 6A). Similar anomalies also occur in isolated areas in the central-western Amazon Basin and extend continuously along the southern and northern margins of the eastern extremity of this basin and into the Solimões Basin (Fig. 6B).

Thus, positive values of residual gravitational anomalies (ranging from 10 to 60 Mgal) confined within sedimentary basins cannot be solely attributed to basement structures or isolated structural bodies (Fig. 6). Therefore, we propose that these anomalies, as interpreted within the residual gravity data, likely stem from high-density rocks associated with CAMP basalts (Figures 6A and 6B).

The residual anomaly maps show geologic structures coincident with the distribution of the CAMP magmatic bodies, independent of the intrusive or extrusive nature of magmatism. For example, in the Parnaíba Basin, the deposits of the Mosquito Formation ( $199 \pm 2.45$  Ma) represent the unique spill interval of the CAMP, which includes basalts interbedded with continental intertrap sediments (Nogueira *et al.* 2021). In contrast, the other occurrences of the CAMP in the Amazonia basins are subvolcanic bodies in the Amazonas and Solimões basins with similar to the youngest volcanic rocks related to the Paraná-Etendeká magmatism ( $\sim 132$ - $137$  Ma), exposed only in the eastern Parnaíba Basin. These volcanic bodies have highlighted kilometric lineaments that reflect structures like arcs and fault zones into the basins (Fig. 7).

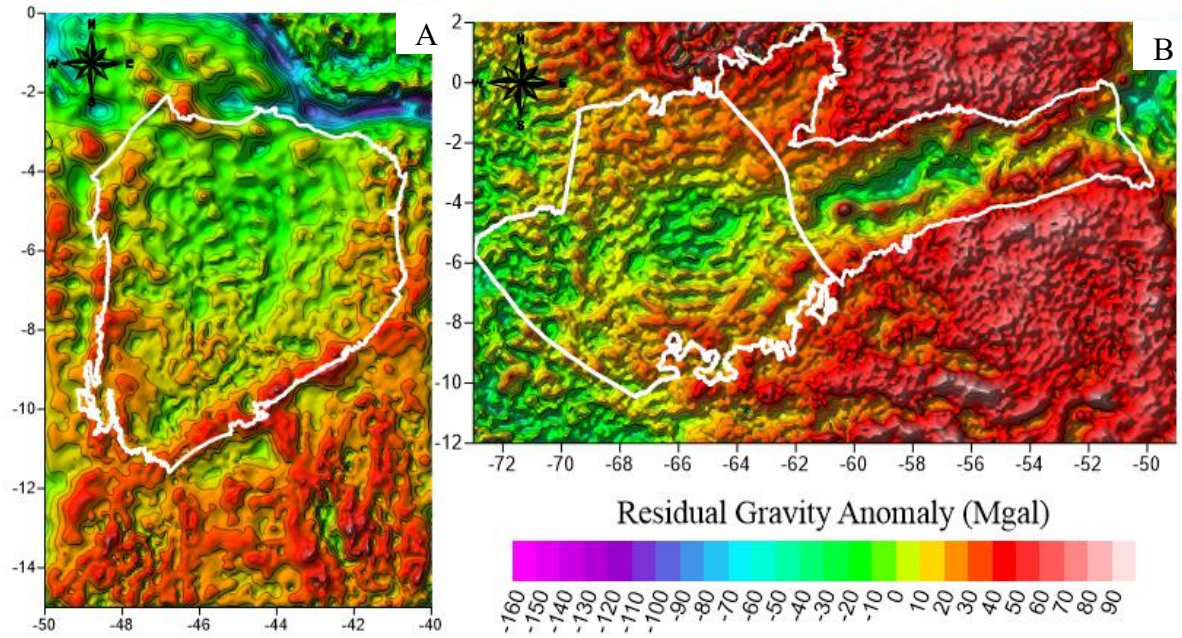


Figure 6 - Residual gravity anomaly showing the gravimetric highs and lows of the Parnaíba, Amazonas, and Solimões basins.

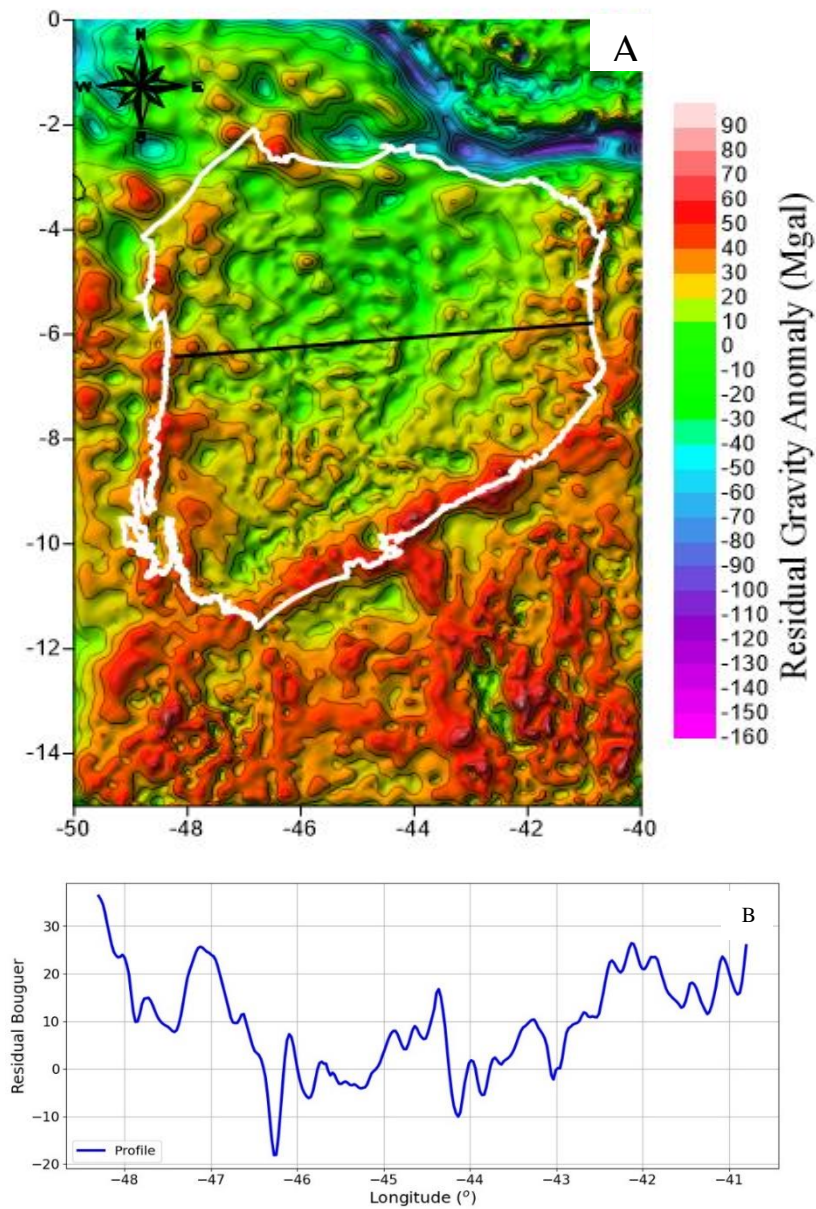


Figure 7 - (A) Residual anomaly map of the Paraíba Basin, which show geologic structures coincident with the distribution of the CAMP magmatic bodies. (B) Graph that show the behavior of the residual signal in a specific area, represented by the solid black line with an eastern and western direction. This delimited area shows the behavior of the gravimetric signal between the gravimetric highs and lows, suggesting that the main structural lineament trends into of this basin, such as Transbrasiliano and Pedro II, have different orientation compared with the Xambioá Arch, predominantly E-W directed, coinciding with crustal fracturing trend related to the Mesozoic magmatism of CAMP and Paraná-Entedeka

The Serra Formosa and Vilhena arcs of the central portion of the Parecis Basin in southeast-northwest and north/south directions, respectively, were previously interpreted as tectonic structures limiting sub-basins (Cf. Baia *et al.* 2007). They were reinterpreted by Rezende *et al.* (2021), through the residual gravity anomaly, coinciding with the CAMP basalt alignment. Although the existence of the arches could not be ruled out, they would probably be associated with the main conduits of the CAMP basalts, whose irregular geometry is due to the irregular volume of the basalt coinciding with the trace of the lineaments (Fig. 8).

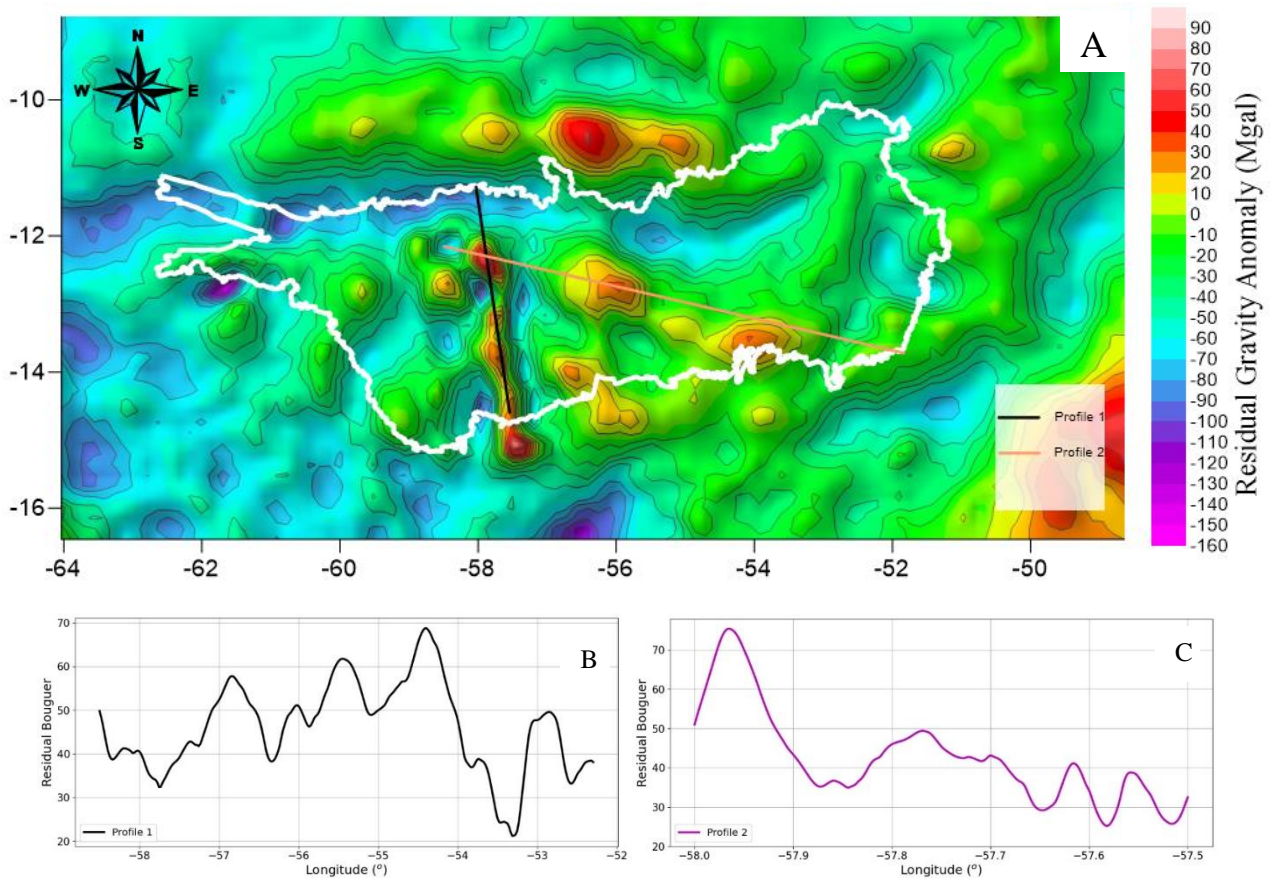


Figure 8 - (A) Residual gravimetric anomaly of the Parecis Basin, which show geologic structures (The Vilhena and Serra Formosa arcs, profile 1 and 2 respectively) coincident with the distribution of the CAMP magmatic bodies. (B) Graph that show the behavior of the residual signal in a specific area, represented by the solid black line with a South/North direction. Graph that show the behavior of the residual signal in a specific area, represented by the solid pink line with a northwest/southeast direction.

Otherwise, the map of the magnetic anomaly related to the deep magnetic field of the Parnaíba Basin suggests that the main structural lineament trends into this basin, such as Transbrasiliiano and Pedro II, have different orientations compared with the Xambioá Arch, predominantly E-W directed, coinciding with crustal fracturing trend related to the Mesozoic magmatism of CAMP and Paraná-Entedeka (Figs. 10A and 10B). This Mesozoic trend is printed in the relief lineament observed in the regions of Araguaína (TO)-Balsas (MA) is related

to the Post-CAMP E-W fracturing probably formed during the Sardinha magmatism (Paraná-Etendeká), which extended to the Floriano region (PI), generating the anomaly observed in aerogeophysical maps of the region (Figs. 10C and 10D). The geophysical and geological data indicate that the Xambioá Arch may be related as a conduit zone or an escape route through the fissural magmatism intruded into the crust. During the Jurassic, the Western Parnaíba Basin was intruded by CAMP magmatism while in the Cretaceous the reactivation of these fault/fracture zones was reactivated during Sardinha magmatism was more effective in the Eastern border of the basin. The E-W alignment of basic volcanic bodies that include Mosquito and Sardinha units in the central basin strongly define the Xambioá Arc (Figs. 7, 10A and 10B).

The Monte Alegre dome, an EoJurassic morphostructure that stands out in the Amazon River plain, is a topographic elevation located on the left bank, approximately 10 km southwest of the homonymous city, in the Central Amazonia (Fig. 9). This structure was intersected by the tholeiitic magmatism of the Lower Jurassic Penatecaua event forming a brachyanticlinal pattern due to the intrusion of magmatic sills or laccolith distributed in an ellipsoidal anticlinal structure with 30 km in length and 20 km in width (Montalvão and Oliveira 1975, Pastana *et al.* 1976, Figueira *et al.* 2012, Abelha *et al.* 2018). Tectonic studies have pointed to an evolution related to the uplift of rocks linked to tectonic control. The asymmetry of the dome is divided into sectors, where the bedding, responsible for the architectural geometry, has different spatial positions (Almeida and Pinheiro 2007). Considering that the dome will have an origin related to uplift due to Mesozoic magmatic intrusions, these faults would be responsible for segmenting this structure into late sectors. However, if we consider the hypothesis that the faults were the main ones responsible for the tilting of the layers, in structural blocks, defining the observed brachyantiform arrangement, this could represent a forced fold, generated in the context of tectonic inversion, linked to the rotations of blocks, in their different domains, controlled by reactivated N-S, NW-SE and NE-SW faults (Almeida and Pinheiro 2007). Following this interpretation, the brachyanticlinal structure will be only a fold of forced regional interference, where the role of uplift by Mesozoic intrusions could gain secondary meaning. These tectonic events occurred after the Penatecaua magmatic event, caused by the Gondwanide Orogeny (Almeida *et al.* 1981, 1984). The first phase of deformation with paleo-tension in the NW-SE direction is related to the Juruá Diastrophism (Caputo 1984, Szatmari 1983, Campos and Teixeira 1988). The second phase of deformation is possibly a result of a major deformation event after the Cretaceous. Figueira *et al.* (2012) have indicated the compression of the South American plate due to its blocking by the Nazca and Cocos plates. Therefore, the dome is far

from the eastern margin of the South American plate to consider any deformational effects. In addition, the faults cut the upper Cretaceous rocks suggesting a Cenozoic tectonic reactivation.

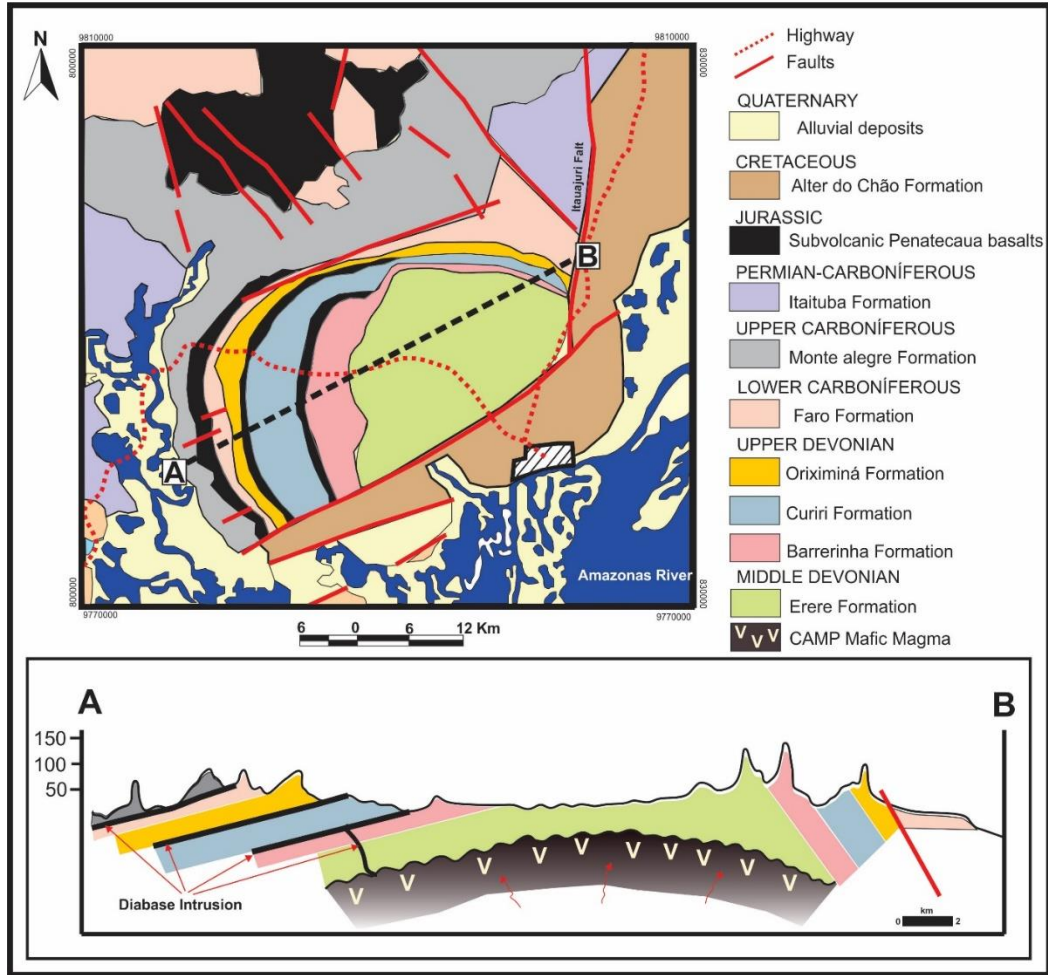


Figure 9 - The Monte Alegre Dome in Amazonas Basin. The dome's origin has been attributed to magmatic intrusions or tectonic deformation. The geologic map and section were based on Pastana (1999) and Figueira *et al.* (2012).



The intense magmatic activities with the injection of Jurassic-Triassic diabase dikes and sills of the CAMP affected practically all previously existing units. The residual gravimetric anomaly of the Amazonas e Solimoes Basins shows geologic structures (Monte Alegre Dome) coincident with the distribution of the CAMP magmatic bodies (Fig. 9, 11A and 11C). The residual gravity anomaly easily defined in the Northeastern border of the Amazonas basin is close to the dome geometry (Fig. 9), which presents a positive gravity signature at the top, similar to the positive signature of the CAMP diabase (Fig. 11C). The primary deformation of the Monte Alegre Dome is more aligned with the emplacement of the CAMP than a putative inversion tectonic that generates an isolated kilometric fold. Until now the faults reactivation never been adequately addressed and these features are not the main conduits for the CAMP basalts that occur as dikes and sills folded in the domic feature (Fig. 9). Sills occur following the folded geometry of the layers indicating that they were emplaced before or during dome formation. The lineaments that divide the different sectors represent normal faults, highlighting the Ererê and Itauajurí faults, on the south and east flanks, with a normal character that were reactivated after the Cretaceous, placing units of different ages and origin in lateral contacts (Fig. 9). Thus, we suggest that the dome was formed during the uplift generated by a magmatic bulge that accommodates volcanic bodies of the CAMP, causing the observed structural aspects (Fig. 9).

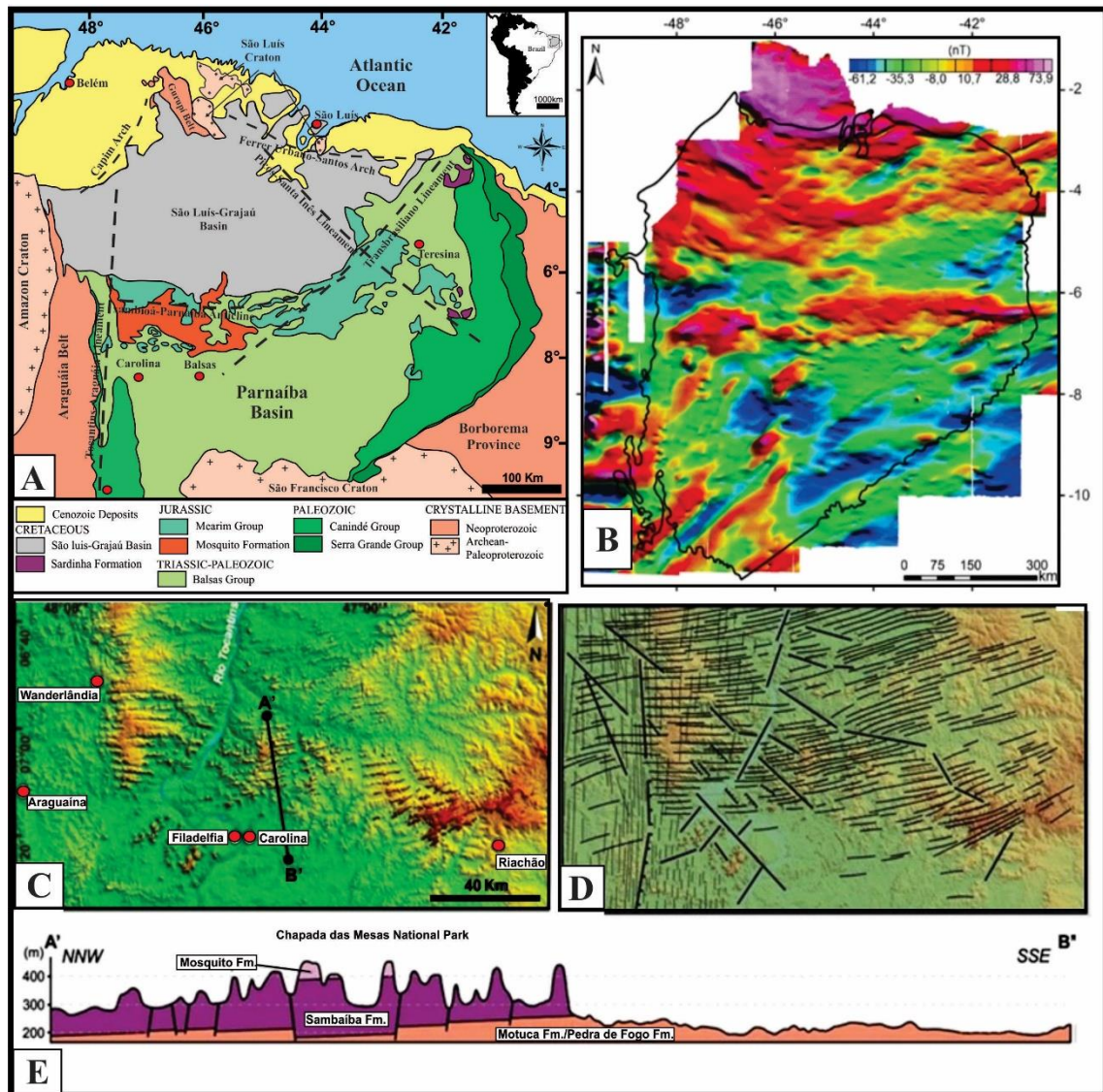


Figure 10 - Correlation between geophysical and geological data from the Parnaíba Basin based on previous works. (A) Tectonic sketch of the structural framework of the Parnaíba Basin (modified from Cordani *et al.* 1984, De Castro *et al.* 2014, 2016, Chamani 2015). (B) Map of magnetic anomalies of the deep magnetic field (adapted from Mocitaiba *et al.* 2017). The dashed rectangle points to an area interpreted as a magnetic signal resulting from a structural source. However, this signal coincides with Mesozoic magmatism, thus requiring new processing and interpretation of the data. (C) Map of the location of the study areas in the Parnaíba Basin, highlighting the main lineaments (modified from Schobbenhaus *et al.* 1984, Santos & Carvalho 2004). (D) Morphostructural context of the central-western portion of the Parnaíba Basin (area of the red square indicated in A based on the analysis of images from SRTM-90 sensors (Modified from Abrantes Jr 2016). (E) Main relief lineaments with the mountains oriented approximately E-W coinciding with the Xambioá Arch (amphiclisis; Modified from Abrantes Jr 2016). Thicker lines represent confirmed and probable failures. The N-S cross-section is based on field data. The area indicated in blue represents the zone of occurrence of Paraná-Etendeká magmatism with occurrences further east of this area.

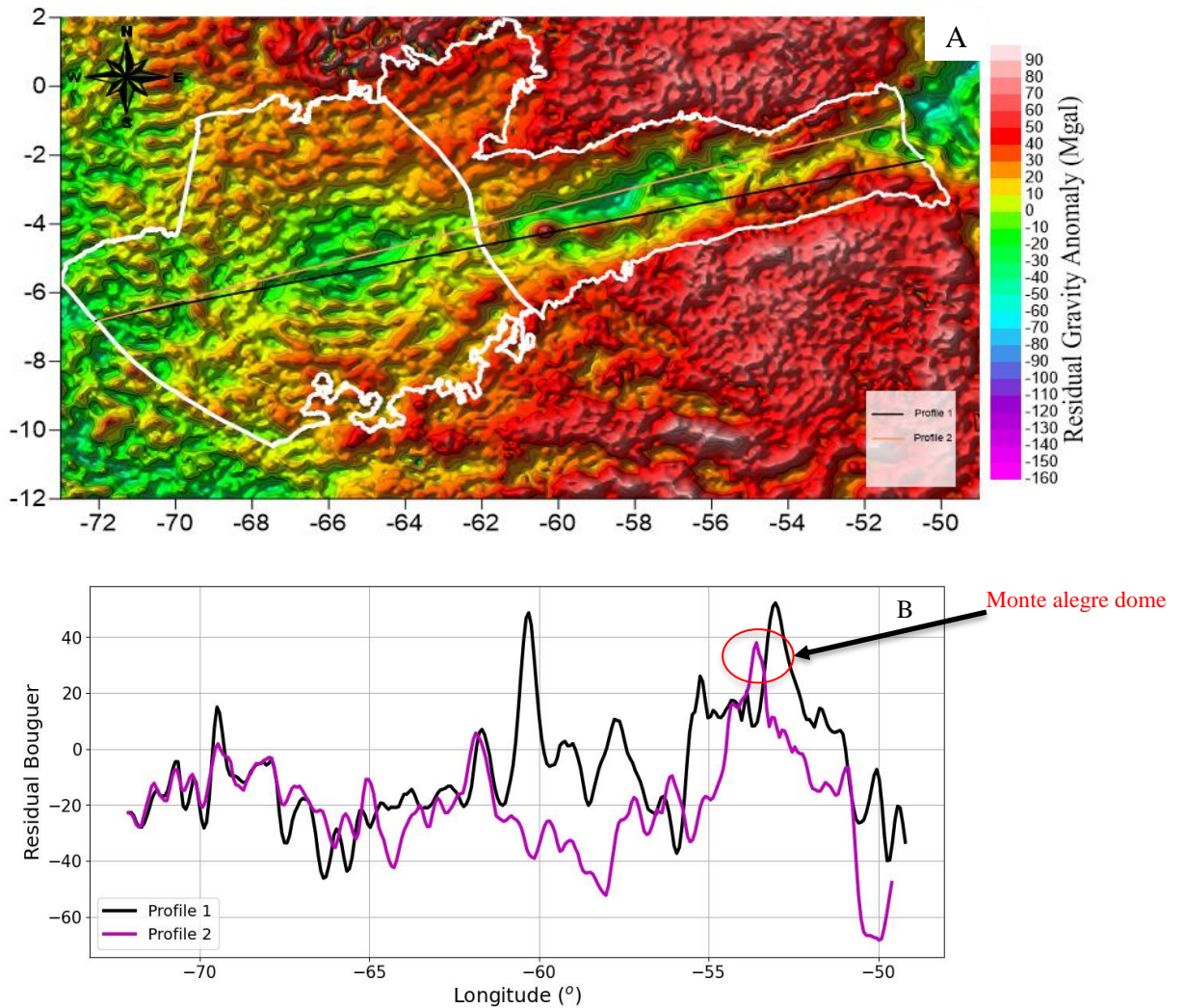


Figure 11 - (A) Residual gravimetric anomaly of the Amazonas e Solimoes Basins, which show geologic structures (Monte alegre Domo, profile 2) coincident with the distribution of the CAMP magmatic bodies. (B) Graph that show the behavior of the residual signal in a specific area, represented by the solid black line with. Graph that show the behavior of the residual signal in a specific area, represented by the solid pink line. By analyzing the residual gravity anomaly of the Amazon Basin with the available geological data, the location of the Monte Alegre Dome is observed (at the peak of the profile 2 at around -55 degrees longitude and 40 mgal), which presents a positive gravity signature at the top, similar to the positive signature of the CAMP diabase.

## 5.5 INTERPRETATIONS

### 5.5.1 Correlation between elastic thickness and Camp Rheology

The measurement of elastic thickness through geophysical methods and direct and inverse modeling techniques (Audet 2014, Eshagh 2020, Ribeiro-Filho 2023, Tesauro 2013) is a valuable tool for understanding the structure and composition of the Earth's crust. These measurements assist scientists in the geological mapping of tectonic structures, identifying hydrocarbon reservoirs, studying magmatic intrusions and effects (Yamasaki 2021), and ultimately understanding tectonic deformation processes (Grandin 2012). This is particularly evident in the Solimões, Amazonas, Parnaíba and Parecis basins, where positive gravimetric anomalies may indicate possible magmatic intrusions and extrusions (Soares *et al.* 2018, Svensen *et al.* 2018, Rezende *et al.* 2021, Castro 2022).

In this study, we observed different forms of CAMP emplacement between the Parnaíba Basin and the Solimões and Amazonas basins. In the Parnaíba Basin, the basalts were outpoured in the surface while in the Solimões and Amazonas basins, they are placed into the crust, i.e., arranged in dykes and sills (Marzoli *et al.* 1999, Vaz *et al.* 2007, Abrantes Jr 2016, Svensen *et al.* 2018, Nogueira *et al.* 2021). The different forms of emplacement of the magmatic bodies in the studied basins were interpreted from the maps based on the elastic thickness parameter. The elastic thickness, together with the Moho depth obtained from it, allows us to infer the crust's resistance to deformational stresses caused by the CAMP's swelling, as well as the rheological extension that the diabases can swell.

By analyzing the maps of elastic thickness and Moho depth of the Parnaíba Basin (Fig.12) and the Solimões and Amazonas basins (Fig.13), it is observed that the Parnaíba Basin has a crust less resistant to deformation, caused by the emplacement of igneous bodies, and an "accommodation" space with greater pressure and fluidity. This suggests that the Parnaíba Basin presents a more fluid rheological behavior than the Solimões and Amazonas basins. Consequently, if the crust is less resistant to deformations, the fluidity of the material easily surpasses the crust layers and overflows to the Earth's surface, as is the case with the CAMP diabase in the Parnaíba Basin (Fig.12). On the other hand, if the crust has high resistance, as observed in the Solimões basins (Fig.13), the fluidity of the diabase towards the surface is lower, resulting in greater resistance to fluid ascent to the surface. Thus, the diabases are disposed subsurface through dykes and sills. Otherwise, together with these geophysical data, we must highlight that the extrusive and intrusive form of these diabase bodies in these basins also directly depend on the anisotropy of the region, in which these basins are located, being an

important factor to be highlighted as a cause for the different forms of occurrences from the camp.

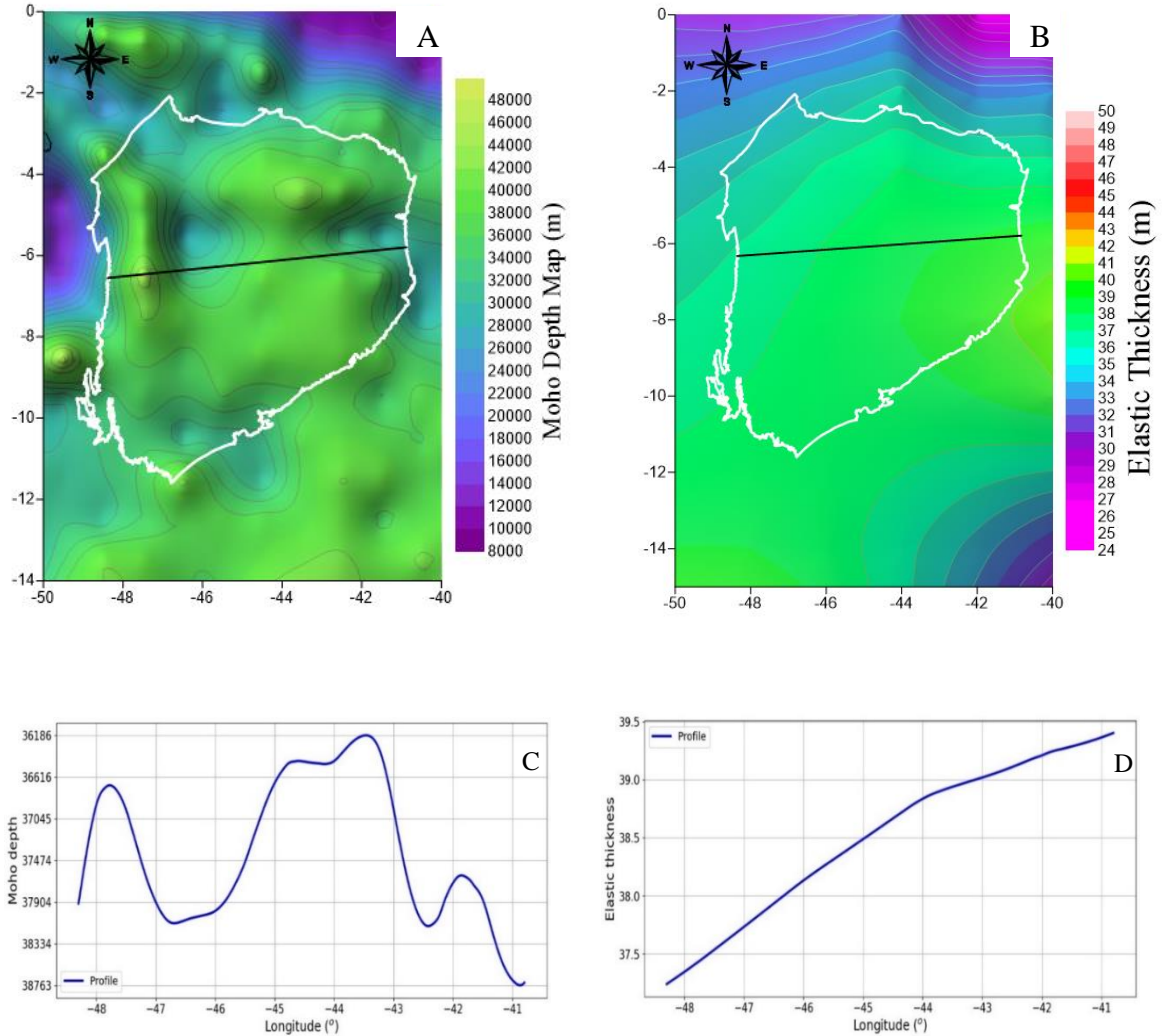


Figure 12 - (A) Moho depth map of the Parnaiba Basin (Uieda and Barbosa 2016). (B) Elastic thickness map of the Parnaiba Basin. (C) Moho depth graph generated from a point area on the map in A (solid black line). (D) Elastic thickness graph generated from a point area on the map in B (solid black line). It is noted that the elastic thickness increases from west to east, while the depth of the Moho is occasionally greater in the areas where the CAMP occurs (western edge).

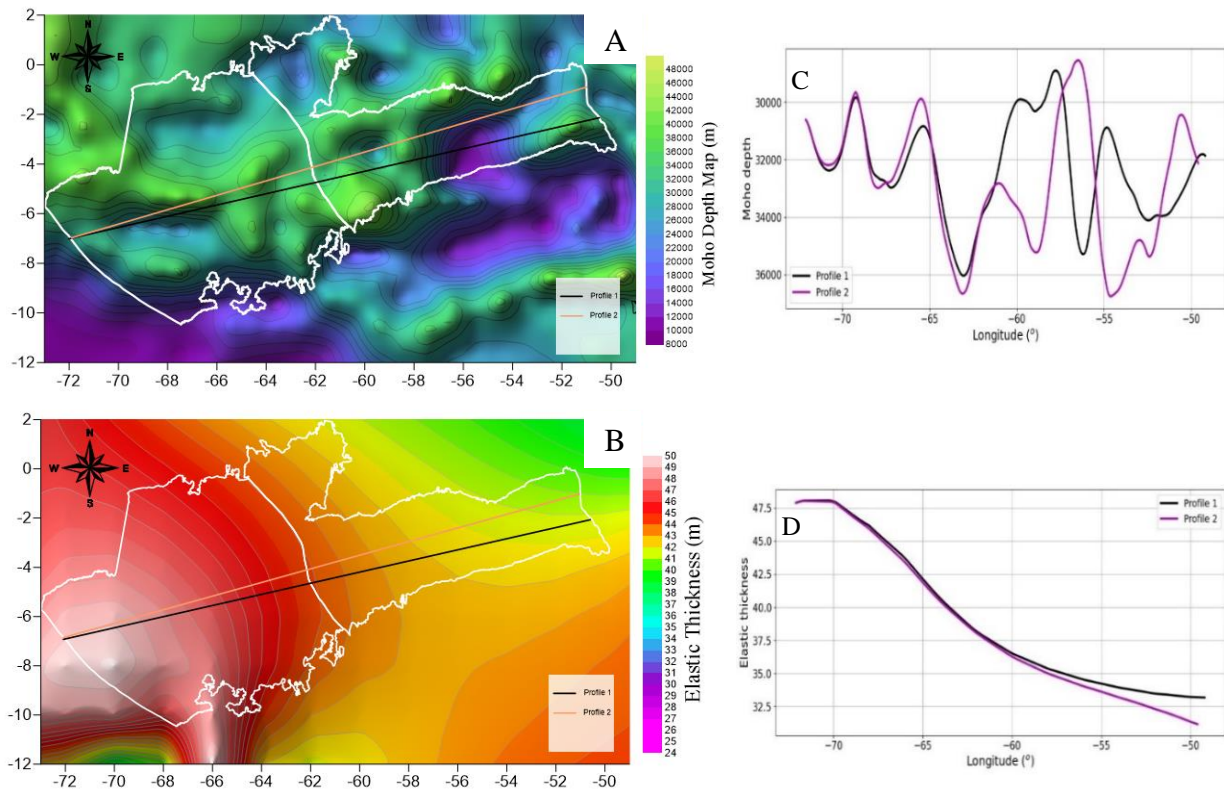


Figure 13 - (A) Moho depth map of the Solimoes and Amazonas basins (Uieda and Barbosa 2016). (B) Elastic thickness map of the Solimoes and Amazonas basins. (C) Moho depth graph generated from two profiles on the map in A (pink and black lines). It is noted that the elastic thickness decreases from western to eastern. (D) Elastic thickness graph generated from two profiles on the map in B (pink and black lines).

These interpretations allowed presuming crustal thickness for the studied area to a more detailed evaluation of stratigraphic units in key locations to determine the intrusive or extrusive nature of the rocks associated with the CAMP in Western Gondwana (Fig.14). From this analysis, it was possible to observe different geotectonic configurations and forms of magmatic body emplacement in the sedimentary basins of the Northern Amazon region, considering important rheological considerations to understand the geological evolution.

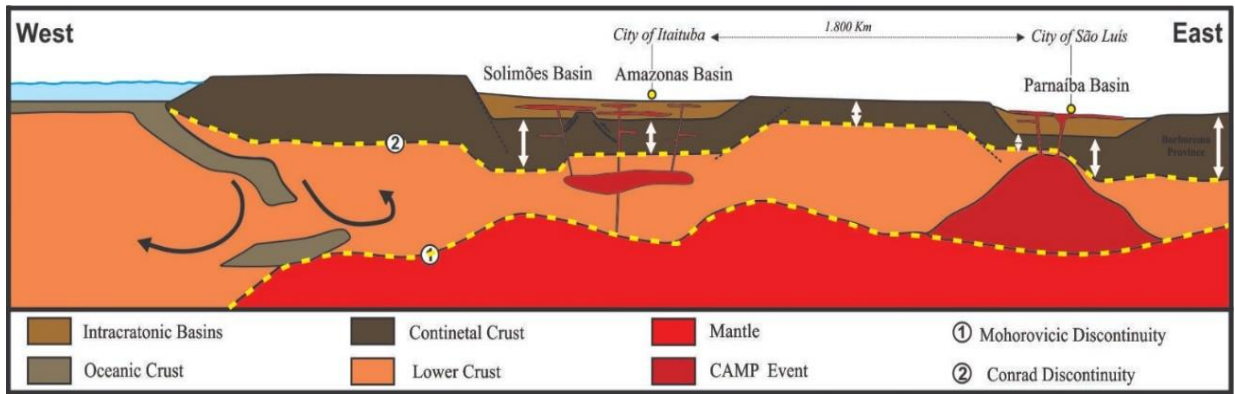


Figure 14 - Representation of crust thickness model 2D of the Amazonas, Solimões, and Parnaíba basins based on interpretations geophysical and geological data.

### 5.5.2 Plume establishment X crustal elasticity

The eastern part of Gondwanaland experienced gradual uplift during the Jurassic due to notable magmatic intrusions causing swelling in the central Amazon basins, evidenced by subsurface Penatecaua magmatism in the Amazonas and Solimões basins. The upper Mesozoic intervals in these basins were disturbed by uplift and erosion from magma accumulation in the subsurface responsible for forming basin-scale unconformities. Contrarily, the western edge of the Gondwana supercontinent, encompassing areas such as the Parnaíba Basin, underwent minor subsidence attributed to thermal and over-burden mechanisms (Köckling *et al.* 2018). In the Atlantic Central margin, there is good geological evidence for post-rift tectonic reactivation, in the form of onshore Cenozoic basins up to 3000 m deep that represent drift Sequences (Neo-Albian to Recent) typical of passive margin thermal subsidence with basaltic magmatism dated for the Neocretaceous, Eocene, and Miocene.

The concentration of the fissure eruptions in the western Parnaíba Basin strongly indicates regional tectonic stress during the emptying and collapse of the magma chamber. This distribution and periods without fissural magmatic activity support the theory of an intermittent magma chamber system lodging in the infracrustal position below the Southwestern Parnaíba Basin (Fig. 16). The Mosquito eruptive system developed in this shallow crustal region is devoid of lava fragments suggesting an effusive eruption, i.e., the magma lost most of its volatiles during ascent through the transport system. In other cases, if the eruption ends up being explosive most or all of a given magma batch is fragmented by the explosive action of volatiles. Besides that, the loss of gas is strongly controlled by the time spent during the magma transport. If the time is short, large super-saturations are required for the nucleation and growth of bubbles and vesiculation proceeds rapidly to magmatic fragmentation. In the case of Mosquito eruption, longer times and slow lava flow are inferred to have allowed both efficient pre-eruptive

degassing by either two-phase flow or gas loss through a permeable network, inducing microlite growth, in response to that degassing, both of which promote effusive rather than explosive activity. The growth of phenocrysts was only possible in the innermost portions of volcanic bodies that cooled more slowly and favored better crystal nucleation. Nevertheless, we cannot rule out feeder dikes can intrude directly from the deep-seated chamber without any tectonic influence, only by the magma injection pressure, since some dikes from a deep-seated magma chamber could propagate directly to the ground surface and cause fissure eruptions of the basaltic lavas.

The interpretations of the residual gravity anomaly indicate a thinner crust in the Parnaíba basin if comparable with those found in the Solimões and Amazonas basins favoring the most magmatic fluid migration that erupted the surface. In contrast, the basins with a thicker basement have experienced magma accumulation in sills fed by dikes that truncate the sedimentary pile (Fig. 14, 15.2 and 15.3). According to Mariane *et al.* (2013), a possible mechanism to create an increased density crust is to associate the dense system lodging in the infracrustal position below the Southwestern Parnaíba Basin to the magmatism, in the sense that the melting basaltic material is emplaced partly as flood basalt at the top of the crust, but partly in the crust, with a density greater than  $2900 \text{ kg/m}^3$ , higher than the reference crust. The thin crust and low elasticity allowed the development of a hot spot in the southwestern Parnaíba Basin, preceding the main continental breakup in Northwestern Pangea. The dense material was emplaced in the mid-lower crust in the form of sills and dikes in the Amazonas e Solimões basins that enter into cracks or at the bottom of the crust, increasing the total volume of the crust. The basic magma flow throughout the infracrust percolating the basement and Paleozoic pile from the Amazonas and Solimões basins. Considering the standard density reference column, CAMP diabase contributes a positive density contrast. This would imply that the underplated material would be seen in the positive gravity signal (Figs 6 and 8). The magma accumulation in a deep-seated basaltic chamber may have caused an infracrust inflate uplifting the region before eruption. It seems that, in general terms, CAMP basalts contribute to a higher density than the crust average increasing the resistance of the crust as the magma swells, creating an infracrustal basaltic layer that makes it difficult to break the crust. Nonetheless, the existence of other shallow magma chambers is not discarded since the sills are observed at ~3–5 km in the sedimentary pile in the basins, hundreds of kilometers to the west of the Parnaíba Basin. On the other hand, depending on crust elasticity the magma percolation can be facilitated by the rock rheology mainly in the basin wedge borders where the concentration of sedimentary rocks has allowed the emplacement as sill and dykes (Figs 12, 13 and 14).



### 5.5.3 Magmatic pulse time estimation

The current age of the CAMP is around 200 to 202 million years, suggesting that the majority of the province's volume was emplaced in ~201, with an estimated duration of around 10 Myrs, probably from the Retetian to the Sinemurian (Schoene *et al.* 2010, Marzoli *et al.* 2018). The geochronological data about the CAMP are scarce and generally, the ages are not positioned stratigraphically, hindering the definition of a more precise time interval estimative, and probably the magmatic pulses had different durations worldwide. By the way, how to estimate the period without activity between the magmatic pulses? The current ages are good for positioning the CAMP in the geological history and in a second-order stratigraphy but are insufficient to distinguish the short time intervals.

Comparing the subvolcanic bodies of the Solimões and Amazonas basins with those found in the Parnaíba Basin, only the Mosquito Formation has stratigraphic markers, the intertrap deposits, and is a prime candidate for estimating the maximum duration of magmatic inactivity. Nevertheless, the intertrap deposits that occur alternated with basalts in the Parnaíba Basin record the last depositional and diagenetic CAMP-related processes in the West Gondwana (Nogueira *et al.* 2021). The intertrap record confirms a time of magmatic inactivity enough to develop a depositional system and suggests an intermittent magmatic chamber.

Sequence stratigraphy concepts have been applied mainly to coastal and marine sediments. However, we tentatively compare the continental meter-scale autogenic cycles in intertrap deposits to the fourth- or fifth-order cycles of a depositional sequence, specifically parasequences (paracycle or small-scale cycle) (Vail *et al.* 1977a, 1977b, 1991, Lehrmann and Goldhammer 1999, Schlager 2004, 2010, Abreu *et al.* 2010, Catuneanu 2011, 2012, 2017 and 2019). Following Vail *et al.* (1991) the parasequence can be estimated as varying from 30.000 to 500.000 yrs. Some authors consider fourth-order parasequences deposited during cycles 100 to 100.000 yrs in duration, but episodic parasequences are of very short duration, generally less than 10 yrs (weber 1995, Schlager 2004, Abreu *et al.* 2010, Catuneanu 2017, 2019).

Is possible, that implantation of a fluvial-eolian system under a volcanic plain can be more an “episodic parasequence” (cf. King 1993, weber 1995) than a normal cycle. In fact, this reduced time is consistent with the recurrent sedimentation of the intertraps whose deposition does not present changes in terms of the depositional system, indicating similar conditions during the deposition of the 3 paracycles. Similar climatic inferences, in a humid desert with

ephemeral rivers and small bed forms meaning reduced accommodation space. The cyclicity was probably induced by thermal subsidence and the strata were preserved by rapid eodiagenetic/hydrothermal cementation (Nogueira *et al.* 2021). These hydrothermal processes occurred mainly during sandwiching by basalt flows. The compaction generated by the weight of mafic rocks also significantly increased the preservation potential of these deposits. Thermal subsidence led to the generation of depressions, ponds, and playas lakes as distal basins. The time constraint of lava emplacement is more difficult to estimate.

The microlithic fabric of the basalt suggests a fast cooling, but due to variations in flow thickness, wind speeds, rainfall amounts, as well as air and ground temperatures, the cooling rates of lava can be significantly influenced. According to the current cooling rate estimation, a 55 m-thicker of lava flow, may require approximately 100.000 yrs to achieve complete solidification (Catuneanu 2017, 2019). Considering this estimative, the 170m-thicker of Mosquito basalt would take less than ~1 Myr for total cooling (15.4C). Consequently, there exists a level of uncertainty regarding the duration for which the interior of a lava flow stays retained as liquid, but this probably does not modify the proposition of a scale of at least, a few hundred years, easily included in the 100.000 yrs of a parasequence. Is possible that the time between the end of the lava flow and the start of fluvial-desertic environment implantation be a significant hiatus because the upper volcanic rocks and most volcanic fragments in the intertrap deposits are weathered, but this is not definitive because is difficult to separate the current and older weathering features (paleosoil, ped features, kaolinized feldspar, etc.) in tropical areas. Although is difficult to estimate precisely the duration time of cycles, the recognition of three magmatic pulses separated by two intertrap successions containing 3 paracycles requires, at least, ~1 Myr for deposition confirming an intermittent activity of a magmatic chamber during the Upper Jurassic in the Parnaíba Basin.

In the eastern Norte American basins, the lava pile of the CAMP was emplaced in a very short time (i.e. 1.6 Myrs) at ~ 199 Ma, synchronously to hydrothermal activity (Jourdan *et al.*, 2009). Although the total CAMP vulcanism ages gathered so far suggest a short duration of the main magmatic activity (2–3 Myrs), they also suggest the possibility of a temporal migration of the active centers throughout CAMP (cf. Nomade *et al.* 2007, Marzoli *et al.* 2011). This provides evidence for the mantle plume hypothesis for CAMP genesis which would also postulate a radial outward migration of magmatism, and which may also be synchronously linked to other models (i.e. mantle upwelling or lithospheric rifting; Marzoli *et al.* 2018). In this instance, estimates of flexural rigidity show heating and weakening of the lithosphere during the Cretaceous, revealing that the magmatism of the Brazilian Paleo-Mesozoic basins resulted

from a remnant plume that settled at the base of the lithosphere due to variations in its thickness (cf. Bizzi *et al.* 2003). The other younger ages (183–194 Myrs) reported previously for dykes and sills in the eastern U.S.A, South America, and Africa (Bertrand 1991, Shabi *et al.* 2005, McHone 2006, Nomade *et al.* 2007, Callegaro *et al.* 2013, Heilbron *et al.* 2018), may suggest the occurrence of a second minor magmatic pulse in the CAMP province. This late activity can be related to a major extensional event, presumably signaling the onset of the oceanization process at ~192 Myrs.

Geological data show that the thickness of basaltic bodies in the Parnaíba Basin reaches a maximum of 300m, while in the Solimões and Amazonas basins they reach volumes greater than 1 km recorded in the subsurface (cf. Nogueira *et al.* 2013, 2021). There is no evidence of extrusive volcanism at CAMP in the Solimões and Amazonas basins, which demonstrates that the behavior of the magma was controlled by the rheology and elasticity of the crust, as well as the elimination of volatiles that allowed greater fluidity for migration. The greater thickness of basalts, as occurs in the Amazon and Solimões basins, is related to the thicker and more elastic crust, which accommodated a greater volume of magma. On the other hand, in the Parnaíba Basin, the volatile-poor magma was quickly pumped through fissures and faults in the crust, as well as the lower elasticity and thickness of this crust led to faster migration to areas of lower pressure, culminating in extrusive pulses (Fig. 15)

A comparative analysis of geological processes with CAMP action in the Amazonas, Solimões, and Parnaíba basins allows us to better understand the temporal contrast about the duration of CAMP occurrences in these basins. Paleoenvironmental, tectonic and geochronological complexities of the Parnaíba indicate swelling and rapid cooling of diabase in this basin (Fig. 15.2 and 15.4). On the other hand, this geological complexity is not visualized in the Amazon and Solimões basins, because the swelling of the CAMP in these basins, allowing their uplift, indicate a longer continuation of the CAMP pulses throughout the Jurassic until the activation of faults and fractures due to tectonism (Juruá Diastrophism; Fig. 15.3).

Therefore, this analysis, even brief of the stratigraphy of these basins, allows us to identify different durations of CAMP occurrences when involving the stratigraphic complexity of the areas studied. The pulses in the Parnaíba basin were alternated with periods of magmatic inactivity with rapid swelling and cooling of diabases in this basin, while in the Solimões and Amazonas basins the CAMP had a continuous duration and lasted for thousands, perhaps millions of years, until the occurrence of Juruá diastrophism (Fig.15)

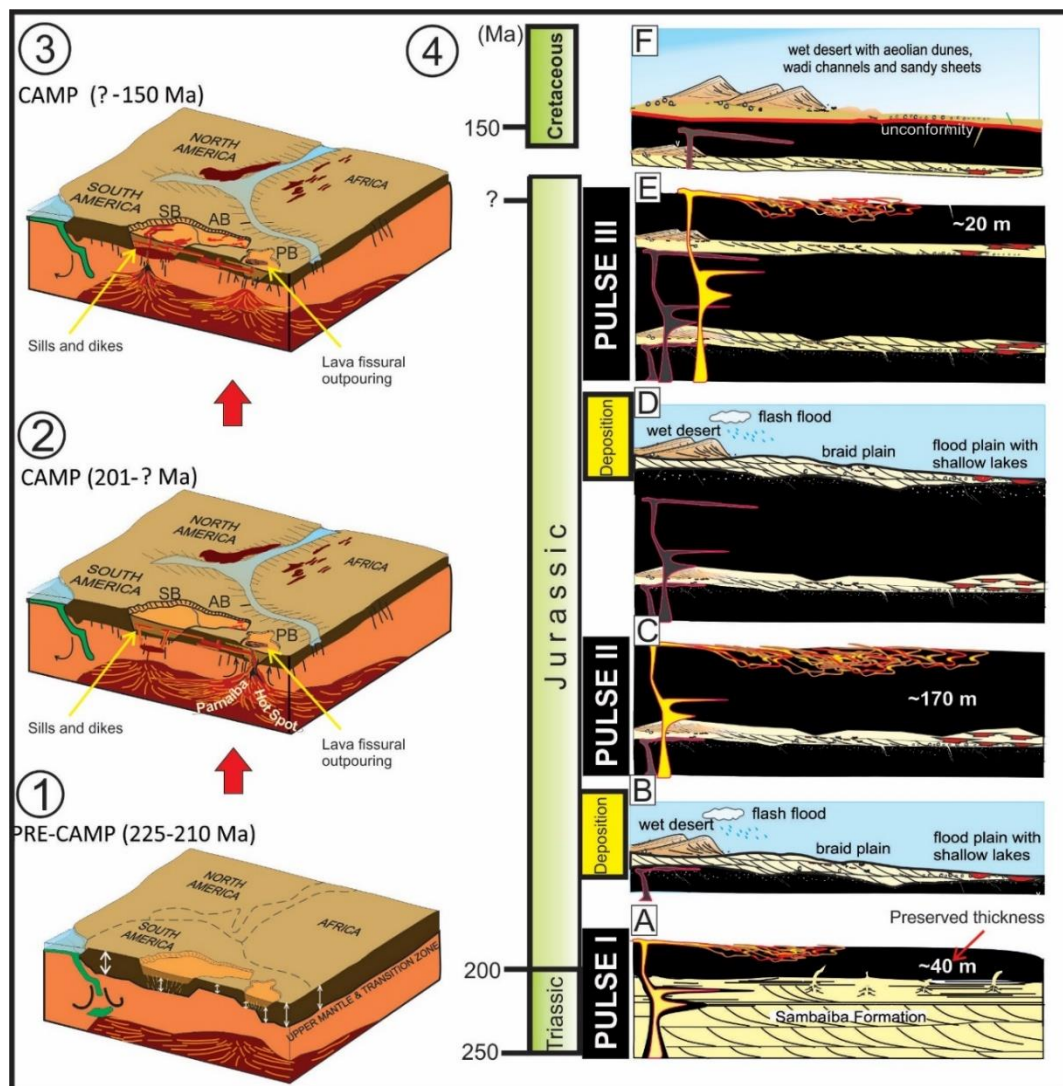


Figure 15 - CAMP Evolution in the Amazon Basins. 1) Previously the main continental break up in Northwestern Pangea the magma accumulation in a deep-seated basaltic chamber may have caused an infra-crust inflate uplifting the region. 2) Due to the thinner crust (elasticity) occurred concentration of the fissure eruptions in the western Parnaiba Basin that allowed the formation of a mantellic plume or hot spot, afterward causing eruption dykes induced by the magma injection pressure. 3) Migration of the CAMP mantle plume of the Parnaiba basin, due to the closure of the CAMP, to the Solimoes and Amazonas basins, allowing increased swelling of the CAMP diabases and continued uplift of these basins until the Middle Jurassic. 4A) previously, the fissure-controlled lava flow event, developed a volcanic substrate in a dry desert setting (Sambaiba Formation). 4B) After a long time of exposure, and weathering of volcanic plain, ephemeral fluvial channels transported basaltic intraclasts that accumulated in depressions and shallow lakes, whereas eolian dunes migrate on the volcanic substrate. 4C) new magmatic pulse with basalts sandwiching the intertrap sands, causing local compaction the eruption climax is associated with the thickest basalt body. 4D) again the implantation of ephemeral fluvial channels incised in volcanic substrate, producing several basaltic intraclasts, and concentrated on depressions that were filled by coarse grains, and fine grains transported toward shallow lakes. 4E) The last magmatic pulse with basalts sandwiched the underlaid intertrap sands. 4F) After the definitive end of the CAMP magmatic pulses, fluvial channels related to the wet desertic system of the Upper Jurassic-Early Cretaceous Corda Formation reworked both volcanic plains and intertrap deposits, producing an unconformity.

#### 5.5.4. Post-camp scenario

Desertic systems and evaporative basins persisted until the Jurassic and Cretaceous periods concomitant with the breakup of Gondwana associated with the implantation of the Mesoatlantic Ridge linked to the evolution of the proto-Atlantic intercontinental rift (Zalán 1991). In West Gondwana, magmatic activities accompanying the continental rapture influenced the sedimentation patterns in coastal and mainly in the intracratonic basins (Svensen *et al.* 2018, Tribaldos and White 2018, Köckling *et al.* 2018). Considering the area of western Pangea, it is observed that there is a large region with magmatic events included in the Central Atlantic Magmatic Province (CAMP) where the area of overflow of Mosquito volcanism is very limited, incompatible with a continental rifting zone. Preceding this punctual overflow event, the final collision of the Laurasia and Gondwana continents (Alleghenian Orogeny), during the Neopermian/Eotriassic, affected the northern portion of South America, producing fractures in the Guianas Craton and the Amazon basins, causing widespread uplifts and, consequently, formation of regional erosive unconformity (Crowley *et al.* 1989, Zalán 1991, Scotese and Mckerrow 2013). This regional uplift was caused by the compressive efforts of Juruá diastrophism and swelling of the crust by Penetecaua magmatism, causing the removal of about 1000 m of sediments from the Paleozoic successions and basement of the Amazonas Basin (Cunha *et al.* 2007). Erosion processes lasted until the end of the Jurassic linked to the beginning of the Wealdenian Reactivation, suppressing the accommodation space for the Jurassic sedimentation. The last record was the siliciclastics of the Permian Andirá Formation of the Amazonas Basin.

It is considered here that possibly the entire region to the West and Northwest of Western Pangea served as a source area for a more depressed region that included the Parnaíba Basin affected by thermal subsidence (Cardoso *et al.* 2019). It cannot be ruled out that it also came from the African continent, which at that time had the same pre-rifting swelling conditions as the Pangea (Fig.16). This new proposal can contribute to the understanding of the probable source areas since it predicts that these were outside the basin, providing a better accommodation of distances for the development of a river-lacustrine system of the Jurassic-Cretaceous limit (contrasting the previous models of Góes (1995), Ballén (2013), Rabelo and Nogueira (2014)).

The fissural nature of the mosquito magmatism indicates that the central zone of the Parnaíba basin was affected by brittle tectonics pre-Waldenian reactivation. At the Jurassic-Cretaceous boundary, it could represent a space created by the lithostatic load of the ~250 m thick basalt, subsided in the central region of the Western Pangea (Fig. 16). A phase similar to a rift but of short duration (~40 Myrs) is admitted, followed by a phase of thermal subsidence that dissipates the heat accumulated during taphrogenesis.

The definitive ceasing of the magmatic pulses and fluvial channels related to the wet desert system of the Jurassic-Cretaceous Corda Formation reworked both volcanic plains and intertrap deposits, forming the unconformity (Fig. 15.4F). This system was characterized by wide sand sheet areas and small-scale eolian dunes. Large-scale lacustrine systems have been linked to thermal subsidence post-dating the CAMP event, which was influenced by decreasing isotherms and crustal loading promoted by basalt beds (Fig.16). These systems contrast with locally concentrated water settings during Permian-Triassic and Triassic-Jurassic times, which evidences the progressive climatic attenuation that affected the Parnaiba Basin throughout the Mesozoic. These climatic conditions were extended to the humid desert system of the Jurassic-Cretaceous Corda Formation, supplied by the erosion of the uplifted areas from the Amazonas Basin, due to the CAMP swelling (Fig. 16)

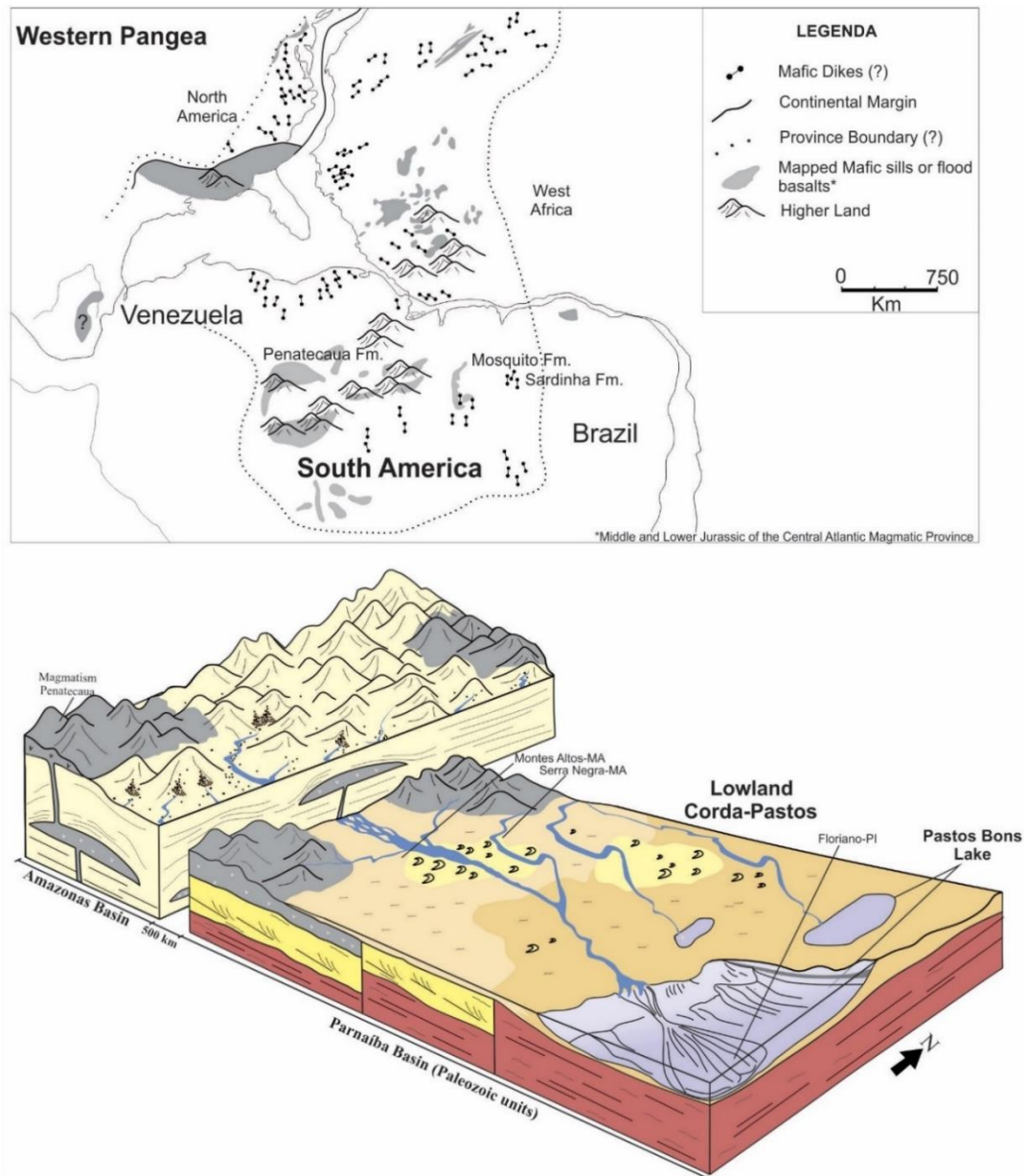


Figure 16 - Paleoenvironmental Reconstruction of the Upper Jurassic and Lower Cretaceous Successions of the Parnaíba Basin and its relationship with West Africa and Solimões and Amazonas basins in the Post-CAMP. Lakes characterized the eastern portion of the basin with deltaic deposits and distal turbidites. The region of the Solimões and Amazon basins, mainly the Amazon Basin, functioned as the main source area for river channels coming from higher areas to the west due to the uplift caused by the CAMP.

## 5.6 CONCLUSIONS

In this work, it was possible to guide detailed geotectonic analyses, using available information on the emplacement of magma bodies, such as the predominantly extrusive Mosquito Formation and the subvolcanic Penetecaua Magmatism. Furthermore, the application of geophysical techniques in combination with previous geologic data enlarges the understanding of the influence of the CAMP in this western region of Gondwana. We suggest a more thorough analysis of the emplacement of igneous bodies in pre-existing structures or those generated during the event. Additionally, the influence of the magmatic pulses on sedimentary events during and after the CAMP is discussed, as outlined in the work of Nogueira *et al.* (2021) in attached, allowing for a more precise description of the CAMP's impact on the Northern Amazonia basins.

Moreover, stratigraphic, sedimentological, and gravimetric evidence in the Northern Amazon Legal basins allowed for the identification of basins with varying degrees of subsidence and elastic thickness, resulting from the weight of diabases in thermal subsidence and crustal elasticity. These data suggest that thermal subsidence, induced by the emplacement of the CAMP, may have led to the reactivation of arc and structure zones, such as the Monte Alegre Dome, enabling the assessment of the role of these structures in accommodating magma bodies during and after the CAMP event. We suggest that such structures and arches as the Arco de Xambioá and Domo de Monte Alegre are possibly evidence or reflections of CAMP Magmatism in the Parnaíba and Amazonas basins, respectively. Thus, the Monte Alegre Dome is possibly evidence caused by the uplift of the Amazon Basin after the swelling of the camp, presenting records of the unconformity at the Jurassic-Cretaceous boundary. This relationship provides a new understanding of the origin of these structures and warns that some structures considered exclusively tectonic are reflections and originated by the CAMP.

The exact value of the camp's age is unknown or poorly known when we include the stratigraphic and sedimentological complexity of the area. More recent dating of the zircon shows low resolution in several basins of western Gondwana, indicating only the time of deposition, with no age of origin, possibly distorting the age values. Analyzing the ages of the pulses in different areas, such as the Amazon Basin and Parnaíba, a contrast in the age of the CAMP was noted when involving the specific complexity of the stratigraphy of these basins. In the Parnaíba Basin, for example, there are evidences that the duration of the CAMP is much shorter than in the Amazonas and Solimões basins. While in the Amazonas e Solimoes basins was uplifting, due to the intrusion of diabases from the CAMP until the Middle to Upper Jurassic, the Parnaíba Basin was experiencing deposition of small deserts (intertraps)



interspersed with CAMP basalts, indicating rapid intrusion and cooling of these basalts that generated small accommodation spaces for the deposition of the so-called intertraps.

The inference of the volume, elasticity, and distribution of magma associated with the CAMP in the sedimentary basins of the Amazon, Solimões, and Parnaíba allowed for the correlation of the region's uplift history with crustal swelling caused by the emplacement of magma bodies, proposing that the anomalously thick crust and densified would be interpreted as the magmatic products that produced the flood basalt in the Parnaíba Basin and magmatic diabase of the lower and upper crustal as sills and dikes which intruded in the crust of the Amazonas e Solimões basins, contributing to increasing the thickness of the crust with rocks of higher density than a normal average crust. At long last, we extend that the humid desert system of the Jurassic-Cretaceous Corda Formation probably had its sedimentation coming from the Amazon Basin, after the uplift, allowing thermal subsidence due to the cooling of the CAMP diabase within the Crust throughout of Jurassic-Cretaceous boundary. These results are important for future work on a new chronostratigraphic, tectonomagmatic, and structural arrangement to the Solimões, Amazonas and Parnaíba basins, from a new geological context with lava-sediment interaction and stratigraphically positioned ages, allowing a better understanding of the history of the CAMP that preceded the main continental rapture in northwestern Pangea

## CAPÍTULO 6 CONSIDERAÇÕES FINAIS

Durante o limite Triássico-Jurássico a intensificação dos processos magmáticos, devido ao rompimento do Pangea, propiciou a implantação de planícies vulcânicas expressivas desenvolvidas por sucessivas erupções basálticas fissurais no Sul e Norte do Craton Amazônico. Esses eventos magmáticos estão associados à província magmática do atlântico central (CAMP). A análise dos dados geofísicos e geológicos existentes permitiu-nos obter evidências em superfície e subsuperfícies do evento CAMP na região.

Os basaltos do CAMP nas bacias dos Parecis, Criogeniano-Ordoviciano tardio Araras-Alto Paraguai, Parnaíba, Amazonas e Solimões provavelmente correspondem a rochas intrusivas (diques ou soleiras) e extrusivas (fluxos de lava) coincidindo com as assinaturas gravitacionais de valores positivos. Os diabásios do CAMP contribuem com um contraste de densidade positivo, considerando a coluna de referência de densidade padrão, implicando que o material subjacente seria visto no sinal de gravidade como positivo. Uma evolução tectonomagmática para a parte do Sul do Cráton Amazônico inclui 1) uma fase inicial antes da ruptura da Pangéia (c. 250 Ma); 2) aumento progressivo do volume dos basaltos devido à ruptura da Pangéia, provocando expansão dos basaltos CAMP na crosta concomitante com a abertura do Oceano Atlântico Central; 3) um evento extensional relacionado à abertura do Atlântico Sul e do Atlântico Equatorial, bem como o primeiro evento tectônico relacionado à orogenia andina, levando à deposição de sedimentos do Cretáceo na Bacia dos Parecis; e 4) a exposição do sul do Cráton Amazônico, causando erosão de rochas do Cretáceo, basaltos CAMP e rochas mais antigas, expondo apenas os canais magmáticos.

Esta tese permitiu interpretar que as bacias com a crosta mais espessa experimentaram acumulação de magmas em soleiras alimentadas por diques que cortam a pilha sedimentar. Interpretou-se que o material denso foi alojado no meio-inferior da crosta em forma de soleiras e diques nas bacias do Amazonas e Solimões que cortam ou ficam abaixo da crosta, aumentando o volume total destas, contribuindo para acumulação de magma em uma câmara magmática profunda, causando uma inflação da infracrusta que elevou a região antes da erupção. Parece que, em termos gerais, os basaltos do CAMP contribuem para uma densidade superior à média da crosta, aumentando a resistência da crosta à medida que o magma ascende, criando uma “camada basáltica infracrustal” que dificulta a ruptura da crosta. No entanto, a existência de uma câmara magmática rasa não é descartada, uma vez que as soleiras são observadas a ~3–5 km na pilha sedimentar nas bacias. Por outro lado, dependendo da elasticidade da crosta, a percolação do magma pode ser facilitada pela reologia das rochas,

principalmente na borda das bacias, onde a concentração de rochas sedimentares permitiu o alojamento como soleiras e diques.

As interpretações das anomalias gravimétricas indicam uma crosta mais fina na bacia do Parnaíba se comparável àquelas encontradas nas bacias do Solimões e do Amazonas, favorecendo a maior migração de fluido magmático que extravasou na superfície. Em contraste, a concentração das erupções fissurais no oeste da Bacia do Parnaíba indica fortemente o estresse tectônico regional durante o esvaziamento e colapso da câmara magmática. No entanto, não podemos descartar a possibilidade de diques alimentadores poderem penetrar diretamente da câmara magmática profunda sem qualquer influência tectônica, apenas pela pressão de injeção de magma, uma vez que alguns diques desta câmara magmática profunda podem se propagar diretamente para a superfície do solo e causar erupções de fissuras das lavas basálticas. Evidências estratigráficas, sedimentológicas e gravimétricas nas bacias aqui estudadas permitiram a identificação de bacias com graus variados de subsidência e espessura elástica, resultantes do peso do diabásio na subsidência térmica e na elasticidade da crosta. Esses dados sugerem que a subsidência térmica, induzida pela colocação do CAMP, pode ter levado à reativação de zonas de arco e estruturas, como o Domo de Monte Alegre, possibilitando avaliar o papel dessas estruturas na acomodação de corpos magmáticos durante e após o evento CAMP.

O valor exato da idade dos pulsos do CAMP é desconhecido ou pouco conhecido quando incluímos a complexidade estratigráfica e sedimentológica da área. A possível inferência do volume, da elasticidade e da distribuição do magma associado ao CAMP nas bacias sedimentares do Amazonas, Solimões, Parnaíba, Parecis e Araras-Alto Paraguai permitiram correlacionar o histórico de soerguimento da região com a densificação crustal causada pela colocação de corpos magmáticos, propondo que a crosta anormalmente espessa está relacionada aos basaltos do CAMP, ou seja, a crosta adensada é presumida como produtos dos diabásios. Por fim, adicionalmente, foi discutida a influência dos pulsos magmáticos nos eventos sedimentares durante e após o CAMP, conforme descrito no trabalho de Nogueira et al. (2021), permitindo uma descrição mais precisa do impacto do CAMP nas bacias legais do Norte da Amazônia e mostrando que a correlação entre geocronologia, estratigrafia e modelagem gravimétrica é satisfatória, embora estudos futuros incluindo dados de magnetometria e proviniência do CAMP possam explicar com mais detalhes ou preencher lacunas da evolução tectonomagmática e deposicional na região.

## REFERÊNCIAS

- Abelha M., Petersohn E., Bastos G. and Araújo D. 2018. New insights into the Parnaíba Basin: results of investments by the Brazilian National Petroleum Agency. *In: Daly M.C., Fuck R.A., Juliã J., Macdonald D.I.M. & Watts A.B. (eds.). Cratonic basin formation: a case study of the Parnaíba basin of Brazil.* London, Geological Society. (Special Publications, 472).
- Abrantes Junior F.R. 2016. *O Permo-Triássico da bacia do Parnaíba, Norte do Brasil: implicações paleoambientais, paleoclimáticas e paleogeográficas para o Pangea Ocidental.* PhD Theses, Universidade Federal do Pará, Instituto de Geociências, Programa de Pós-Graduação em Geologia e Geoquímica, Belém do Pará, xxiv, 130 p.
- Abreu V., Neal J.E., Bohacs K.M., Kalbas J.L. 2010. Sequence stratigraphy of siliciclastic systems - the ExxonMobil Methodology. *In: Concepts in Sedimentology and Paleontology*, 226 p.
- Afonso L.W.J. & Nogueira A.C.R. 2018. Sedimentology and Stratigraphy of Neoproterozoic-Lower Paleozoic Carbonate-siliciclastic succession of the South Western most Amazon Craton, State of Rondônia, Brazil. *Brazilian Journal of Geology*, **48**: 75-93. 38.
- Aguiar G.A. 1969. *Bacia do Maranhão: geologia e possibilidades de petróleo.* Belém, Petrobras, 55 p. (Relatório Técnico, 371).
- Alkmim F.F., Marshak S. and Fonseca M.A. 2001. Assembly Western Gondwana in the Neoproterozoic: clues from the São Francisco craton region, Brazil. *Geology*, **29**: 319-322.
- Amante C. & Eakins B.W. 2009. ETOPO1 Arc-Minute Global Relief Model: procedures, data sources and analysis. *NOAA Technical Memorandum NESDIS NGDC-24, National Geophysical Data Center, Marine Geology and Geophysics Division.* Colorado, USA, 1-20.
- Almeida F.F.M. & Mantovani M.S.M. 1975. Geologia e geocronologia do Granito São Vicente, Mato Grosso. *Anais da Academia Brasileira de Ciências*, **47**: 451-458.
- Almeida F.F.M., Hasui Y., Brito Neves B.B., Fuck R.A. 1981. Brazilian structural provinces: an introduction. *Earth Sci. Rev.* **17**: 1-29.
- Almeida F.F.M., Hasui Y. (eds.). 1984. *O Pré-Cambriano do Brasil.* São Paulo, Edgard Blücher.
- Almeida F. F. M., Brito Neves B.B., Dal Ré Carneiro C. 2000. The origin and evolution of the South American Platform. *Earth-Science Reviews*, **50**: 77-111.
- Almeida F.F.M. & Carneiro C.D.R. 2004. Inundações marinhas fanerozoicas no Brasil e Recursos minerais associados. *In: Mantesso Neto V., Bartorelli A., Carneiro C.D.R., Brito Neves B.B. (eds.). Geologia do continente sul-americano: evolução da obra de Fernando Flávio Marques de Almeida*, 43-48.
- Almeida C. & Pinheiro R.V.L. 2007. O papel das falhas na história tectônica do domo de monte alegre, bacia do médio Amazonas, Pará. *In: Pdpetro. Campinas, São Paulo*, **4**: 1-8.

- Allen P.A. & Allen J.R. 2013. *Basin analysis, principles and applications to petroleum play assessment*. Oxford, Blackwell, 3rd edn.
- Artemieva I. M. 2009. The continental lithosphere: Reconciling thermal, seismic, and petrologic data. *Lithos*, **109**: 23-46.
- Assumpção M., Feng M., Tassara A., Julià J. 2013a. Models of crustal thickness for South America from seismic refraction, receiver functions and surface wave dispersion. *Tectonophysics*, **609**: 82-86.
- Audet P. 2014. Toward mapping the effective elastic thickness of planetary lithospheres from a spherical wavelet analysis of gravity and topography. *Physics of the Earth and Planetary Interiors*, **226**: 48-82.
- Bahia R.B.C. & Pedreira A.J. 1996. Depósitos glaciogênicos da Formação Pimenta Bueno (Carbonífero) na região de Rolim de Moura, Sudeste de Rondônia. *A Terra em Revista*, **1**: 24-29.
- Bahia R.C., Martins-Neto M.A., Barbosa M.S.C., Pedreira A.J. 2006. Revisão estratigráfica da Bacia dos Parecis – Amazônia. *Revista Brasileira de Geociências*, **36**: 692-703.
- Bahia R.C. 2007. *Evolução tectonosedimentar da Bacia dos Parecis*. PhD Theses. Fundação Universidade Federal de Ouro Preto, Ouro Preto, 121 p.
- Bahia R.C., Martins-Neto M.A., Barbosa M.S.C., Pedreira A.J. 2007. Análise da evolução tectonosedimentar da Bacia dos Parecis através de métodos potenciais. *Revista Brasileira de Geociências*, **37**: 639-649.
- Bállen O.A.R., Góes A.M., Negri F.A., Maziviero M.V., Teixeira V.Z.S. 2013. Sistema eólico úmido nas sucessões sedimentares interderrames da Formação Mosquito, Jurássico da Província Parnaíba, Brasil. *Brazilian Journal of Geology*, **43**(4): 695-710.
- Barros M.A.S., Mizusaki A.M.P., Weska R.K., Borba A.W., Chemale J.R.F., Costa E.C. 2007. Petrografia, geoquímica, análises isotópicas (Sr, Nd) e geocronologia Ar-Ar dos basaltos de Tapirapuã (Tangará da Serra, Mato Grosso, Brasil). *Pesquisas em Geociências*, **33** (2): 71-77..
- Barthelmes F. & Kohler W. 2012. International Centre for Global Earth Models (ICGEM), *J. Geod.*, **86** (10): 932-934.
- Basei M. A. S. 1974. Estudo geocronológico do magmatismo ácido da região meridional da Amazônia.
- Baski A.K. & Archibald D.A. 1997. Mesozoic igneous activity in the Maranhão Province, northern Brazil:  $^{40}\text{Ar}/^{39}\text{Ar}$  evidence for separate episodes of basaltic magmatism. *Earth and planetary science letters*, **151**:139-153.
- Batezelli A., Ladeira F.S.B., Assine M.L. 2014. Ambientes deposicionais e evolução estratigráfica do Cretáceo Superior da Bacia dos Parecis. *Geociências*, **33**: 429-448.

Batezelli A. & Ladeira F.S.B. 2016. Stratigraphic framework and evolution of the Cretaceous continental sequences of the Bauru, San franciscana, and Parecis Basins, Brazil. *Journal of South American Earth Sciences*, **65**: 1-24. <https://doi.org/10.1016/j.jsames.2015.11.005>.

Beutel E.K., Nomade S., Fronabargera A.K., Renne P.R. 2005. Pangea's complex breakup: a new rapidly changing stress field model. *Earth and Planetary Science Letters* **236**: 471-48.

Beltrão J. F. 1989. *Uma nova abordagem para interpretação de anomalias gravimétricas regionais e residuais aplicada ao estudo da organização crustal: exemplo da região Norte do Piauí e Noroeste do Ceará*. PhD Theses, Universidade Federal do Pará, Belém, Pará, 156 p.

Beltrão J. F., Silva J. B. C., Costa J. C. 1991. Robust polynomial fitting method for regional gravity estimation. *Geophysics*, **56** (1): 80-89.

Bertrand H. 1991. The Mesozoic tholeiitic province of Northwest Africa: A volcanotectonic record of the early opening of Central Atlantic. In: Kampuzu A.B., Lulaba R.T. (eds.). *Magmatism in extensional settings: the Phanerozoic African plate*. Springer, 147-188.

Bellieni G., Picirillo E.M., Cavazzini G., Petrini R., Cominchiaramonti P., Nardy A.J.R., Civetta L., Melfi A.J., Zantedeschi P. 1990. Low- and high TiO<sub>2</sub>, Mesozoic tholeiitic magmatism of the Maranhão basin (NE-brazil): K–Ar age, geochemistry, petrology, isotope characteristics and relationships with Mesozoic low- and high TiO<sub>2</sub> flood basalts of the Paraná Basin (SE-Brazil). *Neues Jahrbuch. Mineralogischer Abhandlungen*, **162**: 1-33.

Bensalah M.K., Youbi N., Mahmoudi A., Bertrand H., Mata J., El Hachimi H., Madeira J., Martins L.T., Marzoli A., Bellon H., Medina F., Karroum M., Karroum L.A., Ben Abbou M. 2011. The Central Atlantic Magmatic Province (CAMP) volcanic sequences of Berrechid and Doukkala basins (Western Meseta, Morocco): volcanology and geochemistry. *Comunicações Geológicas*, **98**: 15-27.

Bertrand H., Fornari M., Marzoli A., García-Duarte R., Sempere T. 2014. The Central Atlantic Magmatic Province extends into Bolivia. *Lithos* **188**: 33-43

Bizinella G. A. *et al.* 1980. Projeto Tapajós-Sucunduri-relatório final. Manaus: *Ministério das Minas e Energia-Departamento Nacional de Produção Minera*.

Bizzi L.A. *et al.* 2003. Geologia, tectônica e recursos minerais do Brasil: texto, mapas e SIG. CPRM, 692 p.

Blackburn T. J., Olsen P. E., Bowring S. A., McLean N. M., Kent D. V., Puffer J., Et-Touhami M. 2013. Zircon U-Pb geochronology links the end-Triassic extinction with the Central Atlantic Magmatic Province. *Science*, **340**: 941-945, <https://doi.org/10.1126/sci-ence.1234204>. 40.

Blakely R. J. (eds.). 1996. *Potential Theory in Gravity and Magnetics Applications*. Cambridge University Press, 464p, <https://doi.org/10.1017/CBO9780511549816>.

Bertrand H., Fornari M., Marzoli A., García-Duarte R., Sempere T. 2014. The Central Atlantic Magmatic Province extends into Bolivia. *Lithos* **188**: 33-43.

- Bryan S.E. & Ernst R.E. 2008. Revised definition of Large Igneous Provinces (LIPs). *Earth-Science Reviews*, **86** (1- 4): 175-202.
- Callegaro S., Marzoli A., Bertrand H., Chiaradia M., Reisberg L., Meyzen C., Bellieni G., Weems R.E., Merl R. 2013. Upper and lower crust recycling in the source of CAMP basaltic dykes from southeastern North America. *Ear Planet Sci Lett*, **376**: 186–199.
- Callegaro S., Rapaille C., Marzoli A., Bertrand H., Chiaradia M., Reisberg L., Bellieni G., Martin L., Madeira J., Mata J., Youbi N., De Min A., Azevedo M.R., Bensalah M.K. 2014. Enriched mantle source for the Central Atlantic magmatic province: new supporting evidence from Southwestern Europe. *Lithos*, **188**: 15-32.
- Campos J.N.P. & Teixeira L.B. 1988. Estilos tectônicos da Bacia do Amazonas. *In: Congresso Brasileiro de Geologia, Belém, Anais*, **5**: 2161-2172.
- Cardoso A.R., Nogueira A.C.R., Rabelo C.E.N. 2019. Lake cyclicity as response to thermal subsidence: A post-CAMP scenario in the Parnaíba Basin, NE Brazil. *Sedimentary Geology*, **385**: 96-109, <https://doi.org/10.1016/j.sedgeo.2019.03.015> .
- Castro D.L., Fuck R.A., Phillips J.D., Vidotti R.M., Bezerra F.H.R., Dantas E.L. 2014. Crustal structure beneath the Paleozoic Parnaiba basin revealed by airborne gravity and magnetic data, Brazil. *Tectonophysics*, **614**: 128-145.
- Castro D. L., Oliveira D. C., Herrera D. R., Bezerra F. H., Romeiro M. A., Araújo M. N. 2022. Crustal evolution of divergent and transform segments of the Brazilian Equatorial Margin derived from integrated geophysical data: Insights from basement grain heritage. *Earth-Science Reviews*, **232**: 104-132.
- Caputo M.V., Rodrigues R., Vasconcelos D.N.N. 1971. Litoestratigrafia da Bacia do Amazonas Belém, Petrobras - *Sistema de informação de exploração*, 130-405.
- Caputo M.V. 1984. *Stratigraphy, tectonics, paleoclimatology and paleogeography of northern basins of Brazil*. PhD theses, Universidade da Califórnia, Santa Barbara, 583 p.
- Caputo M. V. & Silva O. D. 1990. *Sedimentação e tectônica da Bacia do Solimões: origem e evolução das bacias sedimentares*. Petrobras, Rio de Janeiro, 169-193.
- Capriolo M., Marzoli A., Aradi L. E., Callegaro S., Dal Corso J., Newton R. J., Szabó C. 2020. Deep CO<sub>2</sub> in the end-Triassic Central Atlantic Magmatic Province. *Nature Communications*, **11**: 1670, doi: 10.1038/s41467-020-15325-6.
- Catuneanu O., Galloway W.E., Kendall C.G.StC., Miall A.D., Posamentier H.W., Strasser A., Tucker M.E. 2011. Sequence stratigraphy: methodology and nomenclature. *Newsl. Stratigr*, **44** (3): 173-245.
- Catuneanu O., Martins-Neto M.A., Eriksson P.G. 2012. Sequence stratigraphic framework and application to the Precambrian. *Mar. Petrol. Geol.* **33**: 26–33.
- Catuneanu O. 2017. Sequence stratigraphy: guidelines for a standard methodology. *In: Montenari, M. (Eds.). Stratigraphy and timescales*, UK, Academic Press, **2**:1-57.

- Catuneanu O. 2019. Scale in sequence stratigraphy. *Marine and Petroleum Geology*, doi:10.1016/j.marpetgeo.2019.
- Cebriá J.M., López-Ruiz J., Doblás M., Martíns L.T., Munha J. 2003. Geochemistry of the Early Jurassic Messejana-Plasencia dyke (Portugal-Spain): implications on the origin of the Central Atlantic Magmatic Province. *J Petrol*, **44**: 547-568.
- Coffin M.F. & Eldholm O. 1993. Scratching the surface: estimating dimensions of large igneous provinces. *Geology*, **21**: 515-518.
- Condie K.C. 2004. Supercontinents and super plume events: distinguishing signals in the geologic record time. *Physics of the Earth and Planetary Interiors*, **146**: 319-332.
- Cordani U.G. 1970. Idade do vulcanismo no Oceano Atlântico Sul. *Boletim do Instituto de Geologia e Astronomia*, São Paulo, **1**: 9-76.
- Cordani U.G., Brito neves B.B., Fuck R.A., Porto R., Thomaz filho A., Cunha F.M.B. 1984. Estudo preliminar de integração do Pré-Cambriano com os eventos tectônicos das bacias sedimentares brasileiras, *Boletim de Geociências*, Petrobras, **17** (1): 137-204.
- Cordani U.G., Sato K., Texeira W., Tassinari C.C.G., Basei M.A.S. 2000. Crustal evolution of the South American platform. In: Cordani U.G., Milani E.J., Thomaz Filho A., Campos D.A. (eds.). *Tectonic evolution of South America*. 31<sup>o</sup> International Geological Congress, Rio de Janeiro, 19-40.
- Cordani U.G., Brito Neves B.B., D'Agrella Filho M.S. 2003. From Rodinia to Gondwana: a review of the available evidence from South America. *Gondwana Res.* **6**: 275–283.
- Costa J.B.S., Bemerguy R.L., Hasui Y., Borges M.S. 2001. Tectonics and paleogeography along the Amazon River. *Jour. South Amer. Earth Sc.*, **14**: 335-347.
- Cozzuol M. A. 2006. The Acre vertebrate fauna: age, diversity, and geography. *Journal of South American Earth Sciences*, **21** (3): 185-203. doi:10.1016/j.jsames.2006.03.005.
- Cunha E. D. 1994. *Geografia do alto Purus. Um paraíso perdido: ensaios, estudos e pronunciamentos sobre a Amazônia*. Organização de Leandro Tocantins. Rio de Janeiro: José Olympio.
- Cunha P. R., Gonçalves de Melo J. H., Silva, O. B. 2007. Bacia do Amazonas. *Boletim de geociências da petrobras*, **15**: 227-251.
- Chamani M. A. C. 2015. *Tectônica sinsedimentar no Siluro-Devoniano da Bacia do Parnaíba, Brasil: o papel de grandes estruturas do embasamento na origem e evolução de bacias intracratônicas*. PhD. Theses, Instituto de Geociências – USP, São Paulo, 129 p.
- Chang C. & Liu L. 2019. Distinct responses of intraplate sedimentation to different subsidence mechanisms: insights from forward landscape evolution simulations. *Journal of Geophysical Research: Earth Surface*. doi:10.1029/2018jf004905 .
- Crowley J. K. & Hook S. J. 1996. Mapping playa evaporite minerals and associated sediments



in Death Valley, California, with multispectral thermal infrared images. *Journal of Geophysical Research: Solid Earth*, **101**: 643-660.

Daly M.C., Andrade V., Barousse C.A., Costa R., Mcdowell K., Piggott N., Poole A.J. 2014. Brasiliano crustal structure and the tectonic setting of the Parnaíba basin of NE Brazil: results of a deep seismic reflection profile. *Tectonics*, **33**: 1-19.

Daly M.C., Fuck R.A., Julià J., Macdonald D.I.M., Watts A.B. 2018. Cratonic basin formation: a case study of the Parnaíba Basin of Brazil. London, *Geological Society*, doi:10.1144/sp472.20. (*Special Publications*, 472).

Davies J. H. F. L., Marzoli A., Bertrand H., Youbi N., Ernesto M., Schaltegger U. 2017. End-Triassic mass extinction started by intrusive CAMP activity. *Nature Communications*, <https://doi.org/10.1038/ncomms15596>.

Davies J. H. F. L., Marzoli A., Bertrand, H., Youbi N., Ernesto M., Greber N. D., Schaltegger, U. 2021. Zircon petrochronology in large igneous provinces reveals upper crustal contamination processes: new U–Pb ages, Hf and O isotopes, and trace elements from the Central Atlantic magmatic province (CAMP). *Contributions to Mineralogy and Petrology*, *176*(1). doi:10.1007/s00410-020-01765-2.

Deckart K., Féraud G., Bertrand H. 1997. Age of Jurassic continental tholeiites of French Guyana, Surinam and Guinea: implications for the initial opening of the Central Atlantic Ocean. *Earth and Planetary Sciences Letters*, **150**: 205-220.

Deckart K., Bertrand H., Liégeois J.P. 2005. Geochemistry and Sr, Nd, Pb isotopic composition of the Central Atlantic Magmatic Province (CAMP) in Guyana and Guinea. *Lithos*, **82**: 289-314.

De Castro D. L., Fuck R. A., Phillips J. D., Vidotti R. M., Bezerra F. H., Dantas E. L. 2014. Crustal structure beneath the Paleozoic Parnaíba Basin revealed by airborne gravity and magnetic data, Brazil. *Tectonophysics*, **614**: 128-145.

De Castro D. L., Bezerra F. H., Fuck R. A., Vidotti R. M. 2016. Geophysical evidence of pre-sag rifting and pos-rifting fault reactivation in the Parnaíba Basin, Brazil. *Solid Earth*, **7** (2): 529-548.

De Min A., Piccirillo E.M., Marzoli A., Bellieni G., Renne P.R., Ernesto M., Marques L.S. 2003. The Central Atlantic Magmatic Province (CAMP) in Brazil: petrology, geochemistry,  $^{40}\text{Ar}/^{39}\text{Ar}$  ages, paleomagnetism and geodynamic implications. In: Hames W, McHone G, Renne PR, Ruppel C. (eds.). *The Central Atlantic magmatic province: insights from fragments of Pangaea*, Geophys Monogr, **136**: 91-128.

Eiras J. F., Becker C. R., Gonzaga F. G., Silva J. G., Matsuda N. S., Souza E. M., Feijó F. J. 1994. Bacia do Solimoes. *Boletim de Geociências da Petrobras*.

Ernesto M., Bellieni G. *et al.* 2003. Paleomagnetic and geochemical constraints on the timing and duration of the CAMP activity in northeastern Brazil. In: Hames W., Mchone J., Renne P., Ruppel C. (eds.). *The Central Atlantic Magmatic Province: insights from fragments of Pangea*. American Geophysical Union, Geophysical Monograph Series, **136**: 129-149.

Eshagh M., Tenzer R., Eshagh M. 2020. Elastic thickness of the Iranian lithosphere from gravity and seismic data. *Tectonophysics*, **774**: 228-186.

Espurt N., Baby P., Brusset S., Roddaz M., Hermoza W., Regard V., Bolanos R. 2007. How does the Nazca Ridge subduction influence the modern Amazonian foreland basin? *Geology*, **35** (6): 515-518.

Feng M., Assumpção M., Van der lee S. 2004. Group velocity tomography and lithospheric S-velocity structure of the South American continent. *Physics of the Earth and Planetary Interiors*, **147**: 315-331.

Figueira R.F.I, Salamuni E., Mancini F. 2012. Deformação rúptil em rochas do magmatismo Penatecaua no Domo de Monte Alegre (PA). *Revista Brasileira de Geociências*. **42** (4): 772-784, doi: 10.5327/Z0375-75362012000400009.

Fodor R., Sial A.N., Mukasa S.B., McKee E.H. 1990. Petrology, isotope characteristics, and K-Ar ages of the Maranhão, Northern Brazil, Mesozoic basalt province. *Contrib. Mineral. Petrol.* **104**: 555-567.

Gaia V.C.S., Nogueira A.C.R., Domingos F.H.G., Sans-Jofre P., Bandeira Júnior J.C.S., Oliveira J.G.F., Sial A.N. 2017. The new occurrence of Marinoan cap carbonate in Brazil: the expansion of snowball Earth events to the Southwesternmost Amazon Craton. *Journal of South American Earth Sciences*, **76**: 446-459.

Ghomsí F.E.K.R., Tenzer R., Nguiya S., Mandal A., Nouayou R. 2020. Crustal thickness beneath Atlas region from gravity, topographic, sediment and seismic data. *Geodesy and Geodynamics*, <https://doi.org/10.1016/j.geog.2019.08.002>.

Ghomsí F. E. K., Ribeiro-Filho N., Baldez R., Tenzer R., Martins C. M., Chisenga C., Nouayou R. 2021. Identification of Cameroon's geological structures through a gravity separation and using seismic crustal models. *Journal of African Earth Sciences*, **173**: 27-104.

Ghomsí F. E. K., Pham L. T., Steffen R., Ribeiro-Filho N., Tenzer R., 2022. Delineating structural features of North Cameroon using the EIGEN6C4 high-resolution global gravitational model. *Geological Journal*, **57** (10): 4285-4299.

Granot R. & Dymant J. 2015. The Cretaceous opening of the South Atlantic Ocean. *Earth and Planetary Science Letters*, **414**: 156-163, <https://doi.org/10.1016/j.epsl.2015.01.015>.

Greene S.E., Martindale R.C., Ritterbush K.A., Bottjer D.J., Corsetti F.A., Berelson W. M. 2012. Recognizing ocean acidification in deep time: an evaluation of the evidence for acidification across the Triassic-Jurassic boundary. *Earth Sci. Rev.* **113**: 72-93. <https://doi.org/10.1016/j.earscirev.2012.03.009>.

Góes A.M.O. & Feijó F.J. 1994. Bacia do Parnaíba. *Boletim de Geociências da Petrobras*, **8**: 57-56.

Góes A. M. 1995. *A Formação Poti (Carbonífero Inferior) da Bacia do Parnaíba*. PhD Theses. Instituto de Geociências -USP, São Paulo, 171 p.

Hames W.E., Renne P.R., Ruppel C. 2000. New evidence for geologically instantaneous emplacement of earliest Jurassic Central Atlantic Magmatic Province basalts on the North American margin. *Geology*, **28**: 859-862.

Heilbron M., Guedes E., Mane M., Valeriano C.M., Tupinambá M., Almeida J., Silva L.G.E., Duarte B.P., Favera J.C.D., Viana A. 2018. Geochemical and temporal provinciality of the magmatism of the eastern Parnaíba Basin, NE Brazil. London, *Geological Society*. (Special Publications, 472), <https://doi.org/10.6084/m9.figshare.c.4117985>.

Ingersoll R.V. 2018. Tectonics of sedimentary basins, with revised nomenclature. *In*: Busby C., Azor A.A. (eds.). *Tectonics of Sedimentary Basins: recent Advances*. Oxford, Blackwell Publish, 3- 43, <http://doi.wiley.com/10.1002/9781444347166.ch1>.

HOORN Carina *et al.* 1995. Andean tectonics as a cause for changing drainage patterns in Miocene northern South America. *Geology*, **23** (3): 237-240.

Hoorn C., Wesselingh F. P., Hovikoski J., Guerrero J. 2010. The development of the amazonian mega-wetland (Miocene; Brazil, Colombia, Peru, Bolivia). Amazonia, landscape and species evolution: a look into the past, *Wiley-Blackwell*, 123-142.

Horbe A. M. C., Queiroz M. M. A., Moura C. A. V., Toro M. A. G. 2013. Geoquímica das águas do médio e baixo rio Madeira e seus principais tributários - Amazonas - Brasil. *Acta Amazonica*, **43**(4): 489-504, doi:10.1590/s0044-59672013000400011.

Horbe A. M. C., Trindade I. R., Dantas E. L., Santos R. V., Roddaz M. 2014. Provenance of quaternary and modern alluvial deposits of the Amazonian floodplain (Brazil) inferred from major and trace elements and Pb–Nd–Sr isotopes. *Palaeogeography, palaeoclimatology, palaeoecology*, **411**: 144-154, doi:10.1016/j.palaeo.2014.06.019.

Horbe A.M.C., Roddaz M., Gomes L.B., Castro R.T., Dantas E.L., Carmo D.A. 2019. Proveniência dos sedimentos Neógenos da Formação Solimões (Bacias do Solimões e do Acre), Brasil. *Revista Sul-Americana de Ciências da Terra*, doi:10.1016/j.jsames.2019.05.004.

Hurtado-Alarcón J.C. *et al.* 2018. Phylogeographic patterns in *Maguimithrax spinosissimus* (Decapoda: Mithracidae) from Colombian Caribbean. *New Zealand journal of marine and freshwater research*, **52** (1): 118-137.

Jaillard E., Herail G., Monfret T., Díaz-Martínez E., Baby P., Lavenu A., Dumont J.F. 2000. Tectonic evolution of the Andes of Ecuador, Peru, Bolivia and Northernmost Chile. *In*: Cordani U.G., Milani E.J., Thomaz Filho A., Campos D.A. (Eds.). *Tectonic Evolution of South America*. International Geological Congress, Rio de Janeiro, **31**: 481-558.

Jourdan F., Marzoli A., Bertrand H., Cirilli S., Tanner L.H., Kontak D.J., McHone G., Renne P.R., Bellieni G. 2009.  $^{40}\text{Ar}/^{39}\text{Ar}$  ages of CAMP in North America: implications for the Triassic–Jurassic boundary and the 40K decay constant bias. *Lithos*, **110**: 167-180.

Kasprak A. H., Sepúlveda J., Price-Waldman R., Williford K. H., Schoepfer S. D., Haggart J.W., Whiteside J.H. 2015. Episodic photic zone euxinia in the Northeastern Panthalassic Ocean during the end-Triassic extinction. *Geology*, **43**: 307-310, <https://doi/10.1130/g36371.1>.

Kearey P., Klepeis A.K., Vine J.F. 2009. Global Tectonics. Oxford, *Blackwell Publish*, 3rd edn.

Kiessling W., Roniewicz E., Villier, L., Leonide, P. and Struck U. 2009. An Early Hettangian coral reef in Southern France: Implications for the end-Triassic reef crisis. *Palaios*, **24**: 657–671, <https://doi/10.2110/palo.2009.p09-030r>.

King Jr D. T. 1993. Eustatic and tectonic effects within sequence stratigraphy of the outcropping paralic-marine section, Upper Cretaceous, Alabama, *Geology*, **43**: 157-164.

Knight K.B., Nomade S., Renne P.R., Marzoli A., Bertrand H., Youbi N. 2004. The Central Atlantic Magmatic Province at the Triassic–Jurassic boundary: paleomagnetic and Ar-40/Ar-39 evidence from Morocco for brief, episodic volcanism. *Earth and Planetary Science Letters*, **228**: 143-160.

Korte C., Ruhl M., Pálffy J., Ullmann C. V., Hesselbo S. P. 2019. Chemostratigraphy Across the Triassic-Jurassic Boundary. *Geophysical Monograph Series*, 183-210, <https://doi/10.1002/9781119382508.ch10>.

Klöcking M., White N., MacLennan J. 2018. Role of basaltic magmatism within the Parnaíba cratonic basin, NE Brazil. London, *Geological Society*, (Special Publications, 472), doi:10.1144/sp472.4.

Leite F. P. R., Paz J. D. S., Carmo D., Silva-Caminha S. A. F. 2017. The effects of the inception of Amazonian transcontinental drainage during the Neogene on the landscape and vegetation of the Solimões Basin, Brazil. *Palynology*, **10**: 1-11.

Lehrmann D.J., Goldhammer R.K. 1999. Secular variation in parasequence and facies stacking patterns of platform carbonates: a guide to application of stacking-patterns analysis in strata of diverse ages and settings. In: Harris P.M., Saller A.H., Simo J.A. (eds.). *Advances in Carbonate Sequence Stratigraphy: Application to Reservoirs, Outcrops and Models*. (Society for Sedimentary Geology) Special Publication, 63: 187–225.

Latrubesse E. M., Cozzuol M., da Silva-Caminha S. A., Rigsby C. A., Absy M. L., Jaramillo C. 2010. The Late Miocene paleogeography of the Amazon Basin and the evolution of the Amazon River system. *Earth-Science Reviews*, **99** (3-4): 99-124.

Linsser H. 1958. *Interpretation of the regional gravity anomalies in the Amazonas area*. Rio de Janeiro: Petrobrás.

Louterbach M., Roddaz M., Antoine P. O., Marivaux L., Adnet S., Bailleul J., Calderon Y. 2018. Provenance record of late Maastrichtian–late Palaeocene Andean Mountain building in the Amazonian retroarc foreland basin (Madre de Dios basin, Peru). *Terra Nova*, **30** (1): 17-23.

Lowries W. 2007. *Fundamentals of geophysics*. New York, Cambridge University Press, 393 p.

Lundberg, J. 1997. Paleoclimatic reconstruction and timing of sea level rise at the end of the penultimate glaciation, from detailed stable isotopic study and TIMS dating of submerged Bahamian speleothem. Switzerland, *Speleology*, **1**: 101.

Manenti R. R., Souza W. E., Porsani M. J. 2018. Reprocessing and interpretation of deep structures in a regional transect of the Parnaíba Basin, Brazil. *London, Geological Society, Special Publications*, doi:10.1144/sp472.17

Manspeizer W. 1988. Triassic-Jurassic rifting and opening of the Atlantic: an overview. In: Manspeizer W. (eds.). *Triassic-Jurassic rifting, Continental Breakup and the Origin of the Atlantic Ocean and Passive Margins*, 41-79.

Martínez-Moreno F., Galindo-Zaldívar J., Pedrera A., Teixidó T., Peña J., González-Castillo L. 2015. Regional and residual anomaly separation in microgravity maps for cave detection: the case study of Gruta de las Maravillas (SW Spain). *Journal of Applied Geo-physics*, **114**: 1-11.

Martins L. T., Madeira J., Youbi N., Munhá J., Mata J., Kerrich R. 2008. Rift-related magmatism of the Central Atlantic Magmatic Province in Algarve, Southern Portugal. *Lithos*, **101**: 102-124, <https://doi/10.1016/j.lithos.2007.07.010>. 44.

Marzoli A., Renne P.E., Piccirilli E.M., Ernesto M., Bellieni G., De Min A. 1999. Extensive 200-million-year-old continental flood basalts of Central Atlantic Magmatic Province. *Science*, **284**: 616–618.

Marzoli A., Bertrand H., Knight K.B., Cirilli S., Buratti N., Verati C., Nomade S., Renne P.R., Youbi N., Martini R., Allenbach K., Neuwerth R., Rapaille C., Zaninetti L., Bellieni G. 2004. Synchrony of the Central Atlantic Magmatic Province and the Triassic–Jurassic boundary climatic and biotic crisis. *Geology*, **32**: 973–976.

Marzoli A., Jourdan F., Puffer J.H., Cuppone T., Tanne, L.H., Weems R.E., Bertrand H., Cirilli S., Bellieni G., De Min A. 2011. Timing and duration of the Central Atlantic Magmatic Province in the Newark and Culpeper basins, Eastern U.S.A. *Lithos*, **122**: 175-188.

Marzoli A., Callegaro S., Corso J., Joshua H.F.I., Chiaradia M., Youb I. N., Bertrand H., Reisberg L., Merle R., Jourdan F. 2018. The Central Atlantic Magmatic Province (CAMP): a review. In: Tanner L.H. (eds.). *The late Triassic World: Earth in a time of transition*. New York, Springer, 100-135.

Matsuda N. S. 2002. *Carbonate sedimentation cycle and origin of dolomite on the Lower Pennsylvanian intracratonic Amazon Basin, Northern Brazil*. PhD Theses, Tóquio Department of Earth and Planetary Science.

Matsuda N.S., Dino R., Wanderley filho J.R. 2004. Lithostratigraphic review of the Tapajós Group, Middle Carboniferous-Permian of the Amazonas Basin, Brazil: revisão litoestratigráfica do Grupo Tapajós, Carbonífero Médio-Permiano da Bacia do Amazonas. *Boletim de Geociências da Petrobras*.

Matsuda N. S., Góes A. T. M. O., Wanderley filho J. R. 2006. *Relatório geológico do Paleozoico do Rio Tapajós, borda sul da bacia do Amazonas, Pará*. Petrobrás, Manaus, 87 p.

- Matsuda N. S., Winter W. R., Wanderley Filho J. R., Cacela A. S. M. 2010. The paleozoic of Amazonas basin south edge: Tapajos river, Pará state. O paleozoico da borda sul da bacia do Amazonas: rio Tapajos, estado do Pará. *Boletim de Geociências da Petrobras*, 18 p.
- Melfi A.J., Piccirillo E.M., Nardy A.J.R. 1988. Geological and magmatic aspects of the Paraná Basin: an introduction. In: Melfi A.J. & Piccirillo E.M. (eds.). *The Mesozoic Flood Volcanism of the Paraná Basin: Petrogenetic and Geophysical Aspects*. São Paulo, Instituto Astronômico e Geofísico, 1-13.
- Mendes A.C., Truckenbrodt W.H.W., Nogueira A.C.R. 2012. Análise faciológica da Formação Alter do Chão (Cretáceo, Bacia do Amazonas), próximo à cidade de Óbidos, Pará, Brasil.
- Menegazzo M. C., Catuneanu O., Chang H. K. 2016. The South American retroarc foreland system: the development of the Bauru Basin in the back-bulge province. *Marine and Petroleum Geology*, **73**: 131-156, <https://doi/10.1016/j.marpetgeo.2016.02.027>.
- Melo J.H.G. 1988. The malvinokaffric realm in the Devonian of Brazil. In: Mcmillan, N.J., Embry, A.F. and Glass, D.J. (eds.). *Devonian of the World*. Canadian Society of Petroleum Geologists Memoirs, **14**: 669-703.
- Merle R., Marzoli A., Bertrand H., Reisberg L., Verati C., Zimmerman C., Chiaradia M., Bellieni G., Ernesto M. 2011.  $^{40}\text{Ar}/^{39}\text{Ar}$  ages and Sr-Nd-Pb-Os geochemistry of CAMP tholeiites from Western Maranhão Basin (NE Brazil). *Lithos*, **122**: 137-151.
- Milani E. J. & Zalán P. V. 1999. An outline of the geology and petroleum systems of the Paleozoic interior basins of South America. *Episodes Journal of International Geoscience*, **22** (3): 199-205.
- Milani E.J., Thomaz Filho A. 2000. Sedimentary basins of South America. In: Cordani U.G., Milani E.J., Thomaz Filho A., Campos D.A. (eds.). *Tectonic Evolution of South America*. Rio de Janeiro, **31**: 389-449.
- Miyashiro A. 1974. Volcanic rocks series in island arcs and active continental margins. *American Journal of Science*, **274**: 321-355.
- Mizusaki A.M.P., Wanderley Filho J., Aires J.R. 1992. Caracterização do magmatismo básico das bacias dos Solimões e do Amazonas. Petrobrás, Rio de Janeiro, *Relatório Interno*, 45 p.
- Mizusaki A.M.P., Thomaz-Filho A., Cesero P. 1998. Ages of the magmatism and the opening of the South Atlantic Ocean, *geoscience research*, **25**: 47-57.
- Mizusaki A.M.P., Thomaz-Filho A., Milani E.J., Césero P. 2002. Mesozoic and Cenozoic igneous activity and its tectonic control in Northeastern Brazil. *Journal of South American Earth Sciences*, **15**: 183-198.
- Mocitaiba L.S.R., Castro D.L., Oliveira D.C. 2017. Cartografia geofísica regional do magmatismo mesozoico na Bacia do Parnaíba. São Paulo, *Revista do Instituto de Geociências*, **17** (2): 16-192, doi: 10.11606/issn.2316-9095.v17-455.

- Montes Lauer C.R., Pacca I.G., Melfi A.J., Piccirillo E.M., Bellieni G., Petrone R., Rizzieri R. 1994. The Anari and Tapirapuã Jurassic formations, Western Brazil: paleomagnetism, geochemistry and geochronology. *Earth and Planetary Science Letters*, **128**: 357-71.
- Montalvão R.M.G., Oliveira A.S. 1975. Geologia branquianticlinal de Monte Alegre e da Rodovia Monte Alegre – Prainha. Belém, *Projeto Radam Brasil*, 409 p.
- Moore B. 1961. *South Central Maranhão*: field project. Belém, Petrobrás. (Relatório Técnico).
- Moreira G. 2019. *Paleomagnetismo da Formação Penatecaua da Província Magmática do Atlântico Central na bacia Amazônica, Brasil*. Dissertação (Mestrado). Instituto de Astronomia, Geofísica e Ciências Atmosféricas – USP, São Paulo.
- McGee B., Collins A.S., Trindade R.I.F. 2012. G'day Gondwana – birth of a supercontinent: U/Pb ages for the post-orogenic São Vicente granite, Mato Grosso, Brazil. *Gondwana Research*, **21**: 316-322.
- McHone J. G., 2000. Non-plume magmatism and tectonics during the opening of the Central Atlantic Ocean, *Tectonophysics*, **316**: 287-296.
- McHone J.G. & Puffer J.H. 2003. Flood basalt province of the Pangean Atlantic rift: regional extent and environmental significance. In: LeTourneau P.M. & Olsen P.E. (eds.). *The great rift valleys of Pangea in Eastern North America, Aspects of Triassic–Jurassic Rift Basin*. Columbia University Press, **1**: 141-154.
- McHone J.G. 2006. Igneous Features and Geodynamic Models of Rifting and Magmatism around the Central Atlantic Ocean. Disponível em: <http://www.mantleplumes.org/CAMP.html>.
- Nagy D. 1966. The gravitational attraction of a right rectangular prism. *Geophysics*, **31** (2): 362-371.
- Neves B.B., Riccomini C., Fernandes T.M.G., Santanna L.G. 2004. O Sistema tafrogênico terciário do Saliente Nordeste na Paraíba: um legado proterozóico. *Revista Brasileira de Geociências*, **4**: 127-134.
- Nogueira A.C.R. & Riccomini C. 2006. O Grupo Araras (Neoproterozóico) na parte norte da Faixa Paraguai e Sul do Cráton Amazônico, Brasil. *Rev. Bras. Geoc.*, **36** (4): 576-587.
- Nogueira A.C.R. 2008. Guinada para o Atlântico. In: Furtado R. (eds.). *Scientific American Brasil*. Coleção Amazônia Origens, **1**: 22-27.
- Nogueira A. C. R., Silveira R., Guimarães J. T. F. 2013. Neogene–Quaternary sedimentary and paleovegetation history of the eastern Solimões Basin, central Amazon region. *Journal of South American Earth Sciences*, **46**: 89-99.
- Nogueira A. C. R., Romero G. R., Sanchez E. A. M., Domingos F. H. G., Bandeira J., dos Santos, I. M., Soares J.L., Lafon J.M., Afonso J.L.P., Santos H.P., Rudnitzki I.D. 2019. The Cryogenian–Ediacaran boundary in the Southern Amazon Craton. *Geophysical Monograph Series*, 89-114, <https://doi/10.1002/9781119382508.ch6>. 46.

- Nogueira A.C.R., Rabelo C.E.N., Góes A.M., Cardoso A.R., Bandeira J., Rezende G.L., Santos, R.F., Truckenbrodt W. 2021. Evolution of Jurassic intertrap deposits in the Parnaíba Basin, Northern Brazil: The last sediment-lava interaction linked to the CAMP in West Gondwana. *Palaeogeography, palaeoclimatology, palaeoecology*, <https://doi.org/10.1016/j.palaeo.2021.110370>.
- Nomade S., Knight K.B., Beutel E., Renne P.R., Verati C., Feraud G., Marzol, A., Youbi N., Bertrand H. 2007. Chronology of the Central Atlantic Magmatic Province: implications for the Central Atlantic rifting processes and the Triassic–Jurassic biotic crisis. *Palaeogeography. Palaeoclimatology. Palaeoecology*, **244**: 326–344.
- Nunn J. A. & Aires, J. R. 1988. Gravity anomalies and flexure of the lithosphere at the Middle Amazon Basin, Brazil. *Journal of Geophysical Research: Solid Earth*, **93**: 415-428. doi:10.1029/jb093ib01p00415.
- Northfleet A.A. & Melo M. 1967. Geologia da região norte de Balsas, Maranhão, 268 p.
- Oliveira D.C. & Mohriak W.U. 2003. Jaibaras through: an important element in the early tectonic evolution of the Parnaíba interior sag basin, Northern Brazil. *Marine and Petroleum Geology*, **20**: 351-383.
- Oliveira A.L., Pimentel M.M., Foda R.A., Oliveira D.C. 2018. Petrologia de formações basálticas do Jurássico e Cretáceo da Bacia do Parnaíba, NE do Brasil: correlações e associações com grandes províncias ígneas. London, *Geological Society*. (Special Publications, 472). doi:10.1144/sp472.21.
- Oliveira A. L., Schmitz M.D., Wall C. J., Crowley J. L., Macêdo Filho A. A., Hollanda M. H. B. M. 2023. New U–Pb geochronology for the Central Atlantic Magmatic Province, critical reevaluation of high-precision ages and their impact on the end-Triassic extinction event. *Scientific Reports*, **13**: 54-84, <https://doi.org/10.1038/s41598-023-32534-3>.
- Olsen P.E. 1999. Giant lava flows, mass extinctions and mantle plumes. *Science*, **284**: 604-605.
- Oyarzun R., Doblás M., López-Ruiz J., Cebriá J.M. 1997. Opening of the Central Atlantic and asymmetric mantle upwelling phenomena: implications for long-lived magmatism in western North Africa and Europe. *Geology*, **25**: 727–730.
- Pastana J.M.N., Souza A.M.M., Vale A.G.V., Faria C.A.S., Santos M.E., Assunção, P.R.S., *et al.* 1978. Projeto sulfeto de Alenquer, Monte Alegre, *relatório final*. Belém, Ministério das Minas e Energias.
- Pastana S.M.N. 1999. *Síntese geológica e favorabilidade para tipos de jazimentos minerais do município de Monte Alegre-PA*. Belém, CPRM/ PRIMAZ, 34 p.
- Pedreira A.J. & Bahia, R.B.C. 2000. Sedimentary basins of Rondônia State, Brazil: response to the geotectonic evolution of the Amazonian Craton. *Revista Brasileira de Geociência*, **30**: 477-480.



Pedreira A.J. & Bahia R.B.C. 2004. Estratigrafia e evolução da Bacia dos Parecis, região Amazônica, Brasil: integração e síntese de dados dos projetos Alto Guaporé, Serra Azul, Serra do Roncador, Centro-Oeste de Mato Grosso e Sudeste de Rondônia. Brasília: CPRM: Serviço Geológico do Brasil/DEPAT/DIEDIG, 39.

Piqué A. & Laville E. 1996. The central Atlantic rifting: reactivation of Palaeozoic structures. *Journal of Geodynamics*, **21**: 235–255.

Pinto Filho F.P., Freitas A.F., De Melo C.F., Romanini S.J. 1977. Projeto Sudeste de Rondônia. DNPM/CPRM, Porto Velho, *Relatório final*, 4 v.

Plouff D. 1976. Gravity and magnetic fields of polygonal prisms and application to magnetic terrain corrections. *Geophysics*, **41**: 727-41.

Rabelo C.E.N. & Nogueira A.C.R. 2015. The Upper Jurassic humid desert system of the Parnaíba Basin, region between the desert system of the Upper Jurassic of the Parnaíba Basin, in the region between Formosa da Serra Negra and Montes Altos, State of Maranhão, Brazil. *Geologia USP*, **15**: 3-21.

Rabelo C.E.N., Cardoso A.R., Nogueira A.C.R., Soares J.L., Góes A.M. 2019. Genesis of poikilotopic zeolite in aeolianites: an example from the Parnaíba Basin, NE Brazil. *Sedimentary Geology*, **385**: 61-78.

Reis N.J., Szatmari P., Wanderley Filho J.R., York D., Evensen N.M., Smith P.E. 2006. Dois eventos de magmatismo máfico mesozóico na fronteira Brasil-Guiana, escudo das Guianas: enfoque à região do rifte do Tacutu-North Savanna. In: *SBG, 43º Congresso Brasileiro de Geologia*. Salvador, 459-464.

Renne P.R., Ernesto M., Pacca I.G., Coe R.S., Glen J.M., Prévot M., Perrin M. 1992. The age of Paraná flood volcanism, rifting of Gondwanaland, and Jurassic-Cretaceous boundary. *Science*, **258**: 975-979.

Rezende N.G.A.M. 2002. *A zona zeolítica da Formação Corda-Bacia do Parnaíba*. Dissertação - Mestrado, Universidade Federal do Pará, Belém, 141 p.

Rezende G.L., Nogueira A.C.R., Martins C.M., Ribeiro Filho N., Domingos F.H.G. 2021. Evidence for the Central Atlantic Magmatic Province (CAMP) in Precambrian and Phanerozoic sedimentary basins of the southern Amazonian Craton, Brazil. *J. S. Am. Earth Sci.* 1-9. <https://doi.org/10.1016/j.jsames.2021.103216>.

Ribeiro Filho N., Martins C. M., Sena Santos R. 2018. A novel regional-residual separation approach for gravity data through crustal modeling. *Brazilian Journal of Geophysics*, **36** (4): 491-505.

Ribeiro-Filho N., Martins C. M., Baldez R. M., Souza Júnior I. R., Ghomsy F. E. K. 2023. Determining the effective elastic thickness through cross-correlation between isostatic disturbances. *Geodesy and Geodynamics*, **15** (3): 241-251.

- Rocha-Campos A.C., Cordani U.G., Kawashita K., Sonoki H.M., Sonok, I.K. 1998. Age of the Paraná flood volcanism. In: Piccirillo E.M. & Melfi A.J. (eds.). *The Mesozoic flood volcanism of the Paraná Basin: petrogenetic and geophysical aspects*. São Paulo - USP, 25-45.
- Roddaz M., Baby P., Brusset S., Hermoza W., Darrozes J. M. 2005. Forebulge dynamics and environmental control in Western Amazonia: The case study of the Arch of Iquitos (Peru). *Tectonophysics*, **399** (1-4): 87-108.
- Roddaz M., Viers J., Brusset S., Baby P., Hérail G. 2005. Sediment provenances and drainage evolution of the Neogene Amazonian foreland basin. *Earth and Planetary Science Letters*, **239** (1-2): 57-78.
- Rosa J. W. C. & Fuck R. A. 2016. The structure of the Amazonian craton: Available geophysical evidence. *Journal of South American Earth Sciences*, **70**: 162-173. doi:10.1016/j.jsames.2016.05.0.
- Rodrigues J.B. 2014. *Relatório interno. Projeto Opala*. Brasília, DF, Serviço Geológico do Brasil (CPRM).
- Rubert R. R. *et al.* 2019. Mesozoic tectonic in the deposition and evolution of Cretaceous sedimentary packages of the Parecis Basin, Center-Western Brazil. *Journal of South American Earth Sciences*, **93**: 140-154.
- Ruhl M., Bonis N. R., Reichart G. J., Damste J. S. S., Kurschner W. M. 2011. Atmospheric carbon injection linked to end-Triassic mass extinction. *Science*, **333**: 430-434, <https://doi/10.1126/science.1204255>.
- Ruiz-Martínez V. C., Torsvik T. H., Van Hinsbergen D. J. J., Gaina C. 2012. Earth at 200 Ma: Global palaeogeography refined from CAMP palaeomagnetic data. *Earth and Planetary Science Letters*, 331–332, <https://doi/10.1016/j.epsl.2012.03.008>.
- Saunders A. D. 2005. Large igneous provinces: Origin and environmental consequences. *Elements*, **1**: 259-263, <https://doi/10.2113/gselements.1.5.259>. 48.
- Sanchez-Rojas J. 2012. New bouguer gravity maps of Venezuela: representation and analysis of free-air and bouguer anomalies with emphasis on spectral analyses and elastic thickness. *International Journal of Geophysics*, 1–15. doi:10.1155/2012/731545.
- Santos J.O.S. & Oliveira J.R. 1980. Principais associações máficas não metamorfizadas da Plataforma Amazônica. SBG, *Congresso Brasileiro de Geologia*, **31**: 2253-2262.
- Santos J.O.S. *et al.* 2000. A new understanding of the Provinces of the Amazon Craton based on integration of field mapping and U-Pb and Sm-Nd geochronology. *Gondwana Research*, **3** (4): 453-488.
- Santos M.E.C.M., Carvalho M.S.S. 2004. *Paleontologia das Bacias do Parnaíba, Grajaú e São Luís*. Rio Janeiro, 212 p.
- Santos H.P., Mángano M. G., Soares J.L., Nogueira A.C.R., Bandeira J., Rudnitzki I.D.M. 2017. Ichnologic evidence of a Cambrian age in the Southern Amazon Craton: implications for

the onset of the Western Gondwana history. *Journal of South American Earth Sciences*, **76**: 482-488.

Sahabi M., Aslanian D., Olivet J.L. 2004. A new starting point for the history of the central Atlantic. *Compt Rend Geosci*, **336**:1041-1052.

Silva W.R.L. 1980. Dispersão geoquímica dos elementos Si, Al, Fe, Mn, Na, K, Cu e Zn nos solos e sua aplicação na caracterização de áreas geoquimicamente homogêneas.

Silva-Caminha S., Jaramillo C., Absy M.L. 2010. Neogene palynology of the Solimões Basin, Brazilian Amazonia. *Palaeophytology*, **283**: 1-67.

Siqueira L.P. 1989. Bacia dos Parecis. *Boletim de Geociências da Petrobrás*, **3**: 3-16.

Siqueira L.P. & Teixeira L.B. 1993. Bacia dos Parecis: nova fronteira exploratória da Petrobrás. In: SBGeof, *Congresso Internacional da Sociedade Brasileira de Geofísica*, Resumos Expandidos, **3**: 168-170.

Scomazzon A. K., Moutinho L. P., Nascimento S., Lemos V. B., Matsuda N. S. 2016. Conodont biostratigraphy and paleoecology of the marine sequence of the Tapajós Group, Early-Middle Pennsylvanian of Amazonas Basin, Brazil. *Journal of South American Earth Sciences*, **65**: 25-42.

Schlager W. 2004. Fractal nature of stratigraphic sequences. *Geology*, **32**: 185-188.

Schlager W. 2010. Ordered hierarchy versus scale invariance in sequence stratigraphy. *Int. J. Earth Sci.* **99**: 139-151.

Schaller M.F., Wright J.D., Kent D.V., Olsen P.E. 2012. Rapid emplacement of the Central Atlantic Magmatic Province as a net sink for CO<sub>2</sub>. *Earth and Planetary Science Letters*, **323-324**: 27-39.

Schoene B., Guex J., Bartolini A., Schaltegger U., Blackburn T. J. 2010. Correlating the end-Triassic mass extinction and flood basalt volcanism at the 100-ka level. *Geology*, **38**: 387-390, <https://doi/10.1130/G30683.1>.

Schobbenhaus C. A. 1984. Evolução da plataforma Sul-americana no Brasil e suas principais concentrações minerais. *Geologia do Brasil*, 9-53.

Sheth H. 2007. Large Igneous Provinces (LIPs): definition, recommended terminology, and a hierarchical classification. *Earth Science Reviews*, **85**: 117-124.

Spector A. & Grant F. 1970. Statistical models for interpreting aeromagnetic data. *Geophysics*, **35**: 293-302.

Svensen H.H., Planke S., Chevallier L., Malthe-Sorensen A., Corfu F., Jamtveit B. 2007. Hydrothermal venting of greenhouse gases triggering Early Jurassic global warming. *Earth and Planetary Science Letters*, **256**: 554-566, <https://doi/10.1016/j.epsl.2007.02.013>.

- Svensen H.H., Torsvik T.H., Callegaro S., Augland L., Heimdal T.H., Jerram D.A., Planke S., Perreira E. 2018. Gondwana Large Igneous Provinces: plate reconstructions, volcanic basins and sill volumes. *The Geological Society of London*, **463**: 17-40, <https://doi/10.1144/SP463.7>.
- Szatmari P. 1983. Amazon rift and Pisco-Juruá fault; their relation to the separation of North America from Gondwana. *Geology*, **11** (5): 300-304.
- Tassinari C.C.G., Cordani U.G., Nutman A.P., Van Schmus W.R., Bettencourt J.S., Taylor P.N. 1996. Geochronological systematics on basement rocks from the Rio Negro-Juruena Province (Amazonian Craton) and tectonic implications. *Int. Geol. Rev.*, **38**: 161–175.
- Teixeira L.B. 2001. Evidências geofísicas de rifts precursores nas bacias Paleozóicas do Amazonas, Paraná, Parecis, Parnaíba, Solimões e Alto Tapajós. *In: Workshop sobre correções de Sequências Paleozóicas Sul-Americana*, 1-8.
- Teixeira W., Reis N.J., Bettencourt J.S., Klein E.F., Silva D.C. 2018. Intraplate Paleo to Mesoproterozoic magmatism in the Amazonian Craton reviewed: geochronology and crustal tectonics and barcode matches. *In: Srivastava R. Ernst (eds.). Dyke swarms of the world. A modern perspective (IDC-7 Special Volume)*. Accepted.
- Telford W.M., Geldart L.P., Sheriff R.E. 1990. *Applied geophysics*. Cambridge, Cambridge University Press, 770 p.
- Tenzer R., Gladkikh V., Novak P., Vajda P. 2012. Spatial and spectral analysis of refined gravity data for modelling the crust-mantle interface and mantle-lithosphere structure. *Surveys in Geophysics*, **33**: 817-839.
- Tesauro M., Kaban M. K., Cloetingh S. A. 2013. Global model for the lithospheric strength and effective elastic thickness. *Tectonophysics*, **602**: 78-86.
- Tribaldos R.V. & White N. 2018. Implications of preliminary subsidence analyses for the Parnaíba cratonic basin. London, *Geological Society*, **472** (1): 147-156.
- Trosdorf JR, J. M., Morais N. S. F., Santos C. V., Portela F. T. A., Dall O. A. C. M., Silva A.M. 2018. Phanerozoic magmatism in the Parnaíba Basin: characterization of igneous bodies (well logs and 2D seismic sections), geometry, distribution and sill emplacement patterns. London, *Geological Society*, **472**: 321-340 <https://doi.org/10.1144/SP472.10>.
- Teisserenc P. & Villemain J. 1989. Sedimentary Basin of Gabon-Geology and oil systems. *In: Edwards J.D. & Santogrossi P.A. (eds.). Divergent/Passive Margin basins*. American Association of Petroleum Geologists, 117-199. (Memoir, 46).
- Turcotte D. L. & Schubert G. 2002. *Geodynamics*. Cambridge university press.
- Uieda L. & Barbosa V.C.F. 2016. Fast nonlinear gravity inversion in spherical coordinates with application to the South American Moho. *Geophysical Journal International*, **208**: 162-176, <https://doi/10.1093/gji/ggw390>.
- Vail P.R., Mitchum Jr R.M., Thompson III S. 1977a. Seismic stratigraphy and global changes of sea level, Part 3: relative changes of sea level from coastal onlap. *In: Payton C.E. (Eds.)*.

*Seismic stratigraphy - applications to hydrocarbon exploration*. American Association of Petroleum Geologists, Memoir, **26**: 63-81.

Vail P.R., Mitchum Jr R.M., Thompson III S. 1977b. Seismic stratigraphy and global changes of sea level, Part 4: global cycles of relative changes of sea level. In: Payton C.E. (Eds.). *Seismic stratigraphy - applications to hydrocarbon exploration*. American Association of Petroleum Geologist, Memoir, **26**: 83-97.

Vail P.R., Audemard F., Bowman S.A., Eisner P.N., Perez-Cruz C. 1991. The stratigraphic signatures of tectonics, eustasy and sedimentology - an overview. In: Einsele G., Ricken W., Seilacher A. (Eds.). *Cycles and events in stratigraphy*. Springer-Verlag, 617–659.

Vaz P.T., Rezende N.G.A.M., Filho J.R.W., Travassos W.A.S. 2007. Bacia do Parnaíba. Rio de Janeiro, *Boletim de Geociências da Petrobras*, **15**: 253-263.

Vasquez M.L., Rosa-Costa L.T., Silva C.M.G., Ricc, P.S.F., Barbosa J.P.O., Klein E.L., Lopes E.C.S., Macambira E.M.B., Chaves C.L., Carvalho J.M.A., Oliveira J.G.F., Anjos G.C., Silva H.R. 2008. Unidades litoestratigráficas. In: Vasquez M.L., Rosa-Costa L.T. *Geologia e recursos minerais do Estado do Pará: Sistema de Informações Geográficas – SIG*. Belém, 113-215.

Verati C., Rapaille C., Fèraud G., Marzoli A., Bertrand H., Youbi N. 2007. 40Ar/39Ar ages and duration of the Central Atlantic Magmatic Province volcanism in Morocco and Portugal and its relation to the Triassic–Jurassic boundary. *Palaeogeography, palaeoclimatology, palaeoecology*, **244**: 308-325.

Wanderley Filho. J.R. 1991. *Evolução estrutural da Bacia do Amazonas e sua relação com o embasamento*. Dissertação de Mestrado, Centro de Geociências, Universidade Federal do Pará, Belém do Pará, 125 p.

Wanderley-Filho J. R., Eiras J. F., da Cruz Cunha P. R., Van der Ven P. H. 2010. The Paleozoic Solimões and Amazonas basins and the Acre foreland basin of Brazil. Amazonia: landscape and species evolution: a look into the past, 29-37, doi:10.1002/9781444306408.ch3.

Watts A. B. 2001. *Isostasy and flexure of the lithosphere*. Cambridge University Press, 480 p.

Weber L. J., Sarg J. F., Wright F. M. 1995. Sequence stratigraphy and reservoir delineation of the middle Pennsylvanian (Desmoinesian), paradox basin and Aneth field, Southwestern USA, In: Read J. F., Weber L. J., Sarg J. F., Wright F. M. (eds.). *Milankovitch sea-level changes, cycles, and reservoirs on carbonate platforms in Greenhouse and Ice-House Worlds*: SEPM Short Course, 79 p.

Wesselingh F. P., Hoorn M. C., Guerrero J., Räsänen M. E., Romero Pittman L., Salo J. S. 2006. The stratigraphy and regional structure of Miocene deposits in Western Amazonia (Peru, Colombia and Brazil), with implications for late Neogene landscape evolution, *Scripta Geol.*, **133**: 291-320.

Wienecke S. 2006. *Universitätsbibliothek Der FU Berlin, Universitätsbibliothek Der FU Berlin, a new analytical solution for the calculation of flexural rigidity: significance and application*. PhD theses, Freie Universität Berlin, <https://doi.org/10.17169/REFUBIUM->

4365.

Wienecke S., Braitenberg C., Götze H. J. 2007. A new analytical solution estimating the flexural rigidity in the Central Andes. *Geophysical Journal International*, **169** (3): 789-794.

Wilson C., Charlou J. L., Ludford E. 1997. Hydrothermal anomalies in the Lucky Strike segment on the Mid-Atlantic Ridge (37° 17 N). *Oceanographic Literature Review*, **5** (44): 463-464.

Withjack M.O., Schlische R.W., Olsen P.E. 1998. Diachronous rifting, drifting, an inversion on the passive margin of central eastern North America: an analog for other passive margins. *American Association of Petroleum Geologists Bulletin*, **82**: 817-835.

Whiteside J. H., Olsen P. E., Eglinton T., Brookfield M. E., Sambrotto R. N. 2010. Compound-specific carbon isotopes from Earth's largest flood basalt eruptions directly linked to the end-Triassic mass extinction. *Proceedings of the National Academy of Sciences of the United States of America*, **107**: 6721-6725, <https://doi/10.1073/pnas.1001706107>.

Yamasaki T., Sigmundsson F., Iguchi M. 2022. Variable inflation rate of a magmatic deformation source beneath Air a caldera after the 1914 eruption of Sakurajima volcano: inferences from a linear Maxwell viscoelastic model constrained by geodetic data. *Journal of Volcanology and Geothermal Research*, **421**: 107-446.

Zalán P.V. 1991. Influence of Pre-Andean orogenies on the Paleozoic intracratonic basins of South America. *In: 4. Simpósio Bolivariano, Exploración Petrolera em las Cuencas Subandinas, Bogotá. v. 1. (Memórias IV)*.

Zalán P.V. 2004. Evolução Fanerozóica das bacias sedimentares brasileiras, *In: Mantesso - Neto V., Bartorelli A., Carneiro C. D. R., Neve B. B. B. (eds.). Geologia do continente Sul Americano. Evolução da obra de Fernando Flávio Marques de Almeida, Beca Produções Culturais Ltda, São Paulo, 595-612.*



UNIVERSIDADE FEDERAL DO PARÁ  
INSTITUTO DE GEOCIÊNCIAS  
PROGRAMA DE PÓS-GRADUAÇÃO EM GEOLOGIA E GEOQUÍMICA

## PARECER

### Sobre a Defesa Pública da Tese de Doutorado de GABRIEL LEAL REZENDE

A banca examinadora da Tese de Doutorado de **GABRIEL LEAL REZENDE** orientando do Prof. Dr. Afonso César Rodrigues Nogueira (UFPA), e composta pelos professores doutores Juliana Charão Marques (UFRGS), Claudio Riccomini (USP), Rodrigo Bijani Santos (UFF) e Joelson Lima Soares (UFPA), após apresentação da sua tese intitulada "**O CAMP NAS BACIAS DOS SOLIMÕES, AMAZONAS, PARNAÍBA E PARECIS: IMPLICAÇÕES GEOTECTÔNICAS E DEPOSICIONAIS PARA O JURÁSSICO DO GONDWANA OCIDENTAL**", emite o seguinte parecer:

O candidato realizou sua apresentação de forma clara, bem-organizada e segura no tempo estipulado. Na arguição mostrou domínio da temática abordada e respondeu às perguntas formuladas pela banca. O trabalho escrito foi apresentado na forma de dois artigos, sendo um já publicado e outro em revisão, ambos em periódicos internacionais. A banca fez sugestões de melhoria no texto a serem avaliadas pelo candidato. Considerando-se a elevada qualidade do trabalho e a defesa, a banca examinadora decidiu por unanimidade aprovar a tese de doutorado.

Belém, 23 de agosto de 2024

  
Prof. Dr. Afonso César Rodrigues Nogueira (Orientador-UFPA)

Documento assinado digitalmente

gov.br

JULIANA CHARÃO MARQUES

Data: 26/08/2024 11:26:30-0300

Verifique em <https://validar.it.gov.br>

Prof.<sup>a</sup> Dr.<sup>a</sup> Juliana Charão Marques (Membro-UFRGS)

Documento assinado digitalmente

gov.br

CLAUDIO RICCOMINI

Data: 26/08/2024 15:58:35-0300

Verifique em <https://validar.it.gov.br>

Prof. Dr. Claudio Riccomini (Membro-USP)

Documento assinado digitalmente

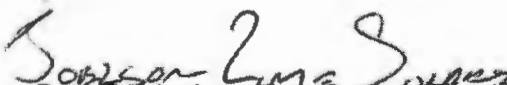
gov.br

RODRIGO BIJANI SANTOS

Data: 29/08/2024 10:12:14-0300

Verifique em <https://validar.it.gov.br>

Prof. Dr. Rodrigo Bijani Santos (Membro-UFF)



Prof. Dr. Joelson Lima Soares (Membro-UFPA)